21. Vinchi F, Gastaldi S, Silengo L, Altruda F, Tolosano E: **Hemopexin prevents endothelial damage and liver congestion in a mouse model of heme overload.** *Am J Pathol* 2008, **173:**289–299.
22. Lagan AL, Melley DD, Evans TW, Quinlan GJ: **Pathogenesis of the systemic inflammatory syndrome and acute lung injury: role of iron mobilization and decompartmentalization.** *Am J Physiol Lung Cell Mol Physiol* 2008, **294:**L161–174.
23. Nielsen MJ, Moestrup SK: **Receptor targeting of hemoglobin mediated by the haptoglobins: roles beyond heme scavenging.** *Blood* 2009, **114:**764–771.
24. Nielsen MJ, Moller HJ, Moestrup SK: **Hemoglobin and heme scavenger receptors.** *Antioxid Redox Signal* 2010, **12:**261–273.
25. Lopez JL: **Two-dimensional electrophoresis in proteome expression analysis.** *J Chromatogr B Analyt Technol Biomed Life Sci* 2007, **849:**190–202.
26. Sa-Correia I, Teixeira MC: **2D electrophoresis-based expression proteomics: a microbiologist's perspective.** *Expert Rev Proteomics* 2010, **7:**943–953.
27. Aggarwal K, Choe LH, Lee KH: **Shotgun proteomics using the iTRAQ isobaric tags.** *Brief Funct Genomic Proteomic* 2006, **5:**112–120.
28. Treumann A, Thiede B: **Isobaric protein and peptide quantification: perspectives and issues.** *Expert Rev Proteomics* 2010, **7:**647–653.
29. Xu J, Khor KA, Sui J, Zhang J, Tan TL, Chen WN: **Comparative proteomics profile of osteoblasts cultured on dissimilar hydroxyapatite biomaterials: an iTRAQ-coupled 2-D LC-MS/MS analysis.** *Proteomics* 2008, **8:**4249–4258.
30. Yang X, Yang S, Wang J, Zhang X, Wang C, Hong G: **Expressive proteomics profile changes of injured human brain cortex due to acute brain trauma.** *Brain Inj* 2009, **23:**830–840.
31. Gerashchenko BI, Gun'ko VM, Gerashchenko II, Mironyuk IF, Leboda R, Hosoya H: **Probing the silica surfaces by red blood cells.** *Cytometry* 2002, **49:**56–61.
32. Murashov V, Harper M, Demchuk E: **Impact of silanol surface density on the toxicity of silica aerosols measured by erythrocyte haemolysis.** *J Occup Environ Hyg* 2006, **3:**718–723.
33. Slowing II, Wu CW, Vivero-Escoto JL, Lin VS: **Mesoporous silica nanoparticles for reducing hemolytic activity towards mammalian red blood cells.** *Small* 2009, **5:**57–62.
34. Lin YS, Haynes CL: **Impacts of mesoporous silica nanoparticle size, pore ordering, and pore integrity on hemolytic activity.** *J Am Chem Soc* 2010, **132:**4834–4842.
35. Yu T, Malugin A, Ghandehari H: **Impact of silica nanoparticle design on cellular toxicity and hemolytic activity.** *ACS Nano* 2011, **5:**5717–5728.
36. Manuel Y, Defontaine MC, Bourgoin JJ, Dargent M, Sonneck JM: **Serum haemopexin levels in patients with malignant melanoma.** *Clin Chim Acta* 1971, **31:**485–486.
37. Coombes RC, Powles TJ, Neville AM: **Evaluation of biochemical markers in breast cancer.** *Proc R Soc Med* 1977, **70:**843–845.
38. Maes M, Delange J, Ranjan R, Meltzer HY, Desnyder R, Cooremans W, Scharpe S: **Acute phase proteins in schizophrenia, mania and major depression: modulation by psychotropic drugs.** *Psychiatry Res* 1997, **66:**1–11.
39. Immenschuh S, Song DX, Satoh H, Muller-Eberhard U: **The type II hemopexin interleukin-6 response element predominates the transcriptional regulation of the hemopexin acute phase responsiveness.** *Biochem Biophys Res Commun* 1995, **207:**202–208.
40. Liang SC, Nickerson-Nutter C, Pittman DD, Carrier Y, Goodwin DG, Shields KM, Lambert AJ, Schelling SH, Medley QG, Ma HL, Collins M, Dunussi-Joannopoulos K, Fouser LA: **IL-22 induces an acute-phase response.** *J Immunol* 2010, **185:**5531–5538.

doi:10.1186/1556-276X-7-555
Cite this article as: Higashisaka *et al.*: Hemopexin as biomarkers for analyzing the biological responses associated with exposure to silica nanoparticles. *Nanoscale Research Letters* 2012 7:555.

Regular Article

THROMBOSIS AND HEMOSTASIS

Anti-factor IXa/X bispecific antibody ACE910 prevents joint bleeds in a long-term primate model of acquired hemophilia A

Atsushi Muto,[1] Kazutaka Yoshihashi,[1] Minako Takeda,[1] Takehisa Kitazawa,[1] Tetsuhiro Soeda,[1] Tomoyuki Igawa,[1] Zenjiro Sampei,[1] Taichi Kuramochi,[1] Akihisa Sakamoto,[1] Kenta Haraya,[1] Kenji Adachi,[1] Yoshiki Kawabe,[1] Keiji Nogami,[2] Midori Shima,[2] and Kunihiro Hattori[1]

[1]Research Division, Chugai Pharmaceutical Co, Ltd, Gotemba, Shizuoka, Japan; and [2]Department of Pediatrics, Nara Medical University, Kashihara, Nara, Japan

Key Points

- A long-term acquired hemophilia A model expressing spontaneous joint bleeds and other bleeds was newly established in nonhuman primates.
- Weekly SC dose of the anti-FIXa/X bispecific antibody ACE910 prevented joint bleeds and other bleeds in the primate hemophilia A model.

ACE910 is a humanized anti-factor IXa/X bispecific antibody mimicking the function of factor VIII (FVIII). We previously demonstrated in nonhuman primates that a single IV dose of ACE910 exerted hemostatic activity against hemophilic bleeds artificially induced in muscles and subcutis, and that a subcutaneous (SC) dose of ACE910 showed a 3-week half-life and nearly 100% bioavailability, offering support for effective prophylaxis for hemophilia A by user-friendly SC dosing. However, there was no direct evidence that such SC dosing of ACE910 would prevent spontaneous bleeds occurring in daily life. In this study, we newly established a long-term primate model of acquired hemophilia A by multiple IV injections of an anti-primate FVIII neutralizing antibody engineered in mouse-monkey chimeric form to reduce its antigenicity. The monkeys in the control group exhibited various spontaneous bleeding symptoms as well as continuous prolongation of activated partial thromboplastin time; notably, all exhibited joint bleeds, which are a hallmark of hemophilia. Weekly SC doses of ACE910 (initial 3.97 mg/kg followed by 1 mg/kg) significantly prevented these bleeding symptoms; notably, no joint bleeding symptoms were observed. ACE910 is expected to prevent spontaneous bleeds and joint damage in hemophilia A patients even with weekly SC dosing, although appropriate clinical investigation is required. (*Blood.* 2014;124(20): 3165-3171)

Introduction

Patients with severe hemophilia A (<1% of normal factor VIII [FVIII] level) typically suffer from recurrent bleeding episodes, primarily in the musculoskeletal system.[1,2] Approximately 85% of the bleeding episodes are into joints,[3] and repeated joint bleeding from early childhood results in a chronic degenerative arthritis. Although traditional on-demand treatment by a FVIII agent cannot prevent hemophilic arthropathy, routine prophylaxis with FVIII to maintain ≥1% FVIII:C is beneficial in preventing it.[4,5] However, the need for frequent IV injections of FVIII negatively affects patients' quality of life and their adherence to the routine prophylactic regimen, which is particularly problematic when treating pediatric patients at home.[2,6]

Furthermore, ~30% of severe patients develop alloantibodies against FVIII (FVIII inhibitors),[2,7] which largely restrict treatment with FVIII. FVIII inhibitors make hemorrhage more difficult to be controlled because alternative bypassing agents have shorter half-lives and are not always effective.[7,8] Attempts to induce immune tolerance to FVIII inhibitors with high doses of FVIII are very expensive and do not always work.[9]

Therefore, a novel drug is needed: one that is long-lasting, subcutaneously injectable, effective regardless of FVIII inhibitors, and does not induce FVIII inhibitors.[10-13] To achieve this desirable profile, we produced a series of humanized immunoglobulin G (IgG) antibodies bispecific to factors IXa and X (anti-FIXa/X antibodies) that mimic the FVIII cofactor function by binding and placing FIXa and FX into spatially appropriate positions (supplemental Figure 1, see supplemental Data available on the *Blood* Web site),[14] and identified a clinical investigational drug termed ACE910.[15] In a short-term primate model of acquired hemophilia A, ACE910 at a single IV dose of 1 or 3 mg/kg exerted hemostatic activity against artificial ongoing bleeds in muscles and subcutis to the same extent as recombinant porcine FVIII (rpoFVIII) at twice-daily IV doses of 10 U/kg.[16] Furthermore, a multiple-dosing simulation calculated from the pharmacokinetic (PK) parameters of ACE910 in cynomolgus monkeys suggested that the plasma ACE910 concentration capable of stopping even ongoing bleeds would be maintained by once-weekly subcutaneous (SC) administration of 0.64 to 1.5 mg/kg ACE910.[16]

Submitted July 2, 2014; accepted September 14, 2014. Prepublished online as *Blood* First Edition paper, October 1, 2014; DOI 10.1182/blood-2014-07-585737.

Presented in abstract form at the World Federation of Hemophilia 2014 World Congress, Melbourne, Australia, May 11-15, 2014.

The online version of this article contains a data supplement.

The publication costs of this article were defrayed in part by page charge payment. Therefore, and solely to indicate this fact, this article is hereby marked "advertisement" in accordance with 18 USC section 1734.

Prevention of joint bleeding is of major importance in the care of hemophilia A patients.[3] However, it remained unproven whether repeated SC dosing of ACE910 could actually prevent spontaneous bleeding episodes, including the joint bleeds that are a pathologic hallmark of hemophilia A. To address this question nonclinically, we required a primate model because ACE910 is highly species-specific in its FVIII-mimetic cofactor activity.[16]

In this study, we aimed first to establish a long-term acquired hemophilia A model expressing spontaneous bleeding episodes, including joint bleeds, in nonhuman primates, and second to evaluate the preventive effect of once-weekly SC dosing of ACE910 in this model for investigating the potential of a prophylactic treatment in hemophilia A patients.

Materials and methods

ACE910

ACE910 was expressed in HEK293 or CHO cells cotransfected with a mixture of plasmids encoding the anti-FIXa heavy chain, anti-FX heavy chain, and common light chain.[15] ACE910 was purified by protein A and ion-exchange chromatography from the culture supernatants.

Anti-primate FVIII neutralizing antibodies

A mouse monoclonal anti-primate FVIII neutralizing antibody, termed VIII-2236, was prepared from hybridoma culture supernatants.[14,16] A chimeric mouse-monkey anti-primate FVIII neutralizing antibody, termed cyVIII-2236, was constructed comprising the mouse variable region from VIII-2236 and the monkey constant region of IgG, which we originally cloned from cynomolgus monkey thymus. The cyVIII-2236 antibody was produced in HEK293 cells and isolated by protein A and gel permeation chromatography from the culture supernatants.

Comparison of cyVIII-2236 with VIII-2236 in an APTT assay

First, to compare the FVIII-neutralizing activity between cyVIII-2236 and VIII-2236, each was added to citrated plasma pooled from 3 normal male cynomolgus monkeys. Then, activated partial thromboplastin time (APTT) was measured with a standard method using Thrombocheck APTT-SLA (Sysmex) and coagulation analyzer KC4 Delta (Stago). Second, to compare the effect of cyVIII-2236 and VIII-2236 on the APTT-shortening activity of ACE910, each was added to FVIII-deficient human plasma (George King) at the final plasma concentration of 300 μg/mL together with various concentrations of ACE910, then APTT was measured.

Animals

Ten male cynomolgus monkeys (2.35-4.25 kg, aged 3-4 years) were purchased from Hamri. All animal studies were approved by the institutional animal care and use committee of Chugai Pharmaceutical, and were conducted in accordance with the approved protocols and the Guidelines for the Care and Use of Laboratory Animals at the company. Chugai Pharmaceutical is fully accredited by the Association for Assessment and Accreditation of Laboratory Animal Care (AAALAC) International.

Long-term primate model of acquired hemophilia A

In the first part of this study, 2 cynomolgus monkeys received weekly IV injections (3 or 10 mg/kg each) of VIII-2236. Citrated blood was collected over time. Blood hemoglobin (Hgb) concentration was measured by hematology analyzer SF-3000 (Sysmex) to monitor hemorrhagic anemia. APTT was assessed with a standard method using Data-Fi APTT (Siemens) and coagulation analyzer AMAX CS-190 (Trinity). In addition, bleeding symptoms (bruises [dark-red areas on the body surface], hematuria, limping, and general condition including joint swelling) were monitored on 21 working days from day 0 until day 28. To observe bruises easily, the body hair was sheared on day 0, and the area of bruises and the number of days when bruises had been detected were assessed.

In the second part of this study, another 8 cynomolgus monkeys received weekly IV injections (10 mg/kg) of cyVIII-2236. Two groups (n = 4 each) were established: a control group (the vehicle group) treated with vehicle and a test group (the ACE910 group) treated with ACE910. ACE910 was administered as an initial 3.97 mg/kg SC dose 2 hours after cyVIII-2236 injection on day 0, and thereafter as weekly 1 mg/kg SC doses. The same dosing regimen of vehicle (histidine buffer containing a surfactant) was applied to the vehicle group. Citrated blood was collected over time. Blood Hgb concentration was measured; the change in blood Hgb level was expressed as a percentage of that on day 0 (2 hours after cyVIII-2236 injection). APTT was measured with Thrombocheck APTT-SLA and KC4 Delta. Bleeding symptoms were monitored on 41 working days until day 56. Necropsy was performed on day 56; organs and tissues from the whole body were macroscopically examined, and hemorrhagic findings in joints (shoulder, elbow, wrist, hip, knee, and ankle on both sides) were scored. Then, they were histopathologically examined.

We assessed cyVIII-2236 concentration, FVIII-neutralizing titer of cyVIII-2236, ACE910 concentration, and development of anti-ACE910 alloantibodies. The methods are described in detail in the supplemental Methods. Briefly, cyVIII-2236 concentration was determined with a sandwich enzyme-linked immunosorbent assay (ELISA) using recombinant human FVIII and an anti-human IgG antibody. FVIII-neutralizing titers of cyVIII-2236 on days 0 (just after cyVIII-2236 injection) and 56 were assessed with a modified Bethesda assay. ACE910 concentration was determined with a sandwich ELISA to quantify human IgG.[16] Anti-ACE910 alloantibodies present at necropsy were examined with an electrochemiluminescent bridging immunoassay using labeled ACE910.[16]

In both parts, the monkeys were carefully monitored under the supervision of the attending veterinarian to determine the necessity of pain relief or other treatment. Consequently, no monkeys received an analgesic drug.

Statistical analysis and multiple-dosing simulation

The data are presented as individual values or as mean ± standard deviation (SD). In the in vivo efficacy study, some were analyzed by 2-tailed Student *t* test (SAS Preclinical Package, version 5.00) between the vehicle and the ACE910 groups. A P value of .05 or less was considered statistically significant. Multiple doses of ACE910 were simulated on the basis of the PK parameters previously determined[16] with SAAM II, version 1.2 software (SAAM Institute).

Results

Failure of long-term neutralization of endogenous FVIII by VIII-2236 in cynomolgus monkeys

First, we attempted to establish a long-term acquired hemophilia A model by weekly IV injection of VIII-2236 in cynomolgus monkeys. APTT prolongation was observed for the first 2 weeks (Figure 1), but gradually shortened after the third injection, and finally disappeared by the end of the fourth week, suggesting the development of alloantibodies to VIII-2236. VIII-2236 is a mouse IgG, and therefore entirely foreign to primates. In addition, no sign of joint bleeds was observed, although some bruises and a transient decrease in blood Hgb were detected (data not shown). Consequently, we sought an alternative way of establishing a longer-term primate model of acquired hemophilia A.

Chimerization of VIII-2236 to cyVIII-2236

As an attempt to avoid anti-VIII-2236 alloantibody development, we chimerized VIII-2236 (mouse IgG) by replacing its constant region with that of cynomolgus monkey IgG. The chimerized VIII-2236 (cyVIII-2236) successfully prolonged APTT in cynomolgus monkey plasma in vitro with a similar concentration dependency to that of original VIII-2236 (Figure 2A). Additionally, cyVIII-2236 did not interfere with the APTT-shortening activity of ACE910, the same results were also found with VIII-2236 (Figure 2B). These results indicate that VIII-2236 was successfully chimerized to cyVIII-2236 while retaining the original characteristics.

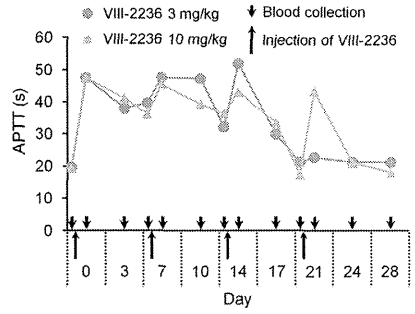

Figure 1. Change in APTT after weekly IV injection of the mouse anti-primate FVIII neutralizing antibody VIII-2236 in cynomolgus monkeys. VIII-2236 was injected at 3 or 10 mg/kg IV doses to cynomolgus monkeys on days 0, 7, 14, and 21. Citrated blood was collected on days 0, 3, 7, 10, 14, 17, 21, 24, and 28 (before and 2 hours after VIII-2236 injection on days 0, 7, 14, and 21). The time course of APTT is shown for each monkey.

Establishment of a long-term acquired hemophilia A model expressing spontaneous joint bleeds in cynomolgus monkeys

Using cyVIII-2236, we retried to establish long-term neutralization of endogenous FVIII, expecting reproducible development of spontaneous joint bleeds. The experimental protocol is illustrated in Figure 3A. In all the monkeys given vehicle (n = 4), APTT was prolonged to approximately twice the normal baseline for 8 weeks (Figure 3B). Plasma cyVIII-2236 concentration fluctuated, but remained over 58.6 μg/mL (nearly 400 nM) (supplemental Figure 2). As over 400 nM cyVIII-2236 prolonged APTT by twofold in vitro (Figure 2A), these observations seemed consistent. Thus, an acquired hemophilia A state was successfully maintained by using cyVIII-2236.

In this long-lasting acquired hemophilia A state, all the control monkeys given vehicle developed abnormal leg motion known as limping: a behavior to avoid using the affected leg (Figure 3C). The limping continued until the experiments ended, with days when limping was detected reaching 25.0 ± 8.3 days (61% ± 20%) of the 41 observation days. Two control monkeys (#3 and #4) developed joint swelling at the ankle in the limping limb from days 28 to 42 and from days 18 to 42, respectively. Macroscopic observation at necropsy on day 56 revealed intraarticular dark red areas (consistent with hemorrhagic findings in the histopathological examination) in joints (elbow, hip, or ankle) of all the control monkeys; the number of bleeding joints was 2.0 ± 0.8 per head (Figure 3D, Table 1). Bleeding was detected in the hip or ankle joint of the side that limped. Representative macroscopic findings of the hip joints are shown in Figures 3Ei-ii. Hemorrhagic findings or reactive findings associated with hemorrhage were histopathologically confirmed in the joints that limped: hemorrhage/hemosiderin deposition, mononuclear cell infiltration, and vascular proliferation in the synovial membranes; synovial hyperplasia; granulation tissue; and destruction of articular cartilage or underlying bone (Figure 4A-C). Thus, a long-term acquired hemophilia A model expressing spontaneous joint bleeds was successfully established in cynomolgus monkeys.

Other spontaneous bleeding symptoms, that is, bruises and hematuria, were detected by daily observation in the vehicle group (data not shown). By macroscopic observation at necropsy, hemorrhagic findings were also observed in skeletal muscle (lower abdomen and femoral region), urinary bladder, seminal vesicle, rectum, and subcutis (back) in 1 or 2 of the 4 control monkeys (Table 1). Additionally, blood Hgb temporarily decreased during the observation period with the lowest values reaching 64% to 87% (Figure 5), suggesting substantial hemorrhagic blood loss.

Bleeding preventive effect of ACE910 in the long-term acquired hemophilia A model

The preventive effect of a weekly SC dose of ACE910 on spontaneous joint bleeds was evaluated in the model described in "Establishment of a long-term acquired hemophilia A model expressing spontaneous joint bleeds in cynomolgus monkeys." The dosing regimen was simulated to maintain the plasma concentration trough at >30 μg/mL from the first week after administration using the PK parameters of ACE910 in cynomolgus monkeys previously obtained because around 26 μg/mL of plasma ACE910 would show hemostatic activity

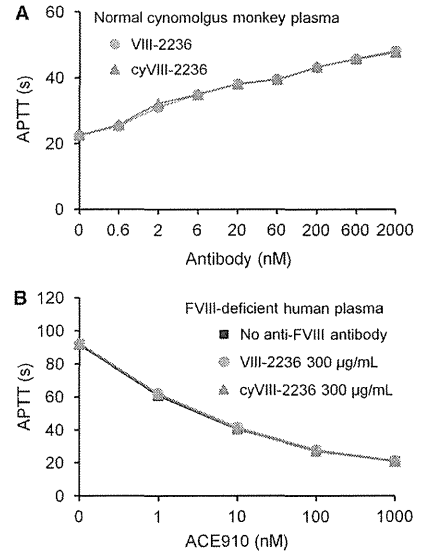

Figure 2. Comparison of the mouse-monkey chimeric anti-primate FVIII neutralizing antibody cyVIII-2236 with the original mouse antibody VIII-2236 in an APTT assay. (A) Effects of cyVIII-2236 and VIII-2236 on APTT in normal cynomolgus monkey plasma. (B) Influence of 300 μg/mL cyVIII-2236 and VIII-2236 on APTT-shortening activity of ACE910 in FVIII-deficient human plasma. Data are expressed as means ± SD (n = 3). The bars depicting SD are shorter than the height of the symbols. The symbols for the group without anti-FVIII antibody are hidden behind the symbols for the other groups in panel B.

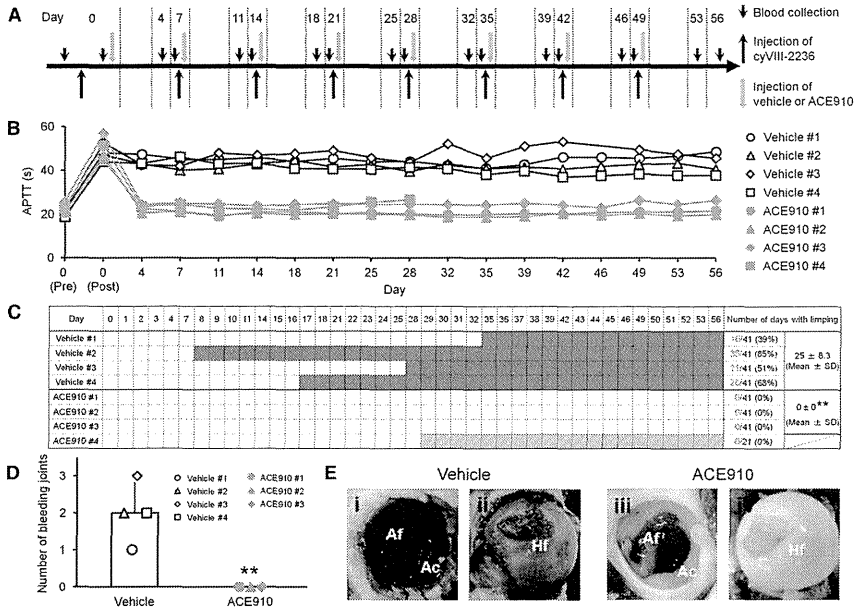

Figure 3. Preventive effects of ACE910 on spontaneous joint bleeds in a long-term primate model of acquired hemophilia A. (A) Experimental protocol used for evaluating preventive effects of ACE910 in a long-term hemophilia A model induced by the weekly IV doses of 10 mg/kg cyVIII-2236. The 8 cynomolgus monkeys received weekly IV injections of cyVIII-2236 on days 0, 7, 14, 21, 28, 35, 42, and 49. ACE910 was administered as an initial 3.97 mg/kg SC dose 2 hours after cyVIII-2236 injection on day 0, and thereafter as a weekly 1 mg/kg SC dose on days 7, 14, 21, 28, 35, 42, and 49. Citrated blood was collected on days 0, 4, 7, 11, 14, 18, 21, 25, 28, 32, 35, 39, 42, 46, 49, 53, and 56 (before and 2 hours after cyVIII-2236 injection on day 0; just before cyVIII-2236, vehicle, and ACE910 injections on days 7, 14, 21, 28, 35, 42, and 49). (B) The time courses of APTT are shown as individual values for respective cynomolgus monkeys (#1-4) of the vehicle and ACE910 groups. The APTT of the vehicle #3 monkey on day 46 was not determined due to a handling failure. (C) The days in which limping was observed are shown in red for the individual cynomolgus monkeys. The gray boxes indicate that no data are available because the ACE910 #4 monkey was killed for humane reasons on day 28 (See "Results"). The number of days with limping (C) and the number of bleeding joints at necropsy (D) are shown as individual values (#1-4) and as means ± SD in the vehicle group (n = 4) and the ACE910 group (n = 3). $^{**}P < .01$ indicates significant differences from the vehicle group (2-tailed Student *t* test). (E) Representative macroscopic findings of the joints at necropsy. Left hip joint with limping in the vehicle #1 monkey; dark-red area in the Af (i) and Hf (ii) is detected. Left hip joint without limping in the ACE910 #3 monkey; no abnormalities are noted in the Af (iii) and Hf (iv). Ac, acetabulum; Af, acetabular fossa; Hf, head of femur.

comparable to that of 10 U/kg (twice-daily) rpoFVIII in a short-term primate model of acquired hemophilia A.[16]

In all the monkeys treated with ACE910 (n = 4), APTT was initially prolonged to approximately twice the normal baseline after the first IV injection of cyVIII-2236, as in the group treated with vehicle. Then, repeated ACE910 administration shortened the prolonged APTT to the baseline level over the entire dosing period (Figure 3B), although careful observation indicates that the APTT-shortening effect was slightly reversed in 1 monkey (ACE910 #4) on days 25 and 28. It should be noted that the APTT of FVIII-neutralized cynomolgus monkey plasma was normalized even at around 30 μg/mL (nearly 200 nM) of ACE910, which also indicated rpoFVIII relative activity of <10% on the basis of peak height in the thrombin generation assay.[16] This is assumedly because ACE910 does not require an activation process to exert its cofactor activity, whereas FVIII needs additional time to be activated by thrombin or FXa in the APTT assay. Therefore, the effect of ACE910 on APTT should be carefully interpreted in relation to the hemostatic efficacy. Plasma cyVIII-2236 in the ACE910 group remained over 96.1 μg/mL, which exceeded the minimal cyVIII-2236 level (58.6 μg/mL) in the vehicle group (supplemental Figure 2). Furthermore, in all monkeys other than the ACE910 #4 monkey, the FVIII-neutralizing titer measured by the modified Bethesda assay was maintained on day 56 (data not shown). These results suggest that endogenous FVIII was also successfully neutralized in the ACE910 group.

The ACE910 #4 monkey showed a rapid and significant decrease in plasma ACE910 concentration from day 21 to day 28, on which it was only 2.8 μg/mL (Figure 6), and anti-ACE910 alloantibodies were detected in the plasma (data not shown). Furthermore, this monkey accidentally experienced a fracture of the mandibular cuspid on day 28, although no other monkeys experienced such a rare accident. Owing to the consequent massive bleeding in the oral cavity, the blood Hgb concentration decreased to 2.2 g/dL (19% of day 0 values, Figure 5). Therefore, in consideration of animal ethics and the impossibility of maintaining an effective ACE910 level, this monkey was killed humanely on day 28 and macroscopic observation of its organs and tissues was carried out at necropsy.

Table 1. Macroscopic hemorrhagic findings at necropsy on day 56 in a long-term primate model of acquired hemophilia A

Organ/tissue	Site		No. of animals with findings: Vehicle, n = 4	ACE910, n = 3
Joint	Elbow	Left	1	0
		Right	1	0
	Hip	Left	4	0
		Right	1	0
	Ankle	Left	1	0
Skeletal muscle	Lower abdomen		2	0
	Femur		1	0
Urinary bladder	Wall		2	0
Seminal vesicle	Serosa		1	0
Rectum	Serosa		1	0
Skin	Back	Subcutis	1	0

In the other 3 monkeys, plasma ACE910 level remained around the target concentration (30 μg/mL) from day 4 to day 56 (Figure 6), demonstrating that the multiple-dosing simulation worked very well. Anti-ACE910 alloantibodies were examined in plasma collected at necropsy (day 28 for the #4 monkey; day 56 for the other 3 monkeys). In addition to the #4 monkey, 1 other monkey (ACE910 #3) had anti-ACE910 alloantibodies. In this monkey, however, the plasma ACE910 level slightly decreased only after day 49, and remained around 26 μg/mL, a level which is expected to show hemostatic activity.[16]

Regarding the joint bleeding symptoms, no limping and no macroscopic bleeding joints at necropsy were observed in any of the ACE910-treated monkeys, including monkey #4. In the ACE910 group (n = 3; excluding #4 statistically), the number of limping days (Figure 3C) and the number of bleeding joints at necropsy (Figure 3D, Table 1) significantly decreased ($P < .01$, 2-tailed Student *t* test), compared with those of the vehicle group (n = 4). In the ACE910 group, synovial hyperplasia and vascular proliferation in the synovial membranes of joints were histopathologically noted (Figure 4D-F). However, these findings were less severe and less frequent in the ACE910 group than those in the joints with neither macroscopic bleeding nor limping in the vehicle group.

Regarding the other spontaneous bleeding symptoms, bruises (the maximum value of areas and the number of days detected during the observation period) were ameliorated, and no hematuria and no organ bleeds at necropsy were found except for the oral cavity bleeds of the ACE910 #4 monkey (Table 1). Furthermore, monkeys #1 to 3 in the ACE910 group exhibited blood Hgb of 90% or above for 8 weeks (Figure 5). The minimum value of blood Hgb during the observation period was 94.9% ± 4.9% in the ACE910 group (n = 3, excluding monkey #4), which was significantly higher than 75.2% ± 11.3% in the vehicle group (n = 4) ($P < .05$, 2-tailed Student *t* test).

Discussion

Joint damage is one of the most problematic bleeding-related complications in hemophilia A patients. Manco-Johnson et al demonstrated in a prospective clinical study that the progression of joint damage could be decreased by routine alternate-day doses of FVIII from infancy.[4] Although this dosing regimen could render a severe disease (<1% FVIII:C) into a moderate one (1%-5%), its preventive effect on joint bleeds was not perfect,[4,17] and an analysis by den Uijl et al determined that the threshold FVIII:C level required to be free from joint bleeds would be 12%.[18] Our previous study in a primate model of acquired hemophilia A predicted that ≥26 μg/mL ACE910 would exhibit hemostatic activity within the range of the mild phenotype (>5%) and that such a hemostatic level would be maintained by weekly SC doses of 0.64 mg/kg ACE910.[16] Therefore, in the present study, we investigated weekly SC doses of 1 mg/kg ACE910 and demonstrated that such a regimen significantly prevented spontaneous joint bleeding, which also confirmed that the simulation of plasma ACE910 concentrations worked well. Because PK data of therapeutic antibodies from cynomolgus monkeys can be scaled to project human PK profiles,[19,20] a similar PK profile and efficacy are expected for ACE910 in a clinical setting.

In this study, a long-term acquired hemophilia A model was newly established. The FVIII:C in this model was speculated to keep <4% and <3% in the vehicle and ACE910 groups, respectively, according to plasma cyVIII-2236 level and the cyVIII-2236 concentration vs FVIII:C correlation in the pooled cynomolgus monkey plasma (supplemental Figures 2 and 3). In the case of congenital hemophilia A, a small percentage of FVIII:C is considered to render the severity of bleeding; however, in acquired hemophilia A, measured FVIII:C does not necessarily correlate with the severity.[21] Although cyVIII-2236 would not have necessarily decreased FVIII:C in the 1-stage clotting assay to <1% in the monkeys, the control monkeys actually presented severe bleeding symptoms. Thus, we considered that this model was a severe

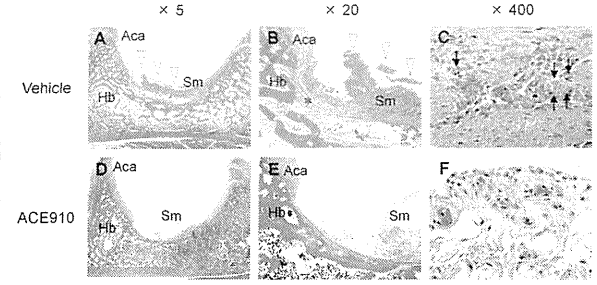

Figure 4. Histopathological findings in a representative joint in a long-term primate model of acquired hemophilia A. Left hip joint with limping in the vehicle #1 monkey (A-C) and left hip joint without limping in the ACE910 #3 monkey (D-F) are shown at original magnification ×5 (A, D), ×20 (B, E), and ×400 (C, F). Hemorrhagic changes (arrowheads) including hemosiderin deposition (arrows) and destruction of articular cartilage/underlying bone (*) are detected in the joint with limping (A-C). No hemorrhagic changes are noted in the joint without limping (D-F). Hematoxylin and eosin stain. Aca, articular cartilage of acetabulum; Hb, hip bone; Sm, synovial membrane.

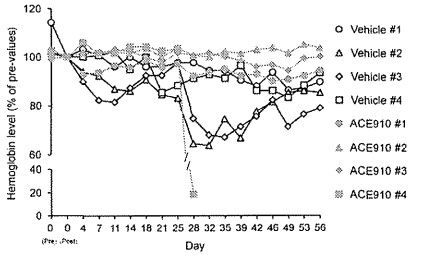

Figure 5. Relative blood Hgb concentrations in a long-term primate model of acquired hemophilia A. The time courses of blood Hgb concentration relative to concentration on day 0 (2 hours after cyVIII-2236 injection) are shown as individual values in respective cynomolgus monkeys (#1-4) of the vehicle and ACE910 groups.

acquired hemophilia A one. In an attempt to further validate this model by looking at reactivity to injected FVIII, we examined the effects of rpoFVIII, which is not neutralized by cyVIII-2236 (data not shown). Aiming to evaluate the marginal level of rpoFVIII efficacy, we administered rpoFVIII for 8 weeks with a twice-weekly 20 U/kg IV dosing regimen, which was set to keep ≥1% rpoFVIII:C for 6 days a week (supplemental Figures 4 and 5A).[22] The prolonged APTT was shortened immediately after the initial rpoFVIII injection (supplemental Figure 5B); however, in 3 of 4 monkeys, the APTT-shortening effect gradually disappeared in the middle of the dosing period, suggesting that anti-rpoFVIII alloantibodies had developed. In terms of bleeding symptoms, the number of days with limping was lower in the rpoFVIII group than in the vehicle group (supplemental Figure 5C); furthermore, the course of blood Hgb tended to worsen when anti-rpoFVIII alloantibodies presumably emerged (supplemental Figure 5D). In the monkey in which rpoFVIII maintained the APTT-shortening effect, limping and decrease in blood Hgb were not observed; nevertheless, 2 bleeding joints were noted by macroscopic observation at necropsy. Although it was difficult to fully evaluate the effect of rpoFVIII because anti-rpoFVIII alloantibodies developed, these results suggest that increasing FVIII activity could ameliorate the bleeding tendency in this model; however, the twice-weekly 20 U/kg IV dosing regimen was not sufficient to fully prevent joint bleeding.

ACE910 and rpoFVIII are proteins foreign to cynomolgus monkeys; therefore, the development of alloantibodies to these is theoretically inevitable.[23] Incidence rates of anti-humanized antibody alloantibodies in cynomolgus monkeys are reported to vary (0%-100%), and antigenicity in cynomolgus monkeys cannot predict that in humans.[19] Although the antigenicity risk score of ACE910 in an in silico T-cell epitope prediction system was comparable to that of trastuzumab and palivizumab, which are nonimmunogenic in a clinical setting,[15] the rate of anti-ACE910 alloantibody development must be evaluated in the actual clinical setting.

In this long-term acquired hemophilia A model, joint damage involving abnormal motion and histopathological features associated with intraarticular hemorrhage were similar to those of hemophilia A patients.[3,24,25] Although a number of animal models have been reported for hemophilia A, it has been difficult to develop reproducible spontaneous joint bleeds.[26-28] The FVIII-deficient mouse model of hemophilia A needs an artificial injuring procedure to induce joint bleeding.[27,29] Although congenital hemophilia A models in dogs, sheep, rats, and pigs have been reported to develop joint bleeds, it seems difficult to express reproducible joint bleeds in individuals and to efficiently evaluate drug efficacy in a practicable experimental period.[28-34] Our model stably developed leg-joint damage within 8 weeks, which was possibly produced by the severe acquired hemophilic state and by bodyweight loading due to the bipedal motion of the monkeys. Thus, this model may be particularly useful in testing the efficacy of therapeutic agents from the orthopedic aspect of hemophilia A. In addition, this primate model should be useful for the many therapeutic antibodies that have poor interspecies cross-reactivity. Moreover, along with our model of hemophilia A, the strategy of using a mouse-host animal chimeric antibody may be beneficial for establishing long-term acquired animal models of other protein-deficiency diseases in the hematology research field.

Although limping and macroscopic intraarticular hemorrhage at necropsy were observed in all 4 control monkeys, joint swelling was noted in only 2 monkeys. Therefore, it was not so reproducible and may be inappropriate for quantitative assessment. The joint swelling was linked to limping in both monkeys. However, in one of the monkeys (vehicle #4), the ankle joint that had swollen did not present macroscopic intraarticular hemorrhage. We assume that the intraarticular hemorrhage may have been absorbed during 2 weeks after the remission of joint swelling.

In this study, although ACE910 completely prevented the macroscopic joint impairment, subclinical histopathological changes in the joint synovium were found, despite the presence of ACE910. We assume that the subclinical or small joint bleeds would occur in this model, and ACE910 prevented them from becoming larger and from leading to clinical symptoms, but did not provide a histopathological complete recovery at around 30 μg/mL of plasma ACE910 concentration. An appropriate clinical investigation will be required to elucidate whether such an action of ACE910 can completely prevent macroscopic and clinical joint damage in the long run.

In conclusion, a long-term acquired hemophilia A model expressing reproducible spontaneous joint bleeds and other bleeds was newly established in cynomolgus monkeys, and weekly SC doses of ACE910 significantly prevented these bleeding symptoms. The difficulty in venous access negatively affects the adoption of and adherence to the routine prophylaxis regimen in home settings.[35]

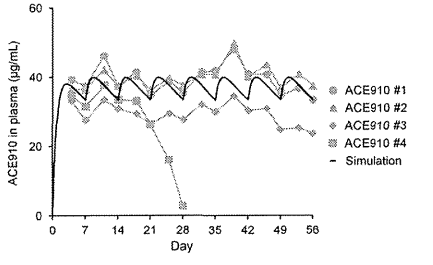

Figure 6. Plasma ACE910 concentrations in a long-term primate model of acquired hemophilia A. ACE910 was administered at an initial SC dose of 3.97 mg/kg on day 0 followed by weekly SC doses of 1 mg/kg on days 7, 14, 21, 28, 35, 42, and 49. The time courses of actual measured and simulated plasma concentrations of ACE910 are shown. The actual measured concentrations are presented as individual values for cynomolgus monkeys (#1-4) of the ACE910 group.

ACE910 is expected to provide hemophilia A patients, regardless of FVIII inhibitors, with a more effective and user-friendly way of bleeding prophylaxis. Clinical investigation of ACE910 is currently ongoing.

Acknowledgments

The authors thank their colleagues at Chugai Pharmaceutical Co, Ltd: T. Matsuura, M. Hiranuma, R. Takemoto, T. Koike, H. Kitamura, and T. Houjo for the in vivo pharmacologic experiments; T. Kojima, T. Wakabayashi, E. Tanaka, K. Esaki, Y. Kikuchi, M. Wada, M. Goto, H. Tsunoda, T. Suzuki, Y. Okuyama-Nishida, A. Harada, M. Funaki, S. Suzuki, T. Toyoda, and M. Ijiri for the preparation of test items and the in vitro experiments; Y. Sakamoto, T. Tachibana, and M. Nanami for the PK studies; and H. Saito for providing advice for the various experiments. The work was carried out at the Research Division, Chugai Pharmaceutical Co, Ltd.

This work was supported by research funding from Chugai Pharmaceutical Co, Ltd.

Authorship

Contribution: A.M., K.Y., M.T., T. Kitazawa, T.S., and Y.K. designed, performed, and analyzed the pharmacologic studies; T.I., Z.S., T. Kuramochi, and A.S. prepared the test items; K. Haraya conducted the PK studies; K.A. conducted the histopathological studies; K.N. and M.S. interpreted data and provided advice from the viewpoints of their medical expertise in hemophilia; K. Hattori provided direction and organized the program; and A.M. and T. Kitazawa wrote this manuscript.

Conflict-of-interest disclosure: A.M., K.Y., T. Kitazawa., T.S., T.I., Z.S., K. Hattori, M.T., T. Kuramochi, A.S., K. Haraya, K.A., and Y.K. are employees of Chugai Pharmaceutical, and the former 7 authors are inventors of the patents relating to anti-FIXa/X bispecific antibodies, of which all rights have been assigned to the company. K.N. and M.S. receive research support paid to their institution from Chugai Pharmaceutical, and have received consulting honoraria from Chugai Pharmaceutical and F. Hoffmann-La Roche.

Correspondence: Atsushi Muto, Research Division, Chugai Pharmaceutical Co, Ltd. 1-135 Komakado, Gotemba, Shizuoka 412-8513, Japan; e-mail: mutoats@chugai-pharm.co.jp.

References

1. Gringeri A, Muça-Perja M, Mangiafico L, von Mackensen S. Pharmacotherapy of haemophilia A. *Expert Opin Biol Ther.* 2011;11(8):1039-1053.
2. Berntorp E, Shapiro AD. Modern haemophilia care. *Lancet.* 2012;379(9824):1447-1456.
3. Roosendaal G, Lafeber FP. Blood-induced joint damage in hemophilia. *Semin Thromb Hemost.* 2003;29(1):37-42.
4. Manco-Johnson MJ, Abshire TC, Shapiro AD, et al. Prophylaxis versus episodic treatment to prevent joint disease in boys with severe hemophilia. *N Engl J Med.* 2007;357(6):535-544.
5. Oldenburg J. Prophylaxis in bleeding disorders. *Thromb Res.* 2011;127(suppl 1):S14-S17.
6. Ragni MV, Fogarty PJ, Josephson NC, Neff AT, Raffini LJ, Kessler CM. Survey of current prophylaxis practices and bleeding characteristics of children with severe haemophilia A in US haemophilia treatment centres. *Haemophilia.* 2012;18(1):63-68.
7. Astermark J, Donfield SM, DiMichele DM, et al; FENOC Study Group. A randomized comparison of bypassing agents in hemophilia complicated by an inhibitor: the FEIBA NovoSeven Comparative (FENOC) Study. *Blood.* 2007;109(2):546-551.
8. Jimenez-Yuste V, Rodriguez-Merchan EC, Alvarez MT, Quintana M, Martin-Salces M, Hernandez-Navarro F. Experiences in the prevention of arthropathy in haemophilia patients with inhibitors. *Haemophilia.* 2008;14(suppl 6): 28-35.
9. Hay CR, DiMichele DM; International Immune Tolerance Study. The principal results of the International Immune Tolerance Study: a randomized dose comparison. *Blood.* 2012; 119(6):1335-1344.
10. Valentino LA, Ismael Y, Grygotis M. Novel drugs to treat hemophilia. *Expert Opin Emerg Drugs.* 2010;15(4):597-613.
11. Lillicrap D. The future of hemostasis management. *Pediatr Blood Cancer.* 2013; 60(suppl 1):S44-S47.
12. Pipe SW. The hope and reality of long-acting hemophilia products. *Am J Hematol.* 2012; 87(suppl 1):S33-S39.
13. Kaufman RJ, Powell JS. Molecular approaches for improved clotting factors for hemophilia. *Blood.* 2013;122(22):3568-3574.
14. Kitazawa T, Igawa T, Sampei Z, et al. A bispecific antibody to factors IXa and X restores factor VIII hemostatic activity in a hemophilia A model. *Nat Med.* 2012;18(10):1570-1574.
15. Sampei Z, Igawa T, Soeda T, et al. Identification and multidimensional optimization of an asymmetric bispecific IgG antibody mimicking the function of factor VIII cofactor activity. *PLoS ONE.* 2013;8(2):e57479.
16. Muto A, Yoshihashi K, Takeda M, et al. Anti-factor IXa/X bispecific antibody (ACE910): hemostatic potency against ongoing bleeds in a hemophilia A model and the possibility of routine supplementation. *J Thromb Haemost.* 2014;12(2):206-213.
17. Collins PW. Personalized prophylaxis. *Haemophilia.* 2012;18(suppl 4):131-135.
18. Den Uijl IE, Mauser Bunschoten EP, Roosendaal G, et al. Clinical severity of haemophilia A: does the classification of the 1950s still stand? *Haemophilia.* 2011;17(6):849-853.
19. Ponce R, Abad L, Amaravadi L, et al. Immunogenicity of biologically-derived therapeutics: assessment and interpretation of nonclinical safety studies. *Regul Toxicol Pharmacol.* 2009;54(2):164-182.
20. Deng R, Iyer S, Theil FP, Mortensen DL, Fielder PJ, Prabhu S. Projecting human pharmacokinetics of therapeutic antibodies from nonclinical data: what have we learned? *MAbs.* 2011;3(1):61-66.
21. Franchini M, Targher G, Montagnana M, Lippi G. Laboratory, clinical and therapeutic aspects of acquired hemophilia A. *Clin Chim Acta.* 2008; 395(1-2):14-18.
22. Srivastava A, Brewer AK, Mauser-Bunschoten EP, et al; Treatment Guidelines Working Group on Behalf of The World Federation Of Hemophilia. Guidelines for the management of hemophilia. *Haemophilia.* 2013;19(1):e1-e47.
23. Dong JQ, Salinger DH, Endres CJ, et al. Quantitative prediction of human pharmacokinetics for monoclonal antibodies: retrospective analysis of monkey as a single species for first-in-human prediction. *Clin Pharmacokinet.* 2011;50(2):131-142.
24. Roosendaal G, Vianen ME, Wenting MJ, et al. Iron deposits and catabolic properties of synovial tissue from patients with haemophilia. *J Bone Joint Surg Br.* 1998;80(3):540-545.
25. Roosendaal G, van Rinsum AC, Vianen ME, van den Berg HM, Lafeber FP, Bijlsma JW. Haemophilic arthropathy resembles degenerative rather than inflammatory joint disease. *Histopathology.* 1999;34(2):144-153.
26. Valentino LA, Hakobyan N, Kazarian T, Jabbar KJ, Jabbar AA. Experimental haemophilic synovitis: rationale and development of a murine model of human factor VIII deficiency. *Haemophilia.* 2004;10(3):280-287.
27. Monahan PE. The expanding menagerie: animal models of hemophilia A. *J Thromb Haemost.* 2010;8(11):2469-2471.
28. Nichols TC, Dillow AM, Franck HW, et al. Protein replacement therapy and gene transfer in canine models of hemophilia A, hemophilia B, von willebrand disease, and factor VII deficiency. *ILAR J.* 2009;50(2):144-167.
29. Hoffman M. Animal models of bleeding and tissue repair. *Haemophilia.* 2008;14(suppl 3):62-67.
30. Nichols TC, Raymer RA, Franck HW, et al. Prevention of spontaneous bleeding in dogs with haemophilia A and haemophilia B. *Haemophilia.* 2010;16(suppl 3):19-23.
31. Porada CD, Sanada C, Long CR, et al. Clinical and molecular characterization of a re-established line of sheep exhibiting hemophilia A. *J Thromb Haemost.* 2010;8(2):276-285.
32. Booth CJ, Brooks MB, Rockwell S, et al. WAG-F8 (m1Ycb) rats harboring a factor VIII gene mutation provide a new animal model for hemophilia A. *J Thromb Haemost.* 2010;8(11):2472-2477.
33. Lozier JN, Nichols TC. Animal models of hemophilia and related bleeding disorders. *Semin Hematol.* 2013;50(2):175-184.
34. Kashiwakura Y, Mimuro J, Onishi A, et al. Porcine model of hemophilia A. *PLoS ONE.* 2012;7(11): e49450.
35. Berntorp E. Joint outcomes in patients with haemophilia: the importance of adherence to preventive regimens. *Haemophilia.* 2009;15(6): 1219-1227.

blood 2014 124: 3165-3171
doi:10.1182/blood-2014-07-585737 originally published online October 1, 2014

Anti-factor IXa/X bispecific antibody ACE910 prevents joint bleeds in a long-term primate model of acquired hemophilia A

Atsushi Muto, Kazutaka Yoshihashi, Minako Takeda, Takehisa Kitazawa, Tetsuhiro Soeda, Tomoyuki Igawa, Zenjiro Sampei, Taichi Kuramochi, Akihisa Sakamoto, Kenta Haraya, Kenji Adachi, Yoshiki Kawabe, Keiji Nogami, Midori Shima and Kunihiro Hattori

Blood (print ISSN 0006-4971, online ISSN 1528-0020), is published weekly by the American Society of Hematology, 2021 L St, NW, Suite 900, Washington DC 20036.

Biochimica et Biophysica Acta 1844 (2014) 1943–1950

Contents lists available at ScienceDirect

Biochimica et Biophysica Acta

journal homepage: www.elsevier.com/locate/bbapap

Review

pH-dependent antigen-binding antibodies as a novel therapeutic modality☆

T. Igawa *, F. Mimoto, K. Hattori

Chugai Pharmaceutical Co. Ltd., Research Division, Japan

ARTICLE INFO

Article history:
Received 31 January 2014
Received in revised form 31 July 2014
Accepted 5 August 2014
Available online 12 August 2014

Keywords:
Monoclonal antibody
Antibody engineering
pH dependent

ABSTRACT

Monoclonal antibodies have become a general modality in therapeutic development. However, even with infinite binding affinity to an antigen, a conventional antibody is limited in that it can bind to the antigen only once, and this results in antigen-mediated antibody clearance when the a membrane-bound antigen is targeted, or in antibody-mediated antigen accumulation when a soluble antigen is targeted. Recently, a pH-dependent antigen-binding antibody that binds to an antigen in plasma at neutral pH and dissociates from the antigen in endosome at acidic pH has been reported to overcome this limitation and to reduce antigen-mediated antibody clearance and antibody-mediated antigen accumulation. A pH-dependent binding antibody against a soluble antigen can be further improved by Fc engineering to enhance the Fc receptor binding. Various approaches, including histidine-based engineering, direct cloning from immunized animals, and synthetic and combinatorial libraries, have been successfully applied to generate pH-dependent binding antibodies against various antigens. This review discusses the features, approaches, advantages, and challenges of developing a pH-dependent binding antibody as a novel therapeutic modality. This article is part of a Special Issue entitled: Recent advances in molecular engineering of antibody.

1. Introduction

With more than 30 monoclonal antibodies already approved for therapeutic use [1] and more than 300 under clinical development [2], monoclonal antibodies are clearly expected to play an important role in future therapeutics. Therefore, antibody engineering technologies that improve the therapeutic potency of monoclonal antibodies have been extensively studied in this decade. Such technologies include improving the binding affinity to a target, the specificity, the pharmacokinetics, and the effector function mediated by the Fc region of an antibody. Binding affinity can be improved by several methods, such as *in vitro* affinity maturation by library display [3] and computer-based *in silico* design [4]. For pharmacokinetics, lowering the isoelectric point of the variable region of an antibody is reported to prolong the antibody half-life by reducing the non-specific clearance of the antibody [5]. Fc engineering to enhance the binding affinity to FcRn at acidic pH also improves pharmacokinetics by increasing the recycling efficiency from the endosomes after non-specific uptake into cells [6]. Modulation of the antibody effector function by optimizing the interaction between the Fc region and an Fc gamma receptor is reported to improve the therapeutic efficacy of a monoclonal antibody [7]. Another noteworthy technology that has recently been reported provides bispecific antibodies with a unique function that conventional monoclonal antibodies cannot achieve; they can neutralize two different disease-related cytokines [8]. In addition, bispecific antibodies can also redirect cytotoxic T cells to cancer cells by binding to CD3 and a tumor antigen [9], and they can mimic the function of coagulation factor VIII by binding to coagulation factor IXa and X [10].

Although these technologies have bestowed improved potency on therapeutic antibodies, it is now becoming more important to generate monoclonal antibodies that have further improved properties and are differentiated from conventional high-affinity monoclonal antibodies. In terms of modulating the interaction between an antigen and an antibody, achieving a high affinity binding to the antigen by affinity maturation has been the only approach for improvement. However, even with an infinite binding affinity to the antigen, a conventional antibody can bind to the antigen only once during its lifetime in plasma, and it is fundamentally limited by its consequent inability to neutralize further antigens, if the *in vivo* produced molar amount of antigen is larger than the amount of antibody injected.

If an antibody is targeting a membrane-bound antigen with a high rate of synthesis, such as IL-6 receptor (IL-6R), EGFR, CD4, or CD40 [11–14], the antibody is rapidly eliminated from plasma through antigen-mediated clearance. As a result, targeting these types of membrane antigen cannot be improved by affinity maturation and requires a high dose. Similarly, a high antibody dose is also required to neutralize soluble antigen at a high plasma concentration. The plasma

☆ This article is part of a Special Issue entitled: Recent advances in molecular engineering of antibody.

* Corresponding author. Tel.: +81 550 87 3029; fax: +81 550 87 5326.
E-mail address: igawatmy@chugai-pharm.co.jp (T. Igawa).

http://dx.doi.org/10.1016/j.bbapap.2014.08.003
1570-9639/

concentration of soluble antigen after antibody administration is determined by two factors: the baseline concentration and the antibody-mediated antigen accumulation. Some soluble antigens, such as IgE and C5, have a plasma baseline concentration that is already very high [15,16]; other soluble antigens without a high baseline concentration in plasma accumulate more than 1000-fold because the recycling function of an antibody inhibits degradation of the antigen and results in a very high concentration [17]. This accumulation after antibody administration occurs because an antigen in complex with an antibody has a longer half-life than the antigen alone [18,19]. The resulting high plasma antigen concentration requires a high antibody dose to neutralize the antigen. For both membrane-bound and soluble antigens, the limitation of conventional antibodies in only binding to the antigen once, even when the binding affinity is infinite, requires a high antibody dose.

Recently, we and others have reported that a pH-dependent antigen-binding property could overcome this limitation of conventional antibodies [20–22]. An antibody with a pH-dependent antigen-binding property dissociates the bound antigen in acidic endosomes after internalization into cells. Consequently, the dissociated antigen is trafficked to the lysosome and degraded, whereas the dissociated antibody, free of antigen, is recycled back to plasma by FcRn. The recycled free antibody can bind to another target antigen. By repeating this cycle, *a pH-dependent antigen-binding antibody can bind to the target* molecule more than once. Moreover, we have shown that the therapeutic potency of a pH-dependent antigen-binding antibody can be further enhanced by increasing its binding affinity to FcRn at neutral pH [23]. These studies demonstrate that pH-dependent antigen-binding antibodies can overcome the limitation of conventional antibodies and allow novel antibody therapeutics with differentiating properties to be generated. In this review, the features, advantages, and challenges of pH-dependent antigen-binding antibodies, and how they can be generated and optimized are discussed.

2. Effect of a pH-dependent antigen-binding antibody

2.1. Against a membrane-bound antigen

Fig. 1A describes the fate of a conventional antibody bound to a membrane-bound antigen. A conventional antibody bound to the cell surface antigen is internalized into cells, after which the antibody–antigen complex passes through the sorting endosome and is transferred to a lysosome, where eventually both the antibody and antigen are degraded by proteolysis. This means that, even with infinite binding affinity to the antigen, a conventional antibody is limited to binding to an antigen only once. Conventional antibodies against membrane-bound antigens, such as IL-6R, EGFR, CD4, and CD40, exhibit non-linear clearance *in vivo* through antigen-mediated antibody clearance [11–14]. When a membrane-bound antigen is highly expressed in the body, the antibody is rapidly cleared from plasma, thereby requiring a high dose to neutralize this type of antigen over a long period.

Fig. 1B describes the fate of a pH-dependent antigen-binding antibody, which we also refer to as a recycling antibody, bound to a membrane-bound antigen. The recycling antibody bound to the cell surface antigen is internalized into the cells in the same way as a conventional antibody. However, in the sorting endosome, where the pH of the vesicle is acidic, the pH-dependent binding antibody is dissociated from the antigen. The antigen is transferred to the lysosome and degraded by proteolysis, while the dissociated antibody binds to FcRn in the endosome and is recycled back to the cell surface. Since FcRn does not bind to the antibody at neutral pH, the antibody dissociates from FcRn at the cell surface and returns back to plasma. A recycling antibody exhibits less non-linear antigen-mediated antibody clearance *in vivo* than conventional antibody and shows prolonged pharmacokinetics by avoiding antigen-mediated clearance. By repeating this cycle of binding at the cell surface and dissociating within the endosomes, a recycling *antibody can bind to multiple antigens and overcomes the limitation of* a conventional antibody.

The effect of a recycling antibody on a membrane-bound antigen was first demonstrated by our group using a monoclonal antibody against IL-6R [20]. A conventional antibody against IL-6R, tocilizumab, was engineered by a histidine mutagenesis approach (details described in section 4-1) to generate a pH-dependent binding antibody against IL-6R, named recycling tocilizumab. Importantly, tocilizumab and recycling tocilizumab have similar binding affinity to IL-6R at pH 7.4, while only recycling tocilizumab rapidly dissociates IL-6R at pH 6.0, allowing us to evaluate only the effect of pH-dependent antigen dissociation in the acidic endosomes. In a pharmacokinetic study in human IL-6R transgenic mice, the pharmacokinetics of recycling tocilizumab was better than that of tocilizumab, while in normal mice (whose IL-6R neither of the antibodies can bind) the pharmacokinetics of the two antibodies were similar, demonstrating that engineering the pH dependency reduced IL-6R-mediated clearance but did not influence non-specific clearance. By using a FcRn null variant of each antibody, we confirmed that the reduced IL-6R-mediated clearance by recycling tocilizumab was dependent on FcRn binding, indicating that recycling tocilizumab dissociated within the endosomes and

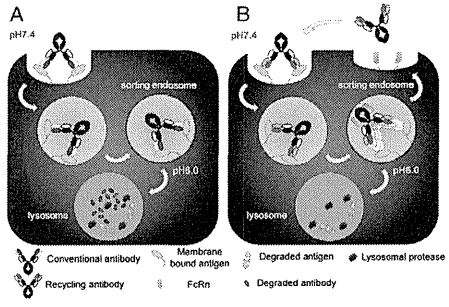

Fig. 1. Models showing the fate of (A) a conventional antibody and (B) a recycling antibody bound to a membrane-bound antigen. (A) A conventional antibody bound to a membrane-bound antigen is internalized into the cell, after which the antibody–antigen complex is trafficked to the sorting endosome and finally to lysosome, where eventually both the antibody and antigen are degraded by lysosomal protease. (B) A recycling antibody bound to a membrane-bound antigen is internalized into the cell in the same way as a conventional antibody. However, in the sorting endosome, where the pH of the vesicle is acidic, the recycling antibody is dissociated from the antigen by means of its pH-dependent antigen-binding property. The antigen is transferred to the lysosome and degraded by proteolysis, while the dissociated antibody is recycled back to the cell surface and plasma by utilizing FcRn.

was recycled back to plasma by FcRn (unpublished data). Chaparro-Riggers *et al.* also showed that FcRn is indispensable for a pH-dependent anti-PCSK9 antibody to be rescued from antigen-mediated clearance [21]. This was demonstrated by the fact that the half-life of the pH-dependent anti-PCSK9 antibody was the same as that of an antibody without pH-dependent binding (0.7 days) in FcRn knockout mice, while in wild-type mice, that of the pH-dependent antibody (14.4 days) was significantly longer than that of the antibody without pH-dependent binding (2.9 days).

A further engineered version of recycling tocilizumab, named SA237, which has a pH-dependent antigen-binding property and enhanced FcRn binding, demonstrated improved pharmacokinetics in cynomolgus monkeys compared to tocilizumab [20]. Whereas a subcutaneous injection of 2 mg/kg of tocilizumab inhibited C-reactive protein production for approximately 10 days, 2 mg/kg of SA237 was effective for more than 28 days. A Phase 1 clinical study of SA237 demonstrated significantly prolonged pharmacokinetics compared to tocilizumab, similar to that observed in cynomolgus monkeys (unpublished data). This study result clinically validated the concept of pH-dependent antigen-binding recycling antibodies.

2.2. Against a soluble antigen

Fig. 2A describes the fate of a conventional antibody bound to a soluble antigen. The conventional antibody bound to the soluble antigen in plasma is taken up into cells by non-specific endocytosis or pinocytosis. The antibody–antigen complex is transferred to a sorting endosome and binds to FcRn at acidic pH. FcRn recycles the antibody–antigen complex to the cell surface, where the complex is dissociated from FcRn back to plasma. Although the antibody is recycled, it is recycled in an antigen-bound form; therefore, the antibody cannot bind to the next antigen. This also limits a conventional antibody to binding only one soluble antigen, just as with a membrane-bound antigen. A soluble antigen in the absence of a conventional antibody is generally transferred to a lysosome and degraded, since most target antigens do not bind to FcRn (only IgG and albumin bind to FcRn). By binding to the soluble antigen, a conventional antibody inhibits the lysosomal degradation pathway of the soluble antigen. Thus, a conventional antibody against a soluble antigen *in vivo* generally results in an increase of total plasma antigen concentration or an accumulation of soluble antigen in plasma, an effect that has been reported for IL-6, MCP1, amyloid beta, hepcidin, and other soluble antigens [17,24–28]. When a soluble antigen is abundant in the body, antigen accumulation results in the antigen binding sites of the antibodies becoming rapidly saturated, and free antibodies that are capable of binding to the antigens is lost.

Fig. 2B describes the fate of a recycling antibody bound to a soluble antigen. The antibody–antigen complex formed by the recycling antibody is also non-specifically taken up into cells in the same way as a conventional antibody. However, within the sorting endosome, the antibody pH-dependently dissociates from the soluble antigen, which is transferred to the lysosome and degraded by proteolysis. On the other hand, the free antibody is recycled back to plasma by FcRn. By repeating this cycle of binding in plasma and dissociating within the endosome, recycling antibodies against soluble antigens can also bind to multiple antigens and overcome the limitation of conventional antibodies. Since an antigen that forms a complex with a recycling antibody is degraded in the lysosome, recycling antibodies can degrade soluble antigens at the rate of non-specific uptake of the antibody–antigen complexes, and thus degrade the antigens more effectively than conventional antibodies. A recycling antibody exhibits reduced plasma antigen accumulation *in vivo* by enhancing soluble antigen clearance, and extends the half-life of the free antibodies.

The effect of a recycling antibody on a soluble antigen was also first demonstrated by the same monoclonal antibodies against IL-6R described above. *Soluble IL-6R (sIL-6R) clearance was compared in normal* mice that received sIL-6R alone, tocilizumab with sIL-6R, or recycling tocilizumab with sIL-6R. While sIL-6R alone was rapidly cleared from plasma, sIL-6R injected together with tocilizumab showed reduced clearance because it was bound to tocilizumab, which has a long half-life. In contrast, sIL-6R injected together with recycling tocilizumab showed accelerated sIL-6R clearance [20]. This antibody–antigen co-injection study can be generally applied to evaluate whether the clearance of a soluble antigen can be accelerated by pH-dependent antigen binding. However, this study does not mimic the clinical situation, where an antibody is injected to plasma at a steady-state soluble antigen concentration. To mimic the clinical situation, mice were implanted with an infusion pump filled with sIL-6R that continuously provided sIL-6R into plasma and maintained a steady-state sIL-6R concentration. In this model, an injection of tocilizumab resulted in approximately 20-fold increase of total plasma sIL-6R concentration, while recycling tocilizumab significantly reduced the accumulation and resulted in only a 2-fold increase of total plasma sIL-6R concentration [23].

Chaparro-Riggers *et al.* reported using a pH-dependent binding antibody against PCSK9 [21]. PCSK9 is a soluble antigen responsible for

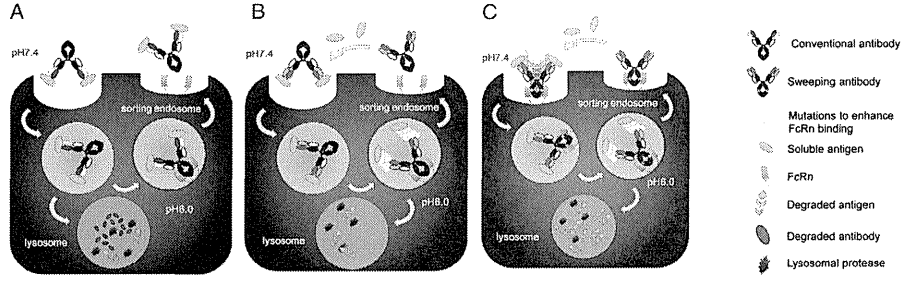

Fig. 2. Models showing the fate of (A) a conventional antibody, (B) a recycling antibody and (C) a sweeping antibody bound to a soluble antigen. (A) A conventional antibody bound to a soluble antigen in plasma is taken up into cells by non-specific endocytosis or pinocytosis. The antibody–antigen complex is transferred to a sorting endosome, where it binds to FcRn at acidic pH and is recycled back to the cell surface and plasma by utilizing FcRn. Although the antibody is recycled, it is recycled in an antigen-bound form; therefore, the antibody cannot bind to the next antigen. (B) A recycling antibody bound to a soluble antigen in plasma is taken up into cells in the same way as a conventional antibody. However, within the sorting endosome, the recycling antibody dissociates the soluble antigen by utilizing its pH-dependent antigen-binding property. The dissociated antigen is transferred to a lysosome and degraded by lysosomal protease. On the other hand, the free antibody is recycled back to plasma by FcRn. (C) A sweeping antibody with enhanced FcRn binding at neutral pH binds to a soluble antigen, and the antibody–antigen complex is rapidly taken up into the cell in a FcRn-mediated manner. By accelerating the uptake of antibody–antigen complexes into cells, a sweeping antibody can degrade a larger amount of soluble antigen than a recycling antibody.

enhancing the degradation of LDL receptors. Inhibition of PCSK9 inhibits LDL receptor degradation and thereby reduces the LDL cholesterol level in plasma. A conventional antibody against PCSK9, J10, showed non-linear clearance in cynomolgus monkeys, which was presumably caused by an accelerated clearance of PCSK9–antibody complexes via an unknown pathway. To overcome the relatively short pharmacokinetics of J10 at low dosages, J17, a histidine-engineered version of J10 with a pH-dependent PCSK9-binding property, was generated. J17 demonstrated significantly improved pharmacokinetics compared to J10 in cynomolgus monkeys, and the LDL cholesterol-lowering effect was longer than that of J10 at the same dose. In the microscopic assay using HepG2 cells, J10 was more efficiently trafficked to lysosomes than J17 when co-incubated with PCSK9, while the trafficking of PCSK9 to lysosomes was comparable in the presence of J10 and J17. The authors demonstrated that a PCSK9-bound antibody shows accelerated lysosomal degradation by an unknown pathway, and this degradation can be avoided by a pH-dependent binding antibody that dissociates from PCSK9 in the endosomes. This study also confirmed the favorable effect of pH-dependent binding against a soluble antigen. Recently, Devanaboyina *et al.* reported a pH-dependent binding antibody against IL-6. In a mouse co-injection study, a conventional antibody against IL-6, clone 0218, significantly reduced the clearance of IL-6, while the pH-dependent binding antibody derived from clone 0218, VH4, accelerated the clearance of IL-6 from plasma [22]. In a microscopic assay using GFP-fused human FcRn variant-transfected HMEC-1 cells, they demonstrated that the conventional antibody against IL-6, clone 0218, colocalized with IL-6 in early endosomes, while the pH-dependent binding antibody, clone VH4, dissociated IL-6 in the early endosomes, and the dissociated IL-6 was subsequently trafficked to lysosomes.

These studies clearly demonstrated that recycling antibody against soluble antigen generally clears soluble antigen faster than conventional antibody and reduces antigen accumulation in plasma. Because administering recycling antibody reduces the total soluble antigen concentration compared with conventional antibody, the antibody dose required to neutralize the soluble antigen can be reduced.

3. Improving a recycling antibody against soluble antigens into a sweeping antibody by Fc engineering

A recycling antibody, with the capability of dissociating soluble antigens in the endosomes, can accelerate the clearance of the soluble antigens from plasma. However, the rate of antigen clearance by a recycling antibody is limited by the slow rate of non-specific uptake of antibody–antigen complexes into cells, so further enhancing the rate of soluble antigen degradation would be very beneficial. To further enhance the clearance of soluble antigens from plasma, we have recently developed a sweeping antibody, which is an Fc-engineered pH-dependent binding antibody [23]. Since uptake of antibody–antigen complexes was the rate-limiting step for antigen degradation, we engineered the Fc region of a pH-dependent antigen-binding antibody to increase the binding affinity to FcRn at neutral pH (wild-type IgG1 just marginally binds to FcRn at pH 7.4). This sweeping antibody, a pH-dependent binding antibody with engineered IgG1, can bind to FcRn at neutral pH on the cell surface, which causes antibody–antigen complexes to be rapidly taken up into the cells in an FcRn-mediated manner and, therefore, degrades more soluble antigens than a recycling antibody (Fig. 2C).

By moderately increasing the binding affinity to FcRn at neutral pH, an *in vivo* study using human FcRn transgenic mice demonstrated that the clearance of soluble antigens can be accelerated approximately 50-fold while the antibody maintains pharmacokinetics similar to a conventional antibody with wild-type IgG1 (Fig. 3). It is important to note that the antigen clearance, not the antibody clearance, was selectively enhanced by simultaneously engineering the pH-dependent antigen binding and moderately increasing the binding affinity to FcRn at neutral pH. For their microscopic assay, Devanaboyina *et al.* used human/mouse chimeric FcRn, which has increased affinity to wild-type human IgG1. In the assay, they reported that, while a soluble antigen remained bound to a non-pH dependent binding antibody in the sorting endosomes, the antigen was dissociated from the pH-dependent binding antibody, and the dissociated antigen was finally transferred to lysosomes [22]. This result also suggests that both pH-dependent antigen binding and enhanced FcRn binding are required to increase antigen uptake into cells. We also observed the same phenomenon in our *in vitro* confocal microscopy assay using the human FcRn–transfected MDCK cell line. While a soluble antigen remained bound to a non-pH-dependent binding antibody in the sorting endosome (Fig. 4A), the soluble antigen was dissociated from a pH-dependent binding antibody with engineered IgG1 and enhanced FcRn binding (Fig. 4B).

It should be noted that previous Fc engineering to increase the binding affinity to FcRn at acidic pH aimed to improve antibody pharmacokinetics by increasing FcRn-mediated IgG recycling [29]. On the other hand, we engineered a pH-dependent antigen-binding antibody to moderately increase its binding affinity at neutral pH to generate a sweeping antibody, which selectively enhanced the clearance of the antigen while maintaining antibody pharmacokinetics similar to wild-type IgG1 (Fig. 3). However, consistent with the report from Vaccaro *et al.* in which they reported that engineering the Fc region of IgG1 to create a strong binding to FcRn at neutral pH modulated *in vivo* concentration of endogenous IgG antibodies [30], a sweeping antibody with strongly increased binding affinity to FcRn at neutral pH resulted in increased antibody clearance, although antigen clearance was more accelerated than that of a sweeping antibody with moderately increased binding affinity to FcRn at neutral pH [23]. An appropriate level of binding affinity to FcRn at neutral pH should be selected, depending on the characteristics of the target soluble antigen.

An alternative approach for enhancing the uptake of antibody–antigen complexes into cells is utilizing uptake mediated by Fc gamma receptor, which has been reported elsewhere as contributing to the clearance of antibody–antigen immune complexes *in vivo* [31]. Especially, the clearance of small immune complexes is dominantly supported by Fc gamma receptor IIb (or CD32b) expressed on liver sinusoidal endothelial cells [32]. Because Fc gamma receptor IIb is reported to be a recycling receptor, enhancing the binding affinity to this receptor could have a similar effect to that observed when the binding affinity to FcRn at neutral pH was enhanced [33]. Previously reported Fc engineering to enhance binding affinity to Fc gamma receptor IIb also enhanced the binding affinity to Fc gamma receptor IIa (or CD32a) with arginine 131 allotype, which represents approximately 70% of the Caucasian population [34]. However, since Fc gamma receptor IIa is not a recycling receptor and is expressed on platelets, enhancing the binding affinity also to Fc gamma receptor IIa could have both pharmacokinetic and safety issues. Recently, we have reported a novel engineered Fc variant that selectively enhances binding to Fc gamma receptor IIb over both the histidine and arginine 131 allotypes of Fc gamma receptor IIa [35]. By combining pH-dependent antigen binding with this novel Fc engineering, we may be able to accelerate the antigen clearance and degrade more soluble antigen than with a recycling antibody.

4. Approaches for generating recycling antibodies

4.1. Experimental approaches

Previously, monoclonal antibodies generated by either animal immunization or *in vitro* antibody library display technology have been selected based on their strong binding affinity to their target antigens at neutral pH and their binding to a functionally appropriate epitope. Therefore, the monoclonal antibodies obtained in such a way seldom had a pH-dependent antigen-binding property. Although most antibodies lose their binding affinity to the antigen at pH 3.0, they do not show

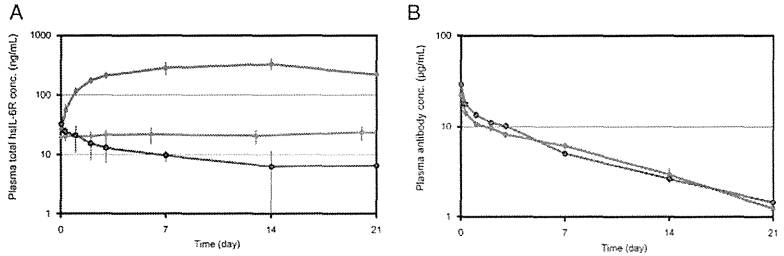

Fig. 3. The effect of a conventional antibody and a sweeping antibody against a soluble antigen in human FcRn transgenic mice. (A) shows the time course of plasma concentration of total soluble antigen, hsIL-6R, after antibodies were administered. (B) shows the plasma antibody concentration. Blue lines indicate a conventional antibody, red lines a sweeping antibody (pH-dependent antigen-binding antibody with enhanced FcRn binding), and gray lines the baseline of the soluble antigen.

rapid enough dissociation of antigens at pH 5.5–6.0 in a sorting endosome.

In our first report of a pH-dependent binding antibody [20], we engineered a conventional antibody against IL-6R, tocilizumab, into a pH-dependent binding antibody, which was identified by mice immunization and subsequent screening of the binding affinity and IL-6–binding neutralizing capability [36]. We took advantage of a natural amino acid, histidine, which has pKa of around 6 (depending on the surrounding environment) and is utilized in naturally occurring pH-dependent protein-protein interactions [37]. We introduced several histidine residues in the CDR or FR of tocilizumab by site-directed mutagenesis. Because of the pKa of the imidazole group, histidine residues are protonated at endosomal acidic pH, which results in destabilizing the antibody–antigen interaction either directly, with histidine residues involved in interacting with the antigen, or indirectly, with histidine residues involved in maintaining the conformation of the CDRs. A crystal structure of tocilizumab Fab fragment in complex with IL-6R suggested that a mutation of the tyrosine residue in the CDR of tocilizumab, which interacts with an arginine residue, into a histidine residue resulted in electrostatic repulsion between the arginine and the protonated histidine residue at acidic pH (unpublished data). A total of three histidine residues and several other mutations were introduced into tocilizumab to compensate for the reduced affinity at neutral pH or to improve its physiochemical properties, and finally histidine-based engineered tocilizumab that rapidly dissociates from IL-6R at pH 6.0 was generated, as we previously reported [20]. The kinetic parameters of tocilizumab and the histidine-based engineered antibody are described in Table 1.

We have applied the same histidine-based engineering approach to several other antibodies against different antigens, and in all cases we have successfully conferred a pH-dependent antigen-binding property. However, in some cases, although introducing histidine(s) in the

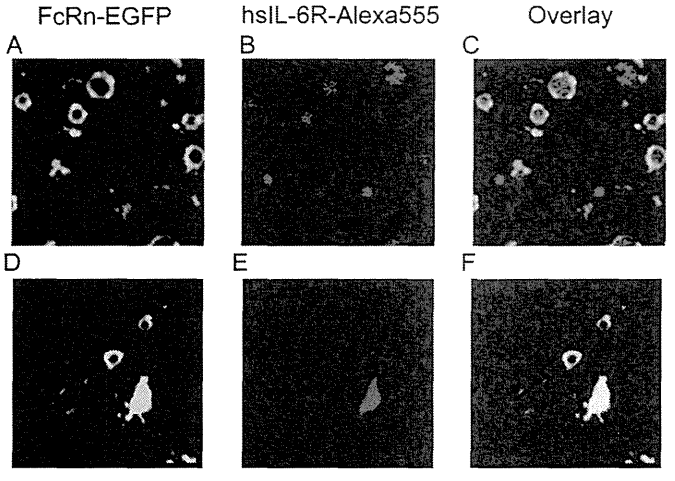

Fig. 4. The intracellular trafficking of an antigen in complex with either a conventional antibody or a pH-dependent antigen-binding antibody in MDCK transfected with human FcRn-EGFP (in green) and beta-2-microglobulin. (A–C) are images of representative endosomes after a pH-dependent antibody with enhanced FcRn binding was incubated in complex with its target antigen, hsIL-6R, which was labeled with Alexa-555 (in red). (D–F) are images of representative endosomes after a conventional antibody with enhanced FcRn binding was incubated in complex with hsIL-6R. (A) and (D) are images of FcRn-EGFP. (B) and (E) are images of hsIL-6R-Alexa555. (C) and (F) are overlays of the FcRn and hsIL-6R images. These are unpublished data.

appropriate position can provide pH dependency (i.e. reduction of the binding affinity at acidic pH), it simultaneously reduces the binding affinity to the antigen at neutral pH to some extent (but less than that at acidic pH). Although such an antibody would elicit a recycling property, the loss of binding affinity at neutral pH would reduce the biological activity of the antibody in plasma. If the biological activity does not meet the therapeutic goal, the binding affinity at neutral pH needs to be improved by the affinity maturation process.

Following our report, Chaparro-Riggers *et al.* reported their pH-dependent binding antibody against PCSK9, which was also generated through histidine-based engineering of the parent antibody [21]. Moreover, Devanaboyina *et al.* recently reported generating a pH-dependent binding antibody against IL-6 in the same way [22]. Changing a single aspartic acid to a histidine residue in HCDR3 conferred pH-dependent binding on IL-6, but the binding affinity to IL-6 at neutral pH was slightly reduced. Other histidine mutations tested in this report either did not display an increased pH dependency or resulted in a substantial loss of the binding affinity at neutral pH.

These reports verify that histidine-based engineering is a general approach for generating pH-dependent binding antibodies that demonstrate a recycling property. However, in some cases, a simultaneous loss of binding affinity at neutral pH may occur. Since the binding affinity at *neutral pH is important for the biological activity of the antibody*, this loss of binding affinity at neutral pH may need to be recovered by subsequent affinity maturation (discussed further in section 6).

The second approach for generating a pH-dependent binding antibody is to isolate the antibody directly from immunized animals. Our trial to screen a large number of antigen-binding antibodies suggested the feasibility of directly isolating rare pH-dependent antigen-binding antibodies (generally less than 5% of the binders) from immunized animals by using direct B cell-cloning technology, which allows antigen-binding antibodies to be identified more efficiently than conventional mouse hybridoma technology [38].

The third approach for generating a pH-dependent binding antibody is to isolate the antibody directly from a synthetic antibody phage library. Since histidine is rarely used in the CDR of human antibodies (0.5%–0.6%), the possibility of directly isolating a pH-dependent binding antibody from naïve or synthetic antibody libraries that mimic the human repertoire is low. Therefore, a library of synthetic antibodies that use more histidine in the CDR in combination with pH-dependent antigen panning (antigen binding at neutral pH and elution at acidic pH) can be used to directly isolate a pH-dependent antigen-binding antibody.

The fourth approach is to use a combinatorial antibody library to generate a pH-dependent binding antibody from a conventional antibody. Murtaugh *et al.* described a combinatorial histidine scanning library approach to engineer a conventional antibody into a pH-dependent binding antibody [39]. In their study, a VHH antibody against RNase A was used as a model antibody, and a combinatorial library was constructed that consisted of combinations of histidine and wild-type residues in the antibody–antigen interface. Antibodies displayed on phages were coselected for high-affinity binding and pH-dependent binding, which resulted in generating pH-dependent VHH antibody against RNase A. Although there was a slight loss in the binding affinity at neutral pH, this approach may be an efficient way to generate a pH-dependent binding antibody from a conventional antibody. Although a histidine-based pH-dependent binding antibody is a promising type of recycling antibody, we are exploring an alternative approach to designing an antibody that dissociates the antigen within sorting endosomes. While the recycling antibodies discussed above take advantage of the pH difference between plasma and endosomes, another environmental difference between plasma and endosomes is calcium ion concentration. Calcium ion concentration in plasma is reported to be 1.2–2 mM in plasma which drops to 3–30 μM in endosomes after endocytosis [40]. Therefore, a calcium ion-dependent binding antibody, which binds to the antigen at the calcium ion concentration in plasma and dissociates the antigen at the calcium ion concentration in endosomes, may be used to generate a recycling antibody.

4.2. Computational approaches

Significant progress has been achieved in the field of computational approaches that design functional proteins, so identifying a pH-dependent antigen-binding antibody by computational design could be an alternative approach. However, although computational design has already been applied to improve antibody–antigen interaction [4] and to generate pH-dependent binding proteins [41,42], there is no report to date of successfully designing a pH-dependent antigen-binding antibody. Strauch *et al.* computationally designed a *pH-dependent protein that binds to the Fc region by utilizing* histidine residues in the Fc region [41]. Sarkar *et al.* designed a pH-dependent granulocyte colony-stimulating factor (GCSF) that maintained the affinity to its receptor at neutral pH. To do this, they computationally identified negatively charged residues in the interface of GCSF and the GCSF receptor (GCSFR). If these negatively charged residues are replaced with histidine residues, the GCSFR binding affinity at neutral pH is expected to stay the same but the binding affinity at acidic pH will be reduced. They selected residues to mutate into histidine by comparing the free energy values at neutral and acidic pH of each histidine-mutated GCSF in complex with GCSFR [42]. A similar approach could be applied to provide antibodies with a pH-dependent antigen-binding property.

5. Advantages of pH-dependent antigen-binding antibodies and potential applications

pH-dependent antigen-binding antibodies have an advantage over conventional antibodies, especially when the target molecules are membrane-bound antigens or soluble antigens abundantly present in the body. Antibodies targeting these antigens require either a high dose that cannot be injected subcutaneously or frequent dosing, both of which are not patient-friendly, especially in chronic diseases.

When an antibody targets an antigen that is both membrane-bound and has a high rate of synthesis, such as IL-6R, EGFR, CD4, or CD40, the antibody is rapidly eliminated from plasma through antigen-mediated clearance [11–14]. In the case of tocilizumab, which targets IL-6R, neither improving the binding affinity to IL-6R nor reducing the non-specific clearance by increasing the binding affinity to FcRn at acidic pH significantly improved the duration of IL-6R neutralization *in vivo* [23]. This is because an antibody that targets IL-6R is mainly cleared from plasma by IL-6R-mediated clearance. Modeling and simulation suggested that the molar amount of IL-6R produced in the body within approximately 18 days is the same as 2 mg/kg of antibody. Since a conventional antibody can bind to the antigen only once, it is evident that, even if a conventional antibody has infinite binding affinity to IL-6R or very low non-specific clearance, a 2 mg/kg dose cannot be effective for more than 18 days. A pH-dependent binding antibody against IL-6R (SA237) that is recycled back to plasma after IL-6R-mediated uptake into cells, can bind to IL-6R multiple times, which allows 2 mg/kg of SA237 to remain effective for more than one month. Importantly, because the amount of an antibody that can be administered in a single subcutaneous injection is limited (generally 1 mL of 150 mg/mL IgG formulation), a pH-dependent binding antibody would be the only way to achieve monthly subcutaneous dosing for an antibody that targets IL-6R. The same strategy can be applied to other antibodies targeting membrane-bound antigens that are rapidly eliminated from plasma through antigen-mediated clearance.

An antibody that targets a soluble antigen with a high baseline plasma concentration, such as IgE or C5, would also require a high dose to neutralize the antigen [15,16]. To use omalizumab, an anti-IgE antibody, in patients with high plasma IgE concentration, subcutaneous injections at two or three sites are required, because plasma IgE concentration (in the range of sub μg/mL) is higher than the concentration of most cytokines (generally in the range of pg/mL) [16]. Similarly, eculizumab, an anti-complement C5 antibody, requires intravenous infusion, because plasma C5 concentration is reported to be 70–140 μg/mL [15]. Although *eculizumab requires chronic dosing, such a large amount of antigen can*not be neutralized by a subcutaneous dose. Administering an antibody against a soluble antigen with rapid clearance, such as amyloid beta, MCP1, hepcidin, IL-6, CD23, or VEGF, results in more than 1000-fold increase of plasma antigen concentration from the baseline by the antigen accumulation effect [17,24–28]. Notably, administering an anti-hepcidin antibody resulted in an accumulation of hepcidin by approximately 5000-fold, which required a 300 mg/kg dose to neutralize hepcidin, despite its picomolar binding affinity [17]. Since soluble antigens with a molecular weight below 60,000 g/L are generally very rapidly eliminated through renal excretion [43], an antibody targeting a soluble antigen with a small molecular weight would suffer from the same issue. Taken together, conventional antibodies targeting soluble antigens with a high baseline concentration and/or a large antigen-accumulation effect require a high dose. Since conventional antibodies can bind to antigens only once and cannot accelerate the antigen clearance, pH-dependent binding antibodies would provide a significant advantage over conventional antibodies against these soluble antigens. pH-dependent binding antibodies would enable subcutaneous dosing or less frequent dosing that cannot be achieved by simple high-affinity conventional antibodies with a long half-life.

Recycling antibodies can be engineered into sweeping antibodies by Fc engineering to enhance the binding to Fc gamma receptor or FcRn. The use of a sweeping antibody against a soluble antigen further reduces the dosage compared to a recycling antibody, providing another advantage over a conventional antibody. Moreover, since a sweeping antibody can actively eliminate the target soluble antigen from plasma, a sweeping antibody against soluble IL-6R that targeted a non-neutralizing epitope and showed no neutralizing activity *in vitro* was able to antagonize the activity of soluble IL-6R *in vivo* by directly removing soluble IL-6R from plasma [23]. Therefore, a sweeping antibody can target a soluble ligand with multiple target epitopes, through which the ligand binds to different receptors that cannot be neutralized by a single monoclonal antibody. Administering a conventional antibody may neutralize the binding of a ligand to its receptor through one epitope, but another epitope remains. In addition, the increase of antibody–antigen complexes in plasma may allow increased signaling to the second receptor through the epitope that is not neutralized. The sweeping antibody, on the other hand, could directly remove such antigens from plasma, allowing multiple epitopes to be antagonized *in vivo*. The same strategy could be applied to toxic antigens that do not have a functional epitope. Similarly to an LDL receptor removing LDL or an asiologlycoprotein receptor removing asiologlycoprotein from plasma, a sweeping antibody could directly remove a toxic antigen from plasma to alleviate the disease condition [44,45]. Since these types of soluble antigen could not be therapeutic targets for conventional antibodies, sweeping antibodies may expand the target antigen space of antibody therapeutics.

Table 1
Kinetic parameters of parent antibody (tocilizumab) and histidine-engineered antibody (recycling tocilizumab).

	k_a at pH 7.4 (s^{-1} M^{-1})	k_d at pH 7.4 (s^{-1})	K_D at pH 7.4 (M)	k_d at pH 6.0 (s^{-1})	pH dependency (k_d at pH 6.0/k_d at pH 7.4)
Tocilizumab	2.2×10^5	1.1×10^{-3}	5.1×10^{-9}	2.3×10^{-3}	2.3
Recycling tocilizumab	5.3×10^5	1.0×10^{-3}	1.9×10^{-9}	1.5×10^{-2}	15

6. Challenges in developing a pH-dependent antigen-binding antibody as a therapeutic

Although a pH-dependent antigen-binding antibody has attractive features, there are several challenges when generating the antibody for therapeutic application. The following challenges are specific to pH-dependent antigen-binding antibodies and need not be considered when developing conventional monoclonal antibodies.

First, histidine-based engineering to generate a pH-dependent antigen-binding antibody sometimes abrogates the binding affinity at neutral pH. In the case of the anti-IL-6 antibody, histidine mutagenesis conferred a recycling property onto the parental antibody, but at the same time it also reduced the binding affinity against IL-6 at pH 7.4 compared to the parent antibody [22]. If the binding affinity at neutral pH of a histidine-based recycling antibody is not sufficient to elicit the desired therapeutic activity, the binding affinity at neutral pH can be improved by the affinity maturation process, which is commonly applied to gener*ate a potent therapeutic antibody [3,4]. Although a general affinity ma*turation strategy can be applied to recover the loss of binding affinity at pH 7.4, such mutations tend to also increase the binding affinity at acidic pH, which is undesirable. Nevertheless, we have been able to successfully generate high-affinity recycling antibodies with nanomolar K_D at pH 7.4 and simultaneously have sufficient pH dependency or large k_d at acidic pH by using histidine-based engineering and affinity maturation in all the antibodies targeting various antigens tested to date.

Second, the extent of pH-dependency required to dissociate the target antigens in acidic endosomes is not clear. An anti-IL-6R antibody with 20-fold larger K_D and 15-fold larger k_d at pH 6.0 than at pH 7.4 showed an improved pharmacokinetic property in cynomolgus monkeys and humans. PCSK9, an antibody with only 2.6-fold larger K_D and 12-fold larger k_d at pH 6.0 than at pH 7.4, showed a prolonged half-life in cynomolgus monkeys, although its binding affinity to cynomolgus monkey PCSK9 at pH 7.4 was also reduced. These results suggest that the pH-dependency in k_d is a more important factor than that in K_D for improving the pharmacokinetics of an antibody, but we assume that the absolute k_d value in acidic pH, not the relative pH-dependency of k_d (the ratio of k_d at pH 7.4 to that at pH 6.0), would also be important to achieve sufficient dissociation of the antigen. However, the absolute k_d value at pH 6.0 required to sufficiently dissociate an antigen from an antibody remains to be elucidated. The absolute K_D at pH 6.0 would also be important if we consider that the internalized antibody–antigen complexes reach a new equilibrium in the acidic endosomes. A detailed kinetic analysis of endosomal trafficking of antibody–antigen complexes would be required to identify the parameters necessary to sufficiently dissociate the antigens in the endosomes. Although these parameters could differ between the pH-dependent binding antibodies that target membrane-bound antigens, those that target soluble antigens, and the Fc-engineered sweeping antibodies, identifying these parameters would be important for generating pH-dependent binding antibodies with optimum *in vivo* properties.

Third, when considering therapeutic application, it would be necessary to predict antibody pharmacokinetics or the rate of antigen clearance in humans by preclinical study. This is often conducted in a pharmacokinetic study using cynomolgus monkeys; therefore, the antibody preferably needs to bind to a cynomolgus monkey antigen with a similar binding affinity as to the human antigen. Although cross-reactivity to cynomolgus monkey antigens is not so challenging for conventional antibodies, it could be more challenging for pH-dependent binding antibodies since the binding kinetics (both K_D and k_d) at pH 6.0 also need to be considered. In the case of the pH-dependent anti-PCSK9 antibody, since pH-dependency of K_D and k_d

and absolute k_d at pH 6.0 is somewhat different between humans and cynomolgus monkeys, predicting human PK/PD from a cynomolgus monkey study could be difficult. Moreover, with sweeping antibodies, since the Fc region is engineered to enhance the binding affinity to an Fc receptor, cross-reactivity of the Fc region also needs to be considered.

7. Conclusion

Recycling antibodies with pH-dependent antigen binding offer significant advantages over conventional antibodies by dissociating the antigens in endosomes and recycling free antibodies back to plasma. Although generating a high-affinity pH-dependent antigen-binding antibody is still challenging, various approaches are currently available and have been successfully applied to various antigens. Because affinity maturation has now become a basic technology for engineering improved antibody therapeutics, pH-dependent binding antibodies should play an important role as a novel modality for antibody therapeutics in the near future.

References

[1] J.G. Elvin, R.G. Couston, C.F. van der Walle, Therapeutic antibodies: market considerations, disease targets and bioprocessing, Int. J. Pharm. 440 (2013) 83–98.
[2] J.M. Reichert, Which are the antibodies to watch in 2013? mAbs 5 (2013) 1–4.
[3] A.R. Bradbury, S. Sidhu, S. Dubel, J. McCafferty, Beyond natural antibodies: the power of in vitro display technologies, Nat. Biotechnol. 29 (2011) 245–254.
[4] S.M. Lippow, K.D. Wittrup, B. Tidor, Computational design of antibody-affinity improvement beyond in vivo maturation, Nat. Biotechnol. 25 (2007) 1171–1176.
[5] T. Igawa, H. Tsunoda, T. Tachibana, A. Maeda, F. Mimoto, C. Moriyama, M. Nanami, Y. Sekimori, Y. Nabuchi, Y. Aso, K. Hattori, Reduced elimination of IgG antibodies by engineering the variable region, Protein Eng. Des. Sel. 23 (2010) 385–392.
[6] W.F. Dall'Acqua, P.A. Kiener, H. Wu, Properties of human IgG1s engineered for enhanced binding to the neonatal Fc receptor (FcRn), J. Biol. Chem. 281 (2006) 23514–23524.
[7] J.R. Desjarlais, G.A. Lazar, Modulation of antibody effector function, Exp. Cell Res. 317 (2011) 1278–1285.
[8] C. Spiess, J. Bevers III, J. Jackman, N. Chiang, G. Nakamura, M. Dillon, H. Liu, P. Molina, J.M. Elliott, W. Shatz, J.M. Scheer, G. Giese, J. Persson, Y. Zhang, M.S. Dennis, J. Giulianotti, P. Gupta, D. Reilly, E. Palma, J. Wang, E. Stefanich, H. Scheerens, G. Fuh, L.C. Wu, Development of a human IgG4 bispecific antibody for dual targeting of interleukin-4 (IL-4) and interleukin-13 (IL-13) cytokines, J. Biol. Chem. 288 (2013) 26583–26593.
[9] A. Satta, D. Mezzanzanica, F. Turatti, S. Canevari, M. Figini, Redirection of T-cell effector functions for cancer therapy: bispecific antibodies and chimeric antigen receptors, Future Oncol. 9 (2013) 527–539.
[10] T. Kitazawa, T. Igawa, Z. Sampei, A. Muto, T. Kojima, T. Soeda, K. Yoshihashi, Y. Okuyama-Nishida, H. Saito, H. Tsunoda, T. Suzuki, H. Adachi, T. Miyazaki, S. Ishii, M. Kamata-Sakurai, T. Iida, A. Harada, K. Esaki, M. Funaki, C. Moriyama, E. Tanaka, Y. Kikuchi, T. Wakabayashi, M. Wada, M. Goto, T. Toyoda, A. Ueyama, S. Suzuki, K. Haraya, T. Tachibana, Y. Kawabe, M. Shima, A. Yoshioka, K. Hattori, A bispecific antibody to factors IXa and X restores factor VIII hemostatic activity in a hemophilia A model, Nat. Med. 18 (2012) 1570–1574.
[11] Y. Ohsugi, T. Kishimoto, The recombinant humanized anti-IL-6 receptor antibody tocilizumab, an innovative drug for the treatment of rheumatoid arthritis, Expert. Opin. Biol. Ther. 8 (2008) 669–681.
[12] M.A. Tabrizi, C.M. Tseng, L.K. Roskos, Elimination mechanisms of therapeutic monoclonal antibodies, Drug Discov. Today 11 (2006) 81–88.
[13] M. Tabrizi, G.G. Bornstein, H. Suria, Biodistribution mechanisms of therapeutic monoclonal antibodies in health and disease, AAPS J. 12 (2010) 33–43.
[14] S.K. Kelley, T. Gelzleichter, D. Xie, W.P. Lee, W.C. Darbonne, F. Qureshi, K. Kissler, E. Oflazoglu, I.S. Grewal, Preclinical pharmacokinetics, pharmacodynamics, and activity of a humanized anti-CD40 antibody (SGN-40) in rodents and non-human primates, Br. J. Pharmacol. 148 (2006) 1116–1123.
[15] N. Hayashi, Y. Tsukamoto, W.M. Sallas, P.J. Lowe, A mechanism-based binding model for the population pharmacokinetics and pharmacodynamics of omalizumab, Br. J. Clin. Pharmacol. 63 (2007) 548–561.
[16] K.M. Zareba, Eculizumab: a novel therapy for paroxysmal nocturnal hemoglobinuria, Drugs Today (Barc) 43 (2007) 539–546.
[17] J.J. Xiao, W. Krzyzanski, Y.M. Wang, H. Li, M.J. Rose, M. Ma, Y. Wu, B. Hinkle, J.J. Perez-Ruixo, Pharmacokinetics of anti-hepcidin monoclonal antibody Ab 12B9m and hepcidin in cynomolgus monkeys, AAPS J. 12 (2010) 646–657.
[18] F.D. Finkelman, K.B. Madden, S.C. Morris, J.M. Holmes, N. Boiani, I.M. Katona, C.R. Maliszewski, Anti-cytokine antibodies as carrier proteins. Prolongation of in vivo effects of exogenous cytokines by injection of cytokine-anti-cytokine antibody complexes, J. Immunol. 151 (1993) 1235–1244.
[19] Charles B. Davis, Leeann P. Tobia, Deborah C. Kwok, Christine M. Oishi, Neil Kherterpal, Timothy W. Hepburn, Lisa J. Benincosa, Fung-Sing Chow, William J. Jusko, Accumulation of antibody-target complexes and the pharmacodynamics of clotting after single intravenous administration of humanized anti-factor IX monoclonal antibody to rats, Drug Deliv. 6 (1999) 171–179.
[20] T. Igawa, S. Ishii, T. Tachibana, A. Maeda, Y. Higuchi, S. Shimaoka, C. Moriyama, T. Watanabe, R. Takubo, Y. Doi, T. Wakabayashi, A. Hayasaka, S. Kadono, T. Miyazaki, K. Haraya, Y. Sekimori, T. Kojima, Y. Nabuchi, Y. Aso, Y. Kawabe, K. Hattori, Antibody recycling by engineered pH-dependent antigen binding improves the duration of antigen neutralization, Nat. Biotechnol. 28 (2010) 1203–1207.
[21] J. Chaparro-Riggers, H. Liang, R.M. DeVay, L. Bai, J.E. Sutton, W. Chen, T. Geng, K. Lindquist, M.G. Casas, L.M. Boustany, C.L. Brown, J. Chabot, B. Gomes, P. Garzone, A. Rossi, P. Strop, D. Shelton, J. Pons, A. Rajpal, Increasing serum half-life and extending cholesterol lowering in vivo by engineering antibody with pH-sensitive binding to PCSK9, J. Biol. Chem. 287 (2012) 11090–11097.
[22] S.C. Devanaboyina, S.M. Lynch, R.J. Ober, S. Ram, D. Kim, A. Puig-Canto, S. Breen, S. Kasturirangan, S. Fowler, L. Peng, H. Zhong, L. Jermutus, H. Wu, C. Webster, E.S. Ward, C. Gao, The effect of pH dependence of antibody–antigen interactions on subcellular trafficking dynamics, mAbs 5 (2013) 851–859.
[23] T. Igawa, A. Maeda, K. Haraya, T. Tachibana, Y. Iwayanagi, F. Mimoto, Y. Higuchi, S. Ishii, S. Tamba, N. Hironiwa, K. Nagano, T. Wakabayashi, H. Tsunoda, K. Hattori, Engineered monoclonal antibody with novel antigen-sweeping activity in vivo, PLoS One 8 (2013) e63236.
[24] J.P. Davda, R.J. Hansen, Properties of a general PK/PD model of antibody–ligand interactions for therapeutic antibodies that bind to soluble endogenous targets, mAbs 2 (2010) 576–588.
[25] J.J. Haringman, D.M. Gerlag, T.J. Smeets, D. Baeten, F. van den Bosch, B. Bresnihan, F.C. Breedveld, H.J. Dinant, F. Legay, H. Gram, P. Loetscher, R. Schmouder, T. Woodworth, P.P. Tak, A randomized controlled trial with an anti-CCL2 (anti-monocyte chemotactic protein 1) monoclonal antibody in patients with rheumatoid arthritis, Arthritis Rheum. 54 (2006) 2387–2392.
[26] P.L. Martin, J. Cornacoff, U. Prabhakar, T. Lohr, G. Treacy, J.E. Sutherland, S. Hersey, E. Martin, Reviews preclinical safety and immune-modulating effects of therapeutic monoclonal antibodies to interleukin-6 and tumor necrosis factor-alpha in cynomolgus macaques, J. Immunotoxicol. 1 (2005) 131–139.
[27] J.C. Byrd, S. O'Brien, I.W. Flinn, T.J. Kipps, M. Weiss, K. Rai, T.S. Lin, J. Woodworth, D. Wynne, J. Reid, A. Molina, B. Leigh, S. Harris, Phase 1 study of lumiliximab with detailed pharmacokinetic and pharmacodynamic measurements in patients with relapsed or refractory chronic lymphocytic leukemia, Clin. Cancer Res. 13 (2007) 4448–4455.
[28] G.C. Jayson, C. Mulatero, M. Ranson, J. Zweit, A. Jackson, L. Broughton, J. Wagstaff, L. Hakansson, G. Groenewegen, J. Lawrance, M. Tang, L. Wauk, D. Levitt, S. Marreaud, F. F. Lehmann, M. Herold, H. Zwierzina, R. European Organisation for, C. Treatment of, Phase I investigation of recombinant anti-human vascular endothelial growth factor antibody in patients with advanced cancer, Eur. J. Cancer 41 (2005) 555–563.
[29] T. Olafsen, Fc engineering: serum half-life modulation through FcRn binding, Methods Mol. Biol. 907 (2012) 537–556.
[30] C. Vaccaro, J. Zhou, R.J. Ober, E.S. Ward, Engineering the Fc region of immunoglobulin G to modulate in vivo antibody levels, Nat. Biotechnol. 23 (2005) 1283–1288.
[31] R.J. Kurlander, D.M. Ellison, J. Hall, The blockade of Fc receptor-mediated clearance of immune complexes in vivo by a monoclonal antibody (2.4G2) directed against Fc receptors on murine leukocytes, J. Immunol. 133 (1984) 855–862.
[32] L.P. Ganesan, J. Kim, Y. Wu, S. Mohanty, G.S. Phillips, D.J. Birmingham, J.M. Robinson, C.L. Anderson, FcgammaRIIb on liver sinusoidal endothelium clears small immune complexes, J. Immunol. 189 (2012) 4981–4988.
[33] C.Y. Zhang, J.W. Booth, Divergent intracellular sorting of Fc{gamma}RIIA and Fc {gamma}RIIB2, J. Biol. Chem. 285 (2010) 34250–34258.
[34] T. Lehrnbecher, C.B. Foster, S. Zhu, S.F. Leitman, L.R. Goldin, K. Huppi, S.J. Chanock, Variant genotypes of the low-affinity Fcgamma receptors in two control populations and a review of low-affinity Fcgamma receptor polymorphisms in control and disease populations, Blood 94 (1999) 4220–4232.
[35] F. Mimoto, H. Katada, S. Kadono, T. Igawa, T. Kuramochi, M. Muraoka, Y. Wada, K. Haraya, T. Miyazaki, K. Hattori, Engineered antibody Fc variant with selectively enhanced FcgammaRIIb binding over both FcgammaRIIa(R131) and FcgammaRIIa(H131), Protein Eng. Des. Sel. 26 (2013) 589–598.
[36] K. Sato, M. Tsuchiya, J. Saldanha, Y. Koishihara, Y. Ohsugi, T. Kishimoto, M.M. Bendig, Reshaping a human antibody to inhibit the interleukin 6-dependent tumor cell growth, Cancer Res. 53 (1993) 851–856.
[37] D.E. Vaughn, P.J. Bjorkman, Structural basis of pH-dependent antibody binding by the neonatal Fc receptor, Structure 6 (1998) 63–73.
[38] S. Tickle, R. Adams, D. Brown, M. Griffiths, D. Lightwood, A. Lawson, High-throughput screening for high affinity antibodies, JALA 14 (2009) 303–307.
[39] M.L. Murtaugh, S.W. Fanning, T.M. Sharma, A.M. Terry, J.R. Horn, A combinatorial histidine scanning library approach to engineer highly pH-dependent protein switches, Protein Sci. 20 (2011) 1619–1631.
[40] J.V. Gerasimenko, A.V. Tepikin, O.H. Petersen, O.V. Gerasimenko, Calcium uptake via endocytosis with rapid release from acidifying endosomes, Curr. Biol. 8 (1998) 1335–1338.
[41] E.M. Strauch, S.J. Fleishman, D. Baker, Computational design of a pH-sensitive IgG binding protein, Proc. Natl. Acad. Sci. U. S. A. 111 (2014) 675–680.
[42] C.A. Sarkar, K. Lowenhaupt, T. Horan, T.C. Boone, B. Tidor, D.A. Lauffenburger, Rational cytokine design for increased lifetime and enhanced potency using pH-activated "histidine switching", Nat. Biotechnol. 20 (2002) 908–913.
[43] C.E. Mogensen, The glomerular permeability determined by dextran clearance using Sephadex gel filtration, Scand. J. Clin. Lab. Invest. 21 (1968) 77–82.
[44] H. Feinberg, D. Torgersen, K. Drickamer, W.I. Weis, Mechanism of pH-dependent N-acetylgalactosamine binding by a functional mimic of the hepatocyte asialoglycoprotein receptor, J. Biol. Chem. 275 (2000) 35176–35184.
[45] T. Yamamoto, H.C. Chen, E. Guigard, C.M. Kay, R.O. Ryan, Molecular studies of pH-dependent ligand interactions with the low-density lipoprotein receptor, Biochemistry 47 (2008) 11647–11652.

Journal of Thrombosis and Haemostasis, **12**: 206–213 DOI: 10.1111/jth.12474

ORIGINAL ARTICLE

Anti-factor IXa/X bispecific antibody (ACE910): hemostatic potency against ongoing bleeds in a hemophilia A model and the possibility of routine supplementation

A. MUTO,* K. YOSHIHASHI,* M. TAKEDA,* T. KITAZAWA,* T. SOEDA,* T. IGAWA,* Y. SAKAMOTO,* K. HARAYA,* Y. KAWABE,* M. SHIMA,† A. YOSHIOKA‡ and K. HATTORI*

Research Division, Chugai Pharmaceutical Co., Ltd, Gotemba, Shizuoka; †Department of Pediatrics, Nara Medical University; and ‡Nara Medical University, Kashihara, Nara, Japan

To cite this article: Muto A, Yoshihashi K, Takeda M, Kitazawa T, Soeda T, Igawa T, Sakamoto Y, Haraya K, Kawabe Y, Shima M, Yoshioka A, Hattori K. Anti-factor IXa/X bispecific antibody (ACE910): hemostatic potency against ongoing bleeds in a hemophilia A model and the possibility of routine supplementation. *J Thromb Haemost* 2014; **12**: 206–13.

Summary. *Background:* We previously reported that a humanized anti-factor IXa/X bispecific antibody, hBS23, mimics the function of FVIII even in the presence of FVIII inhibitors, and has preventive hemostatic activity against bleeding in an animal model of acquired hemophilia A. After further molecular engineering of hBS23, we recently identified an improved humanized bispecific antibody, ACE910, for clinical investigation. *Objectives:* To elucidate the *in vivo* hemostatic potency of ACE910 by examining its effect against ongoing bleeds, and to determine its pharmacokinetic parameters for discussion of its potency for prophylactic use. *Methods:* A non-human primate model of acquired hemophilia A was established by injecting anti-primate FVIII neutralizing antibody. When bleeds emerged following an artificial bleed-inducing procedure, either ACE910 or recombinant porcine FVIII (rpoFVIII) was intravenously administered. rpoFVIII was additionally administered twice daily on the following 2 days. Bleeding symptoms were monitored for 3 days. A pharmacokinetic study and multiple-dosing simulations of ACE910 were also performed. *Results:* A single bolus of 1 or 3 mg kg^{-1} ACE910 showed hemostatic activity comparable to that of 10 U kg^{-1} (twice daily) rpoFVIII against ongoing bleeds. The determined ACE910 pharmacokinetic parameters included a long half-life (3 weeks) and high subcutaneous bioavailability (nearly 100%). The simulation results based on pharmacokinetic parameters indicated that the above hemostatic level could be maintained with once-weekly subcutaneous administration of ACE910, suggesting the possibility of more effective prophylaxis. *Conclusions:* ACE910 may offer an alternative on-demand treatment option for patients with hemophilia A, as well as user-friendly and aggressive routine supplementation.

Keywords: antibodies, catalytic; factor VIII; hemophilia A; hemostasis; therapeutics.

Correspondence: Atsushi Muto, Research Division, Chugai Pharmaceutical Co., Ltd, 1-135 Komakado, Gotemba, Shizuoka 412-8513, Japan.
Tel.: +81 550 87 3411; fax: +81 550 87 1960.
E-mail: mutoats@chugai-pharm.co.jp

Institution where the work was carried out: Research Division, Chugai Pharmaceutical Co., Ltd.

Received 25 April 2013
Manuscript handled by: L. Aledort
Final decision: P. H. Reitsma, 27 November 2013

Introduction

Hemophilia A is a bleeding disorder caused by an inherited deficiency of factor VIII. The severity is known to correlate with the plasma FVIII level: severe, moderate and mild phenotypes are defined by plasma FVIII levels of < 1, 1–5 and > 5 to < 40 U dL^{-1}, respectively. Severe cases have a high propensity to suffer bleeds, including joint bleeds, whereas moderate cases typically experience far fewer bleeding episodes, and mild cases rarely bleed spontaneously [1,2].

Patients are primarily treated with FVIII agents. However, as FVIII agents are exogenous for severely affected patients, ~ 30% of them develop alloantibodies against FVIII (FVIII inhibitors) [2]. FVIII inhibitors largely restrict treatment with FVIII agents, and consequently make it difficult to control bleeding, because alternative bypassing agents have shorter *in vivo* half-lives and are not always effective [3]. The eradication of FVIII inhibitors with high doses of FVIII is very expensive, and does not always work [4]. In patients with severe hemophilia A without FVIII inhibitors, routine prophylaxis with exoge-

nous FVIII to maintain FVIII levels above 1 U dL^{-1} is beneficial to prevent bleeding [5,6]; however, the need for frequent intravenous injections negatively affects patients' quality of life [7].

In order to overcome these shortcomings, we previously created a humanized anti-FIXa/FX bispecific IgG antibody, termed hBS23, which replicated FVIII cofactor function by binding and placing FIXa and FX into spatially appropriate positions [8]. hBS23 had cofactor activity *in vitro*, even in the presence of FVIII inhibitors, and, in a non-human primate model of acquired hemophilia A, hBS23 at an intravenous dose of 0.3 mg kg^{-1} exerted hemostatic activity to prevent the progression of bleeding symptoms to the same extent as recombinant porcine FVIII (rpoFVIII) maintained at a plasma level of $\geq$ 1 U dL^{-1}. However, it remained unproven whether this bispecific antibody approach possessed the potency to ameliorate ongoing bleeds, which would require higher levels of FVIII, or how much hemostatic potency it had in comparison with FVIII. We recently modified hBS23 with a multidimensional optimization approach to improve the FVIII-mimetic cofactor activity, pharmacokinetic properties, immunogenicity, physicochemical stability, and ease of industrial manufacture for clinical application; we consequently identified an improved humanized anti-FIXa/FX bispecific IgG antibody, termed ACE910 [9]. In this study, we elucidate the *in vivo* hemostatic potency of ACE910, including that against ongoing bleeds as compared with rpoFVIII, by using a non-human primate model of acquired hemophilia A.

Furthermore, in order to elucidate the potency of ACE910 in routine supplementation, we performed a pharmacokinetic study of ACE910 in non-human primates to determine its pharmacokinetic parameters, and conducted multiple dosing simulations with those parameters. Routine supplementation with exogenous FVIII is aimed at keeping the FVIII level at 1 U dL^{-1} or above to convert a severe disease to a moderate one [2,5]. This strategy successfully reduces bleeding episodes and the risk of developing hemophilic arthropathy [5]. However, the effect is not necessarily perfect: a recent report suggested that the risk of joint damage remains until the baseline factor level is 10–15 U dL^{-1} or higher [10]. In this study, we also discuss the possibility of once-weekly subcutaneous administration of ACE910 for routine supplementation that is more aggressive than the current one with exogenous FVIII; in other words, a regimen that can convert a severe disease to a mild disease.

Materials and methods

Materials

ACE910 was expressed in human embryonic kidney 293 or Chinese hamster ovary (CHO) cells, which were co-transfected with the mixture of plasmids encoding the humanized anti-FIXa heavy chain, anti-FX heavy chain, and common light chain. ACE910 was purified by protein A and ion exchange chromatography from the culture supernatant [9]. B domain-deleted rpoFVIII [8] was prepared as described in the supporting information (Preparation and analysis of rpoFVIII). Briefly, we expressed it in CHO cells by stable transfection. Then, rpoFVIII was purified from the supernatant by using ion exchange and gel permeation chromatography. We confirmed its purity with SDS-PAGE under reduced conditions, and determined its activity (U dL^{-1}) with an activated partial thromboplastin time (APTT)-based one-stage coagulation assay. Recombinant human FVIII (rhFVIII) was purchased from Bayer HealthCare (Leverkusen, Germany). Anti-primate FVIII neutralizing antibody (VIII-2236) [8] and the other purchased reagents are described in the supporting information (Confirmation of non-reactivity of VIII-2236 to rpoFVIII and ACE910, and the other supporting methods).

Animals and ethics

We used 26 and 12 male cynomolgus monkeys for the *in vivo* hemostatic study (2.6–4.0 kg, aged 3 years; Hamri, Ibaraki, Japan) and for the pharmacokinetic study (2.9–5.0 kg, aged 4–5 years; Japan Laboratory Animals, Tokyo, Japan), respectively. We used 24 female mice (aged 5 weeks; Charles River, Yokohama, Japan, and SLC, Hamamatsu, Japan) and 24 female rats (aged 4 weeks; Charles River) for the immunization to generate anti-idiotype antibodies against the variable region of ACE910. The details of anti-idiotype antibodies are described in the supporting information (Generation and preparation of anti-idiotype antibodies to each variable region of ACE910).

All animal studies were approved by the Institutional Animal Care and Use Committee of Chugai Pharmaceutical, and were conducted in accordance with the approved protocols and the Guidelines for the Care and Use of Laboratory Animals at the company. Chugai Pharmaceutical is fully accredited by the Association for Assessment and Accreditation of Laboratory Animal Care International.

APTT and thrombin generation (TG) assays

APTT and TG assays were performed with standard equipment. In the TG assay, we employed two kinds of triggering solutions that contained, respectively, FXIa and tissue factor (TF). The solution containing human FXIa (Enzyme Research Laboratories, Swansea, UK) was prepared in-house, and the solution containing TF, PPP-Reagent LOW (Thrombinoscope BV, Maastricht, the Netherlands) was purchased. The details are described in the supporting information (APTT and TG assays).

In vivo *hemostatic study in an acquired hemophilia A model*

As ACE910 is highly species-specific in its FVIII-mimetic cofactor activity, non-human primates were used. On day 0, the animals received an intravenous injection of VIII-2236 (10 mg kg^{-1}). Two hours later, the animals were anesthetized with isoflurane inhalation, and bruises on the body surface that might possibly have emerged because of FVIII neutralization were measured. Then, the following two surgical procedures were performed: a 18G-needle was inserted 1 cm deep into the muscle at 22 sites (two sites in each upper arm, three sites in each forearm, four sites on the inside of each thigh, and two sites on the outside of each thigh); and subcutaneous exfoliation was performed by inserting the tip of forceps beneath the abdominal skin to 3 cm at two sites. After administration of buprenorphine, an analgesic drug, the animals were allowed to recover from the anesthesia. (They received this analgesic treatment twice daily [morning and evening] from day 0 to day 2; six doses were given, and the condition of the animals was observed daily.) After recognition of bleeding, approximately 6–8 h after injury, the animals received intravenous ACE910 (0.3, 1 or 3 mg kg^{-1}; $n = 4$ for each group), rpoFVIII (3.4 or 10 U kg^{-1}; $n = 4$ for each group), or no test item (control; $n = 6$). In the rpoFVIII group, rpoFVIII was also intravenously administered in the morning and evening on days 1 and 2 (a total of five administrations). In the morning on days 1, 2, and 3, the animals were anesthetized for measurement of the bruised areas. After the evaluation on day 3, the animals were killed humanely. Citrated blood was collected before and 2 h after the VIII-2236 injection, ~ 10 min after the test item administration on day 0, and before measurement of the bruised area on days 1, 2, and 3. The change in blood hemoglobin level was expressed as a percentage of that on day 0 (2 h after the VIII-2236 injection). The plasma ACE910 concentration was determined with the method described in the supporting information (Measurement of plasma ACE910 concentration).

Pharmacokinetic study

Animals received intravenous ACE910 (6 mg kg^{-1}; $n = 3$) or subcutaneous ACE910 (0.06, 0.6 or 6 mg kg^{-1}; $n = 3$ for each group) in a single dose. For animals dosed intravenously, blood was sampled with a heparinized syringe at 0.25, 2, 8, 24, 48, 72 and 96 h postdose, as well as at 7, 14, 28, 42, 56, 70 and 84 days postdose. For animals dosed subcutaneously, blood was collected in the same way without sampling at 0.25 h. The plasma concentrations of ACE910 and anti-ACE910 alloantibodies were measured with the methods described in the supporting information (Measurement of plasma ACE910 concentration and detection of anti-ACE910 alloantibodies).

Statistical analysis, pharmacokinetic analysis, and multiple-dosing simulation

For the *in vivo* hemostatic study, data are presented as mean ± standard error. Other data are presented as mean ± standard deviation. The parametric Dunnett multiple comparison test (two-tailed) (SAS preclinical package version 5.00; SAS Institute Japan, Tokyo, Japan) was used to determine *P*-values. $P < 0.05$ was considered to be statistically significant.

In the pharmacokinetic study, the plasma ACE910 concentration data were analyzed by non-compartmental analysis with PHOENIX WINNONLIN version 6.2 (Pharsight, St Louis, MO, USA). Multiple-dosing simulations were performed with SAAM II version 1.2 (SAAM Institute, Seattle, WA, USA).

Results

In vitro *cross-reactivity of ACE910 with cynomolgus monkeys*

First, we examined the cross-reactivity of ACE910 with cynomolgus monkeys by use of an APTT assay. ACE910 shortened APTT in FVIII-neutralized cynomolgus monkey plasma with a concentration dependency similar to that in human FVIII-deficient plasma (Fig. 1A,B).

We next examined the cross-reactivity of ACE910 with cynomolgus monkeys by use of one of the global assays, the TG assay [11]. Because we had not clearly detected rpoFVIII activity in the standard low-TF triggering condition in FVIII-neutralized cynomolgus monkey plasma, we instead employed FXIa as a trigger. Beforehand, we had confirmed, in human FVIII-deficient plasma, that the two triggering conditions produced similar peak heights for the purpose of comparing ACE910 with rhFVIII (Figs 1C and S1). ACE910 improved the peak height of the FXIa-triggered TG assay in FVIII-neutralized cynomolgus monkey plasma in a similar concentration-dependent manner to that in human FVIII-deficient plasma (Fig. 1C,D). ACE910 had a similar cofactor activity as rhFVIII or rpoFVIII in improving the peak height in each species. Beforehand, the rpoFVIII that we prepared had been analyzed for qualification (Fig. S2).

In vivo *hemostatic study in an acquired hemophilia A model*

To examine the *in vivo* hemostatic potency of ACE910, including that against ongoing bleeds, we modified the non-human primate model of acquired hemophilia A that we previously reported [8]. Briefly, more intense injury procedures were employed, and the dose timing of the test item was set to after the emergence of bleeding symptoms, so that the hemostatic action of 10 U kg^{-1} rpoFVIII could be properly evaluated.

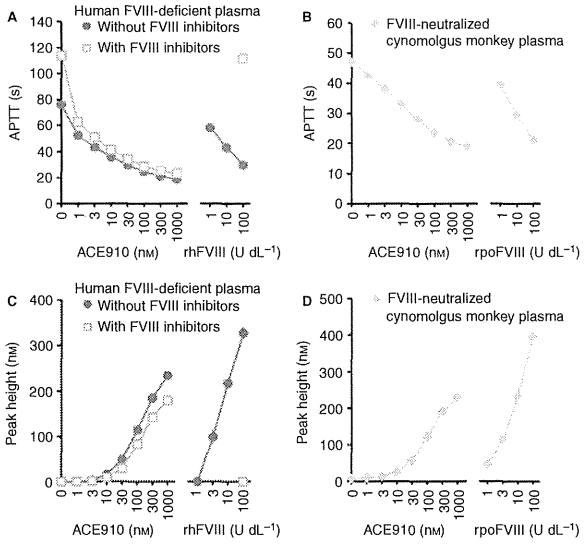

Fig. 1. FVIII-mimetic cofactor activity of ACE910 in human FVIII-deficient plasma without and with FVIII inhibitors and in FVIII-neutralized cynomolgus monkey plasma. Effects of ACE910, recombinant human FVIII (rhFVIII) or recombinant porcine FVIII (rpoFVIII) on activated partial thromboplastin time (APTT) (A, B) and on peak height of thrombin generation triggering the intrinsic pathway (C, D), in human FVIII-deficient plasma without and with FVIII inhibitors (A, C) and in FVIII-neutralized cynomolgus monkey plasma (B, D). Data are expressed as mean ± standard deviation (n = 3).

The experimental protocol is illustrated in Fig. 2A. An acquired hemophilia A status was first established by injecting an anti-primate FVIII antibody, VIII-2236, which neutralizes endogenous FVIII, but neither exogenous rpoFVIII nor ACE910 (Fig. S3). Then, bleeding was artificially induced by inserting a needle in the limb muscles and by subcutaneous exfoliation on the abdomen. The animals in the control group showed a progressive decrease in hemoglobin level (anemia associated with hemorrhage) and expansion of bruised areas (Fig. 2B,C). A single intravenous administration of ACE910 at 6–8 h after bleeding induction, when visible bleeding symptoms had emerged, tended to ameliorate the decrease in hemoglobin level (P = 0.0643 at 3 mg kg^{-1} vs. control). The expansion of bruised areas was significantly reduced at doses of 1 and 3 mg kg^{-1} ACE910 (P < 0.05 vs. control). These hemostatic effects of ACE910 at 1 and 3 mg kg^{-1} were comparable to the hemostatic effect of dosing twice daily with 10 U kg^{-1} rpoFVIII. In such a regimen, the plasma concentration of rpoFVIII would reach 25 U dL^{-1} just after the first injection, and would range between 7.4 and 46 U dL^{-1}, according to a simulation of multiple dosing of rpoFVIII based on the pharmacokinetic parameters obtained from the single-dose injection study of rpoFVIII in cynomolgus monkeys (Fig. S4). The mean plasma concentration of ACE910 (0.3, 1 or 3 mg kg^{-1}) was, respectively, 6.6, 26 or 61 μg mL^{-1} (45, 180 or 420 nM) just after administration, and 3.0, 8.4 or 34 μg mL^{-1} (21, 58 or 230 nM) on day 3 (Fig. 2D). In the clinical setting, 20 U dL^{-1} is often employed as the target initial FVIII level for treatment of ongoing bleeds [12]. Therefore, intravenous administration of 1–3 mg kg^{-1} ACE910, or a plasma concentration of 26–61 μg mL^{-1} (180–420 nM), is also expected to exert hemostatic activity against ongoing bleeds in the clinical setting.

Pharmacokinetic study and multiple-dosing simulation

In order to investigate the potency of ACE910 for routine supplementation, we performed a single-dose pharmacokinetic study of ACE910, to determine the pharmacokinetic parameters for simulating the plasma ACE910 concentration after multiple dosing.

The plasma half-life of ACE910 was 19.4 days after a single intravenous administration at 6 mg kg^{-1}, and in the range of 23.6–26.5 days after a single subcutaneous administration at 0.06, 0.6 or 6 mg kg^{-1} (Table S1). With

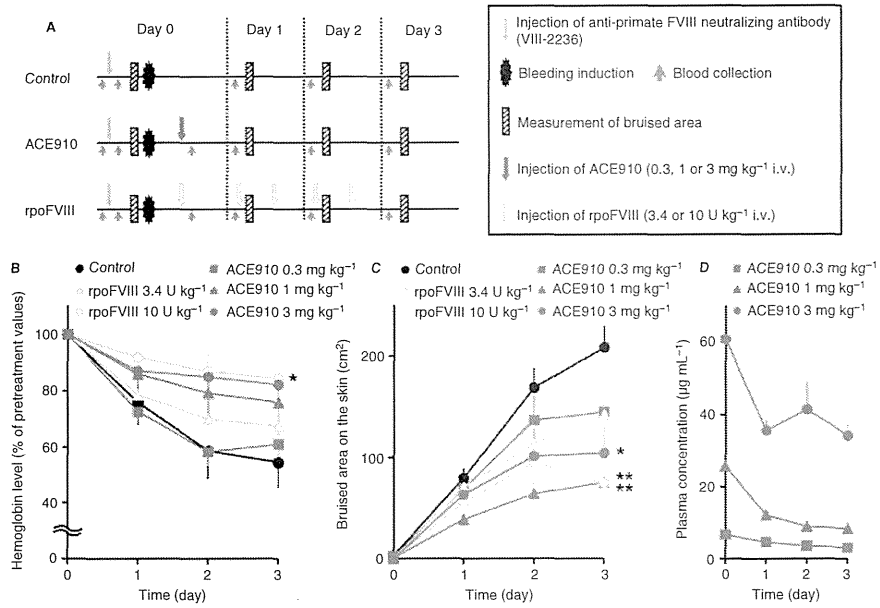

Fig. 2. *In vivo* hemostatic activity of ACE910 against ongoing bleeds in an acquired hemophilia A model. (A) The experimental protocol used. (B, C) Time course changes of (B) hemoglobin level and (C) bruised areas in the control group (no test item; n = 6), the ACE910 group (0.3, 1 or 3 mg kg^{-1}; n = 4 for each group), and the recombinant porcine FVIII (rpoFVIII) group (3.4 or 10 U kg^{-1}; n = 4 for each group). Asterisks show statistical significance of the data on day 3 (*P < 0.05 and **P < 0.01 vs. control). (D) Time course of plasma ACE910 concentration in the ACE910 groups. Data are expressed as mean ± standard error. i.v., intravenous.

subcutaneous administration, the maximum plasma concentration of ACE910 increased in approximate proportion to the dose increment. The subcutaneous bioavailability was 102.3% at the 6 mg kg^{-1} dose. These results were consistent with those of our previous study [9]. For these analyses, we excluded two animals in which anti-ACE910 alloantibodies were detected, respectively, from 28 days after the intravenous administration of 6 mg kg^{-1} and from 56 days after the subcutaneous administration of 0.06 mg kg^{-1}. Their plasma ACE910 concentrations decreased in association with the detection of anti-ACE910 alloantibodies.

In the *in vivo* hemostatic study, the mean initial plasma concentrations of ACE910 were 26 and 61 μg mL^{-1} (180 and 420 nM) in the 1 and 3 mg kg^{-1} groups, respectively. The hemostatic effect in these groups was comparable to that in the rpoFVIII 10 U kg^{-1} group, in which the FVIII level was within the range of a mild phenotype (Fig. S4B). We considered that if, by routine supplementation, a plasma ACE910 level of 26 μg mL^{-1} or above were maintained at all times in patients, a severe phenotype would possibly be converted to a mild phenotype beyond a moderate phenotype. To examine this possibility, multiple-dosing simulations of ACE910 were performed with the parameters obtained from the pharmacokinetic study. The results of the simulations indicated that, if the target trough plasma level of ACE910 were set to 26 or 61 μg mL^{-1}, it could be maintained by once-weekly subcutaneous administrations of 0.64 or 1.5 mg kg^{-1} at a steady state, respectively (Fig. 3).

Discussion

We previously reported the creation of an anti-FIXa/FX bispecific antibody, named hBS23, which restored FVIII cofactor function [8]. Although hBS23 had meaningful hemostatic activity, its molecular structure would have required further optimization in terms of manufacturing efficiency, immunogenicity, pharmacokinetic profile, physicochemical properties, and FVIII-mimetic cofactor activity. To address these remaining issues, we continued to

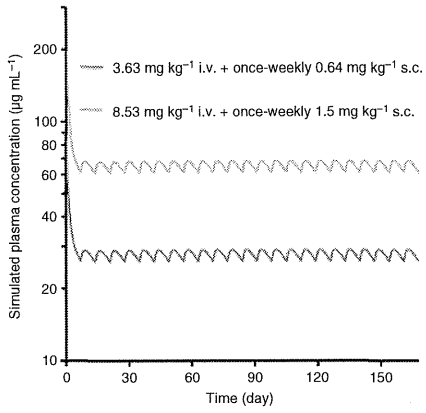

Fig. 3. Examples of simulations; plasma ACE910 concentration after multiple dosing in cynomolgus monkeys. The time course of plasma ACE910 concentration was simulated by use of the pharmacokinetic study data in cynomolgus monkeys for the case of once-weekly subcutaneous (s.c.) administration at 0.64 or 1.5 mg kg^{-1}, starting 7 days after the initial bolus intravenous administration of 3.63 or 8.53 mg kg^{-1}, respectively. i.v., intravenous.

optimize the bispecific antibody multidimensionally, and finally identified an improved one, ACE910, for clinical investigation [9]. ACE910 had twice the effect on increasing catalytic efficiency, 1.5 times the *in vivo* half-life and higher subcutaneous bioavailability than hBS23. Furthermore, ACE910 was able to be purified on a large manufacturing scale and formulated into a subcutaneously injectable liquid formulation. However, the degree of *in vivo* hemostatic potency of ACE910 remained unproven. We hypothesized that approximately 300 nM (44 μg mL^{-1}) of plasma ACE910 would exert an *in vivo* hemostatic activity equivalent to 10 U dL^{-1} FVIII, as 300 nM ACE910 showed *in vitro* cofactor activity similar to that of 10 U dL^{-1} FVIII, in terms of the peak height in the TG assay in human FVIII-deficient plasma (Fig. 1C) [9]. When making this hypothesis, we did not use the APTT data. ACE910 strongly shortened APTT, even beyond the level achieved with 100 U dL^{-1} FVIII at more than 300 nM (Fig. 1A), but we considered that this phenomenon could be attributed to the fact that FVIII requires additional time to be activated by thrombin or FXa, whereas ACE910 does not.

In order to prove the hypothesis, we had to detect appropriately the *in vivo* hemostatic activity of a plasma level of approximately 10 U dL^{-1} rpoFVIII. For this purpose, we employed more intensive injury procedures, and changed the timing of administration of the test items to after bleeding symptoms had emerged. In the clinical setting, the treatment of ongoing bleeds minimally requires a plasma FVIII level of 10–20 U dL^{-1}, which is much higher than the level required for prophylactic bleeding prevention (1 U dL^{-1}) [12]. As a result, intravenous administration of 10 U kg^{-1} (twice daily) of rpoFVIII showed a significant hemostatic effect, whereas a hemostatic effect of 3.4 U kg^{-1} (twice daily) of rpoFVIII was not clearly detected in this model. The multiple-dosing simulations of rpoFVIII in cynomolgus monkeys indicated that, with twice-daily doses of 3.4 or 10 U kg^{-1}, the plasma rpoFVIII level would be, respectively, 8.5 or 25 U dL^{-1} at the outset, would remain at more than 2.5 or 7.4 U dL^{-1}, and would reach a maximum of 16 or 46 U dL^{-1} by the end of the observation period (Fig. S4B). Therefore, we judged that this re-established model was well validated in terms of the reactivity to FVIII. Using this validated model, we elucidated the *in vivo* hemostatic potency of ACE910. A single intravenous administration of ACE910 at 1 or 3 mg kg^{-1} ameliorated bleeding symptoms to an extent equivalent to that achieved with twice-daily doses of 10 U kg^{-1} rpoFVIII. Among the results, it seems contradictory that the mean bruised area of the ACE910 1 mg kg^{-1} group was smaller than that of the 3 mg kg^{-1} group. From the viewpoint of ethics for primates, we employed the minimum number of animals possible to detect a hemostatic effect. Therefore, we think that this variation in dose dependency occurred incidentally, because the deviation in the bruised area was rather large.

The pharmacokinetic profiles of ACE910 and rpoFVIII were different, and therefore it is quite difficult to compare their *in vivo* hemostatic activities in terms of plasma level. However, to say the least, the hemostatic activity at the maximum plasma level of ACE910, 26 or 61 μg mL^{-1}, would have reached that at the minimum plasma level of rpoFVIII, 7.4 U dL^{-1}. If the two agents were compared according to their initial plasma levels, 26 or 61 μg mL^{-1} plasma ACE910 would have shown hemostatic activity equivalent to that of 25 U dL^{-1} rpoFVIII. Given that ACE910 should work equivalently in humans and cynomolgus monkeys (Fig. 1C,D), and that ACE910 fully exerted its activity even in the presence of FVIII inhibitors (Fig. 1A,C), ACE910 could be possibly an effective and long-acting treatment option to ameliorate ongoing bleeds in patients with FVIII inhibitors.

We also consider that ACE910 will be highly valuable for routine prophylaxis against bleeding. Current routine prophylaxis with exogenous FVIII is aimed at converting a severe disease (< 1 U dL^{-1} FVIII) to a moderate one (1–5 U dL^{-1}), but it requires frequent venous access, typically three times weekly. This negatively affects both the implementation of and adherence to the supplementation routine, particularly for pediatric patients treated at home [7]. In addition, the development of FVIII inhibitors deprives them of this treatment option. As ACE910 is expected to be a long-acting, subcutaneously injectable agent that is unaffected by the presence of FVIII inhibitors, it will be able to resolve the drawbacks inherent to exogenous FVIII and its prophylactic use [13,14]. Furthermore, although routine prophylaxis with exogenous FVIII effectively reduces joint bleeds and prevents joint damage, its prophylactic effect is not necessarily perfect [5,10]. In line with this, the clinical outcomes of patients with moderate hemophilia A vary, and the proportion of them who suffer from joint impairment is not negligible [1]. Therefore, keeping FVIII levels within the range of a mild phenotype (> 5 U dL^{-1}) may provide patients with substantial benefits in terms of preserving joint status and enabling patients to participate in physical activities [15]. As mentioned above, even by a conservative estimate, 61 μg mL^{-1} plasma ACE910 would be expected to show hemostatic activity within the range of a mild phenotype.

Generally, pharmacokinetic data of therapeutic antibodies from cynomolgus monkeys can be scaled to project human pharmacokinetic profiles [16], and the simulated plasma concentration–time profiles from the pharmacokinetic parameters are known to be comparable to the actual observed profiles for therapeutic antibodies [17]. Therefore, we conducted multiple-dosing simulations with the pharmacokinetic study data in cynomolgus monkeys, and found that 61 μg mL^{-1} plasma ACE910 would be maintained at a steady state by once-weekly subcutaneous administration of 1.5 mg kg^{-1} (Fig. 3). The simulation is, of course, not the same as actual data, but we have since confirmed that the simulation of the time profile of plasma ACE910 concentration with the above pharmacokinetic parameters gave a good prediction of the actual data in another cynomolgus monkey study employing multiple dosing with ACE910 (Y. Sakamoto, unpublished data). Therefore, we think that the simulation would work well.

In the pharmacokinetic study, two of 12 animals developed anti-ACE910 alloantibodies. In cynomolgus monkeys, the development of anti-humanized antibody alloantibodies is theoretically inevitable, and their reported incidence rates vary (0–100%) [18]. Unfortunately, it has been found that the immunogenicity in cynomolgus monkeys cannot predict that in humans [18].

In terms of subcutaneous injection, the upper limit of the dosing amount is generally considered to be 1 mL or less than 2 mg kg^{-1} of therapeutic antibodies [19], and ACE910 has a sufficiently high solubility for such a subcutaneous dosage to be obtained with a small injection volume [9]. Thus, we expect that once-weekly subcutaneous administration of ACE910 will provide more aggressive routine prophylaxis aimed at achieving a mild phenotype in hemophilia A patients both without and with FVIII inhibitors.

In conclusion, this study suggests that ACE910 has the potential not only to ameliorate ongoing bleeds, even in patients with FVIII inhibitors, but also to offer a user-friendly and aggressive routine prophylaxis for patients both without and with FVIII inhibitors. ACE910 may provide great benefits to all patients with severe hemophilia A, including pediatric patients and patients with FVIII inhibitors.

Addendum

A. Muto, K. Yoshihashi, M. Takeda, T. Kitazawa, T. Soeda and Y. Kawabe designed and performed the pharmacologic studies. T. Igawa, Y. Sakamoto and K. Haraya designed and performed the pharmacokinetic studies. M. Shima and A. Yoshioka provided advice from the viewpoints of their medical expertise in hemophilia. K. Hattori provided direction and organized the program. A. Muto and T. Kitazawa wrote the manuscript.

Acknowledgements

We thank our colleagues at Chugai Pharmaceutical – T. Matsuura, M. Hiranuma, R. Takemoto, T. Koike, H. Kitamura and T. Houjo for the *in vivo* pharmacologic experiments; Z. Sampei, T. Kojima, T. Wakabayashi, E. Tanaka, K. Esaki, Y. Kikuchi, A. Sakamoto, M. Wada, M. Goto, H. Tsunoda, T. Suzuki, Y. Okuyama-Nishida, A. Harada, M. Funaki, S. Suzuki, T. Toyoda, Y. Higuchi and M. Ijiri for the preparation of test items and the *in vitro* experiments; T. Tachibana for the pharmacokinetic studies; and H. Saito for providing advice for the various experiments.

Disclosure of Conflict of Interests

A. Muto, K. Yoshihashi, T. Kitazawa, T. Soeda, T. Igawa, K. Hattori, M. Takeda, Y. Sakamoto, K. Haraya and Y. Kawabe are employees of Chugai Pharmaceutical, and the first six of these authors are inventors of the patents relating to anti-FIXa/FX bispecific antibodies, all rights for which have been assigned to the company. M. Shima receives consulting honoraria and research support from Chugai Pharmaceutical. A. Yoshioka previously received research support from Chugai Pharmaceutical.

Supporting Information

Additional Supporting Information may be found in the online version of this article:

Table S1. Pharmacokinetic parameters of ACE910 in cynomolgus monkeys.
Fig. S1. Effects of ACE910 or rhFVIII on peak height of thrombin generation triggered by low TF in human FVIII-deficient plasma without FVIII inhibitors.
Fig. S2. SDS-PAGE analysis of rpoFVIII. Purified rpoFVIII (0.95 μg) was analyzed by SDS-PAGE with 4–20% gradient gel under reducing conditions, followed by staining with Coomassie brilliant blue.

Fig. S3. Influence of VIII-2236 on the APTT-shortening activity of rpoFVIII, ACE910 or rhFVIII in human FVIII-deficient plasma. In the absence of VIII-2236, rpoFVIII, ACE910 and rhFVIII concentration-dependently shortened the APTT of human FVIII-deficient plasma.

Fig. S4. Pharmacodynamic study and multiple dosing simulations of rpoFVIII in cynomolgus monkeys.

References

1 Den Uijl IE, Fischer K, van der Bom JG, Grobbee DE, Rosendaal FR, Plug I. Clinical outcome of moderate haemophilia compared with severe and mild haemophilia. *Haemophilia* 2009; **15**: 83–90.

2 Berntorp E, Shapiro AD. Modern haemophilia care. *Lancet* 2012; **379**: 1447–56.

3 Astermark J, Donfield SM, DiMichele DM, Gringeri A, Gilbert SA, Waters J, Berntorp E. A randomized comparison of bypassing agents in hemophilia complicated by an inhibitor: the FEIBA NovoSeven Comparative (FENOC) Study. *Blood* 2007; **109**: 546–51.

4 Hay CR, DiMichele DM. The principal results of the International Immune Tolerance Study: a randomized dose comparison. *Blood* 2012; **119**: 1335–44.

5 Manco-Johnson MJ, Abshire TC, Shapiro AD, Riske B, Hacker MR, Kilcoyne R, Ingram JD, Manco-Johnson ML, Funk S, Jacobson L, Valentino LA, Hoots WK, Buchanan GR, DiMichele D, Recht M, Brown D, Leissinger C, Bleak S, Cohen A, Mathew P. Prophylaxis versus episodic treatment to prevent joint disease in boys with severe hemophilia. *N Engl J Med* 2007; **357**: 535–44.

6 Oldenburg J. Prophylaxis in bleeding disorders. *Thromb Res* 2011; **127**: S14–17.

7 Ragni M, Fogarty P, Josephson N, Neff A, Raffini L, Kessler C. Survey of current prophylaxis practices and bleeding characteristics of children with severe haemophilia A in US haemophilia treatment centres. *Haemophilia* 2012; **18**: 63–8.

8 Kitazawa T, Igawa T, Sampei Z, Muto A, Kojima T, Soeda T, Yoshihashi K, Okuyama-Nishida Y, Saito H, Tsunoda H, Suzuki T, Adachi H, Miyazaki T, Ishii S, Kamata-Sakurai M, Iida T, Harada A, Esaki K, Funaki M, Moriyama C. A bispecific antibody to factors IXa and X restores factor VIII hemostatic activity in a hemophilia A model. *Nat Med* 2012; **18**: 1570–4.

9 Sampei Z, Igawa T, Soeda T, Okuyama-Nishida Y, Moriyama C, Wakabayashi T, Tanaka E, Muto A, Kojima T, Kitazawa T, Yoshihashi K, Harada A, Funaki M, Haraya K, Tachibana T, Suzuki S, Esaki K, Nabuchi Y, Hattori K. Identification and multidimensional optimization of an asymmetric bispecific IgG antibody mimicking the function of factor VIII cofactor activity. *PLoS ONE* 2013; **8**: e57479.

10 Den Uijl IE, Mauser Bunschoten EP, Roosendaal G, Schutgens RE, Biesma DH, Grobbee DE, Fischer K. Clinical severity of haemophilia A: does the classification of the 1950s still stand? *Haemophilia* 2011; **17**: 849–53.

11 Shima M, Matsumoto T, Ogiwara K. New assays for monitoring haemophilia treatment. *Haemophilia* 2008; **14**: 83–92.

12 Srivastava A, Brewer AK, Mauser-Bunschoten EP, Key NS, Kitchen S, Llinas A, Ludlam CA, Mahlangu JN, Mulder K, Poon MC, Street A. Guidelines for the management of hemophilia. *Haemophilia* 2013; **19**: e1–47.

13 Lillicrap D. The future of hemostasis management. *Pediatr Blood Cancer* 2013; **60**: S44–7.

14 Pipe SW. The hope and reality of long-acting hemophilia products. *Am J Hematol* 2012; **87**: S33–9.

15 Collins PW. Personalized prophylaxis. *Haemophilia* 2012; **18**: 131–5.

16 Deng R, Iyer S, Theil FP, Mortensen DL, Fielder PJ, Prabhu S. Projecting human pharmacokinetics of therapeutic antibodies from nonclinical data: what have we learned? *MAbs* 2011; **3**: 61–6.

17 Dong J, Salinger D, Endres C, Gibbs J, Hsu C, Stouch B, Hurh E, Gibbs M. Quantitative prediction of human pharmacokinetics for monoclonal antibodies: retrospective analysis of monkey as a single species for first-in-human prediction. *Clin Pharmacokinet* 2011; **50**: 131–42.

18 Ponce R, Abad L, Amaravadi L, Gelzleichter T, Gore E, Green J, Gupta S, Herzyk D, Hurst C, Ivens IA, Kawabata T, Maier C, Mounho B, Rup B, Shankar G, Smith H, Thomas P, Wierda D. Immunogenicity of biologically-derived therapeutics: assessment and interpretation of nonclinical safety studies. *Regul Toxicol Pharmacol* 2009; **54**: 164–82.

19 Igawa T, Tsunoda H, Kuramochi T, Sampei Z, Ishii S, Hattori K. Engineering the variable region of therapeutic IgG antibodies. *MAbs* 2011; **3**: 243–52.

Molecular Immunology 58 (2014) 132–138

Contents lists available at ScienceDirect

Molecular Immunology

journal homepage: www.elsevier.com/locate/molimm

Crystal structure of a novel asymmetrically engineered Fc variant with improved affinity for FcγRs

F. Mimoto, S. Kadono, H. Katada, T. Igawa *, T. Kamikawa, K. Hattori

Research Division, Chugai Pharmaceutical Co., Ltd., Japan

ARTICLE INFO

Article history:
Received 26 August 2013
Received in revised form
20 November 2013
Accepted 23 November 2013
Available online 14 December 2013

Keywords:
ADCC
Effector function
X-ray structure
FcγR interactions
Fc engineering

ABSTRACT

Enhancing the effector function by optimizing the interaction between Fc and Fcγ receptor (FcγR) is a promising approach to enhance the potency of anticancer monoclonal antibodies (mAbs). To date, a variety of Fc engineering approaches to modulate the interaction have been reported, such as afucosylation in the heavy chain Fc region or symmetrically introducing amino acid substitutions into the region, and there is still room to improve FcγR binding and thermal stability of the C_H2 domain with these approaches. Recently, we have reported that asymmetric Fc engineering, which introduces different substitutions into each Fc region of heavy chain, can further improve the FcγR binding while maintaining the thermal stability of the C_H2 domain by fine-tuning the asymmetric interface between the Fc domain and FcγR. However, the structural mechanism by which the asymmetrically engineered Fc improved FcγR binding remained unclear. In order to elucidate the mechanism, we solved the crystal structure of a novel asymmetrically engineered Fc, asym-mAb23, in complex with FcγRIIIa. Asym-mAb23 has enhanced binding affinity for both FcγRIIIa and FcγRIIa at the highest level of previously reported Fc variants. The structural analysis reveals the features of the asymmetrically engineered Fc in comparison with symmetric Fc and how each asymmetrically introduced substitution contributes to the improved interaction between asym-mAb23 and FcγRIIIa. This crystal structure could be utilized to enable us to design a more potent asymmetric Fc.

1. Introduction

Effector functions including antibody-dependent cell-mediated cytotoxicity (ADCC) and antibody-dependent cell-mediated phagocytosis (ADCP) significantly contribute to the efficacy and potency of anticancer therapeutic monoclonal antibodies (mAbs) (Scott et al., 2012). According to cumulative evidence, the potency of the antibodies can be enhanced by improving the binding affinity for Fcγ receptors (FcγRs), which are expressed on effector cells such as NK cells and macrophages (Scott et al., 2012). There have been a number of reports about engineering the heavy chain Fc region to improve the binding affinity for FcγRs by methods such as afucosylation of the N-linked glycan attached to Asn297 (Shields et al., 2002; Shinkawa et al., 2003) or symmetrically introducing amino acid substitutions into the heavy chain Fc region with or without the N-linked glycan attached to Asn297 (Green et al., 2002; Jung et al., 2010; Lazar et al., 2006; Richards et al., 2008; Saxena et al., 2009; Strohl, 2009; Stuchbury et al., 2007). These engineered Fc variants enhanced the binding affinity for FcγRIIa and FcγRIIIa or improved the ratio of activating FcγR binding to inhibitory FcγR binding (A/I ratio), which resulted in enhanced ADCP and ADCC activity. However, these symmetric Fc engineering approaches cannot achieve a high affinity for both FcγRIIIa high- and low-affinity allotypes and improve the A/I ratio and maintain thermal stability of the C_H2 domain at the same time. Recently, we have reported a novel potent Fc variant that maximized the effector function by an asymmetric Fc engineering approach (Mimoto et al., 2013). We introduced different amino acid substitutions into each heavy chain Fc region in an asymmetric manner to optimize the asymmetric interface between the Fc region and FcγR to successfully design an asymmetric Fc variant that had the highest affinity for both FcγRIIIa high- and low-affinity allotypes, had superior or at least comparable ADCC with the previously reported symmetrically engineered antibody, and had the

Abbreviations: ADCC, antibody-dependent cell-mediated cytotoxicity; ADCP, antibody-dependent cell-mediated phagocytosis; A/I ratio, activating FcγR binding to inhibitory FcγR binding; asym-mAb23, a novel asymmetrically engineered Fc; FcγR, Fcγ receptor; mAb, monoclonal antibody; PDB, Protein Data Bank; PBMC, peripheral blood mononuclear cells; rms, root-mean-square; SPR, surface plasmon resonance.

* Corresponding author at: 1-135 Komakado, Gotemba, Shizuoka, Japan. Tel.: +81 550 87 6734; fax: +81 550 87 5326.
E-mail address: igawa@chugai-pharm.co.jp (T. Igawa).

0161-5890
http://dx.doi.org/10.1016/j.molimm.2013.11.017

highest A/I ratio. However, the mechanism by which the asymmetrically introduced substitutions contribute to the improved FcγR binding remained unclear.

Here we report a crystal structure of the novel asymmetrically engineered Fc variant, asym-mAb23, in complex with FcγRIIIa. In contrast to the previously reported asymmetrically engineered Fc variant (Mimoto et al., 2013), asym-mAb23 enhanced the binding affinity for both FcγRIIIa and FcγRIIa to a level comparable with that of previously reported Fc variants for both FcγRIIIa (Lazar et al., 2006) and FcγRIIa (Richards et al., 2008). This is the first report describing the structure of asymmetrically engineered Fc variant with increased affinity for FcγRs. This crystal structure sheds light on the molecular mechanisms behind the interaction between FcγRs and asymmetrically engineered Fc variant, which will be beneficial for further designing a more potent asymmetric Fc variant.

2. Materials and methods

2.1. Preparation of antibodies and FcγRs

The antibody variants used in the experiments were expressed transiently in FreeStyle™ 293 cells (Life Technologies) transfected with plasmids encoding heavy and light chains and purified from culture supernatants using rProtein A Sepharose 4 Fast Flow or rProtein G Sepharose 4 Fast Flow (GE Healthcare), as previously described (Mimoto et al., 2013). Asymmetrically engineered Fc variants contained knobs-into-holes substitutions, Y349C/T366W in one of the heavy chains and D356C/T366S/L368A/Y407V in the other, to facilitate heterodimerization (Klein et al., 2012).

The FcγRs used in the experiments were also expressed transiently in FreeStyle™ 293 cells (Life Technologies), as previously described (Mimoto et al., 2013).

2.2. Surface plasmon resonance (SPR) analysis

The kinetic analysis of antibody variants for human FcγRs was monitored by SPR analysis using a Biacore 4000 instrument (GE Healthcare), as previously described (Mimoto et al., 2013). A recombinant protein A/G (Thermo Scientific) was immobilized on a CM5 sensor chip (GE Healthcare) using a standard primary amine-coupling protocol. HBS-EP+ (GE Healthcare) was used as the running buffer. Antibody variants were captured on the chip, followed by injection of FcγRs. The assay concentrations are from 0.001 nM to 16 nM for FcγRI, from 0.49 nM to 2000 nM for FcγRIIa, from 2.0 nM to 8000 nM for FcγRIIb, and from 0.12 nM to 2000 nM for FcγRIIIa. The experiments were conducted independently, in triplicate.

2.3. ADCC assay

Cytotoxicity of antibody against antigen A was measured using a standard calcein-AM release assay, as previously described (Mimoto et al., 2013). We used DLD-1 cells expressing tumor antigen A as target cells for the assay. Peripheral blood mononuclear cells (PBMC) were purified from whole human blood of healthy donors and used as effector cells. Antibody solution was mixed with the target cells (1×10^4 cells) and then the effector cells were added to the solution at a ratio of 50:1 PBMC to target cells.

2.4. Preparation of Fc fragments and FcγRIIIa for crystallization

We cloned a recombinant Fc fragment of asym-mAb23, Fc (asym-mAb23), corresponding to the heavy chain residues from 216 (EU numbering) to C-terminus for the crystallization. Cys220 was replaced with Ser so that the free cysteine would not make disulfide bonds. FcγRIIIa with N35Q, N71Q, and N166Q substitutions was prepared as previously described (Ferrara et al., 2011). The complex of Fc (asym-mAb23) and FcγRIIIa was prepared by mixing the Fc fragment with a little excess of FcγRIIIa, and purified by size exclusion chromatography.

Table 1
Data collection and refinement statistics.

	Fc (asym-mAb23)-FcγRIIIa
Data collection	
Space group	$P2_1$
Cell dimensions	
a, *b*, *c* (Å)	75.03, 72.49, 163.48
α, β, γ (°)	90, 91.15, 90
Resolution (Å)	2.78 (2.85–2.78)[a]
Rsym	0.078 (0.614)
$I/\sigma I$	13.9 (2.1)
Completeness (%)	98.1 (98.2)
Redundancy	3.8 (3.4)
Refinement	
Resolution (Å)	25–2.78
No. reflections	41,404
Rwork/Rfree	23.6/27.4
No. atoms	9961
Average *B* factors	54.7
rms deviations	
Bond lengths (Å)	0.005
Bond angles (°)	0.962
Ramachandran statistics	
Most favored (%)	96.4
Additional allowed (%)	3.3
Disallowed (%)	0.3

Number of crystals for each structure is one.
[a] Values in parentheses are for highest-resolution shell.

2.5. Crystallization

Diffraction-quality crystals were obtained by 1:1 mixing of the 10 mg/ml protein complex of Fc (asym-mAb23) and FcγRIIIa with 0.1 M Bis–Tris pH 6.25, 0.2 M sodium iodide, and 14.5% PEG 3350 in hanging drop vapor diffusion setups with streak seeding at 20 °C.

2.6. Data collection

For data collection, crystals were flash frozen at 95 K in precipitant solution containing 20% ethylene glycol. Diffraction data to 2.78 Å were collected using the Photon Factory beamline BL-NE3A. Data were processed with Xia2 (Winter, 2010), XDS Package (Kabsch, 2010), and Scala (Evans, 2006).

2.7. Structure determination

The crystals belong to the space group $P2_1$ with cell parameters of $a = 75.03$ Å, $b = 72.49$ Å, $c = 163.48$ Å, and $\beta = 91.15°$. The structure was determined by molecular replacement with PHASER (McCoy et al., 2007) using the structure of IgG1-Fc fragment, Fc (IgG1), and FcγRIIIa complex (PDB: 3SGJ) as a search model. The asymmetric unit contains two 1:1 complexes of Fc (asym-mAb23) and FcγRIIIa. A model was built with the program Coot (Emsley et al., 2010) and refined with the program REFMAC5 (Murshudov et al., 2011). Data collection and refinement statistics are summarized in Table 1. When numbering, the standard EU numbering was used for the heavy chain Fc region. For FcγRIIIa, the FcγRII numbering system was used like PDB entry 1E4K (Sondermann et al., 2000). To convert to standard NCBI numbering, it is necessary to add three to the amino acid residue number of FcγRIIIa. All graphical presentations were prepared with PyMOL (DeLano, 2002). Superposition and calculation of root-mean-square (rms) differences were done by LSQKAB (Kabsch, 1976) in CCP4 program suite. Coordinates and

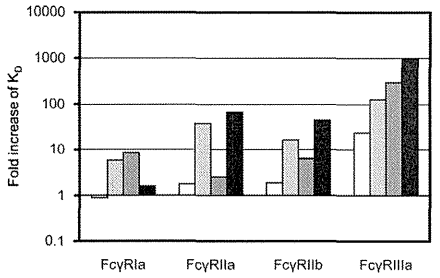

Fig. 1. Affinity analysis of antibody Fc variants for FcγRs by SPR. Fold increase of the binding affinity for each FcγR was calculated by the equation, K_D (control)/K_D (Fc variants). As the control, the K_D value of IgG1 is used for afucosyl mAb and the K_D value of IgG1 with knobs-into-holes substitutions is used for ADE variant, DLE variant, and asym-mAb23. The K_D used for the calculation is the mean value of the triplicate independent experiments. Bar colors are as follows: white, afucosyl mAb; light gray, ADE variant; dark gray, DLE variant; and black, asym-mAb23.

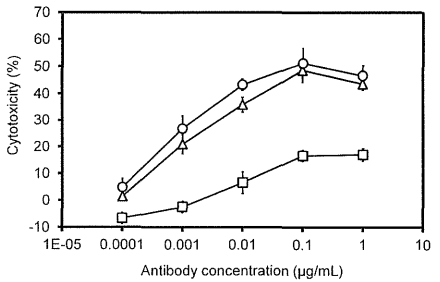

Fig. 2. ADCC of antibody Fc variants. ADCC of IgG1, afucosyl mAb, and asym-mAb23 was determined by percent lysis of DLD-1 cells expressing opsonized tumor antigen A at varying concentrations of antibody Fc variants to tumor antigen A, using PBMC as effector cells. Square, IgG1; triangle, afucosyl mAb; and circle, asym-mAb23. Mean ± S.D. of triplicate wells.

structure factors have been deposited at the Protein Data Bank (PDB) with the codes 3WN5.

3. Results and discussion

3.1. SPR analysis of FcγR binding affinity and ADCC

We optimized Fc variants asymmetrically to increase the binding affinity for both FcγRIIIa and FcγRIIa by utilizing the comprehensive mutagenesis in FcγR binding sites of the C_H2 domain, as we explained in our previous report (Mimoto et al., 2013). As a result, we obtained a variant, asym-mAb23, by introducing L234Y/L235Y/G236W/S239M/H268D/S298A/A327D substitutions into one heavy chain Fc region and D270E/K326D/A330K/K334E substitutions into the other heavy chain Fc region, which enhanced binding affinity for FcγRIIa by 67-fold and for FcγRIIIa by 1000-fold compared with wild-type mAb, as shown in Fig. 1. The kinetic parameters (k_a, k_d, and K_D) of each antibody are shown in supplementary Table 1 and representative sensorgrams are depicted in supplementary Fig. 1. The FcγRIIa binding affinity of asym-mAb23 was comparable with that of the most potent symmetrically engineered Fc variant with G236A/S239D/I332E (ADE) substitutions (Fig. 1). The FcγRIIIa binding affinity of asym-mAb23 was also comparable with that of the most potent symmetrically engineered Fc variant with S239D/A330L/I332E (DLE) substitutions (Fig. 1). Asym-mAb23 achieved the most potent binding to FcγRIIa and FcγRIIIa at the same time, which could not be achieved by symmetrically engineered Fc variants.

The ADCC activity of asym-mAb23 was compared with that of wild-type IgG1 and afucosyl mAb using human PBMC. Asym-mAb23 showed greater ADCC activity than IgG1 and slightly higher or comparable activity with afucosyl mAb (Fig. 2).

3.2. Overall structure of the asymmetrically engineered Fc variant in complex with FcγRIIIa

The 2.78 Å resolution crystal structure was determined for the complex of Fc (asym-mAb23) with human FcγRIIIa. In an asymmetric unit of the crystal, two 1:1 complexes of Fc (asym-mAb23) and FcγRIIIa, complex 1 (Fig. 3A) and complex 2 (Fig. 3B), were observed. In both of the complexes, Fc (asym-mAb23) binds to FcγRIIIa at the lower hinge region and C_H2 domains, as observed in the previously reported crystal structures of Fc and FcγR complexes (Ferrara et al., 2011; Sondermann et al., 2000; Radaev et al., 2001; Ramsland et al., 2011), one of which (PDB ID: 3SGJ) is shown in Fig. 3C. The rms difference of the whole main chain atoms between the two complexes in the asymmetric unit is slightly large, at 2.03 Å. However, the rms difference of the main chain atoms in the binding region consisting of domain 2 of FcγRIIIa and the C_H2 domains of the Fc (asym-mAb23) is 1.60 Å.

Theoretically, an asymmetrically engineered Fc variant is able to interact with FcγRs in two different orientations, since the Fc region recognizes the FcγR asymmetrically from each side of the region. However, in this crystal structure, Fc (asym-mAb23) has the same asymmetric binding orientation toward FcγRIIIa in each complex. The chain of Fc (asym-mAb23) with D270E/K326D/A330K/K334E substitutions binds to the side of FcγRIIIa that comprises W87, W110, and K158, and the other chain with L234Y/L235Y/G236W/S239M/H268D/S298A/A327D substitutions binds to the other side of FcγRIIIa that comprises K117, Y129, and H131. This result suggests that asym-mAb23 *recognized FcγRIIIa or FcγRIIa only in a favorable manner.*

Between the FcγRIIIa and Fc (IgG1) complex (PDB ID: 3SGJ) and complex 1 of the Fc (asym-mAb23) and FcγRIIIa in this crystal, rms difference of the main chain atoms in the binding region is 1.65 Å and between the FcγRIIIa and Fc (IgG1) complex and complex 2, that is 1.03 Å. This result indicates that the protein structure of complex 2 is more similar to the FcγRIIIa and Fc (IgG1) complex than complex 1 is. Most of the key interactions observed between Fc (IgG1) and FcγRIIIa are conserved. For example, P329 in the C_H2-A of complex 1 and complex 2 forms tight hydrophobic interactions with W87 and W110 of FcγRIIIa, and D265 in the C_H2-B of both of the complexes forms a potent electrostatic interaction with K117 of FcγRIIIa in a similar way to the reported FcγRIIIa and Fc (IgG1) complex structures.

The structure of the carbohydrate chains attached to N159 of FcγRIIIa is different between the complexes. In complex 1, the electron density of five branched sugar moieties of FcγRIIIa was observed, similar to that seen in the FcγRIIIa and Fc (IgG1) complex (Ferrara et al., 2011), and those sugar moieties are involved in the interaction with a carbohydrate chain of Fc (asym-mAb23). On the other hand, in complex 2, the electron density of only three sugar moieties was observed, and these are not involved in the interaction with Fc (asym-mAb23).

*These differences observed in the two complexes in an asym*metric unit may suggest that Fc (asym-mAb23) could bind to

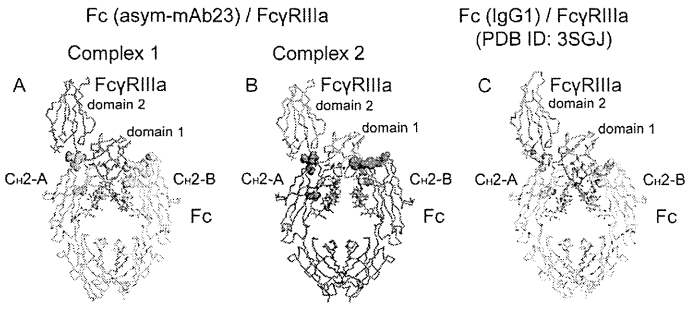

Fig. 3. The overall structure of Fc (asym-mAb23) and FcγRIIIa complexes in the asymmetric unit in comparison with a known Fc (IgG1) and FcγRIIIa complex. (A) The Cα trace of Fc (asym-mAb23) and FcγRIIIa complex 1. Complex 1 consists of two Fc fragments and FcγRIIIa. The Fc fragment with D270E/K326D/A330K/K334E substitutions is shown in green (Fc fragment A) and the other Fc fragment with L234Y/L235Y/G236W/S239M/H268D/S298A/A327D substitutions in cyan (Fc fragment B). FcγRIIIa is shown in magenta. (B) The Cα trace of Fc (asym-mAb23) and FcγRIIIa complex 2. Complex 2 consists of two Fc fragments and FcγRIIIa. Fc fragment A is shown in red and Fc fragment B in blue. FcγRIIIa is shown in orange. (C) The Cα trace of a known Fc (IgG1) and FcγRIIIa complex (PDB ID: 3SGJ). The complex consists of two Fc fragments and FcγRIIIa. Fc fragment A and B are corresponding to those of Fc (asym-mAb23) and FcγRIIIa complex. Both of the Fc fragments are shown in yellow and FcγRIIIa in gray. The substituted residues in Fc (asym-mAb23) and the corresponding residues in Fc (IgG1) are shown by spheres. The carbohydrate chains of the heavy chain Fc region and of FcγRIIIa are shown by sticks.

FcγRIIIa in several different manners, although the difference may also be influenced by the crystal packing environment.

3.3. Structural implication of the contribution of each substitution of asym-mAb23 to the improved FcγRIIIa binding

The interfaces between the C_H2-A of Fc (asym-mAb23) and FcγRIIIa in complexes 1 and 2 are depicted in Fig. 4. In the C_H2-A of Fc (asym-mAb23), four substitutions, D270E/K326D/A330K/K334E, are introduced. Structural superposition of the C_H2-A of FcγRIIIa and Fc (IgG1) complex (PDB ID: 3SGJ) with the C_H2-A of complex 1 and complex 2 results in 0.75 Å and 0.67 Å rms differences of the main chain atoms, respectively. These substitutions do not affect the main chain structure of the C_H2-A, but affect the side chain structures around the residues.

In the C_H2-A, all of the substituted residues are charged, which would improve long-range electrostatic interactions with FcγRIIIa. In both of the complexes in this crystal, D270E would optimize the electrostatic interaction with K111 of FcγRIIIa (Fig. 4A and B); K326D would change electrostatic repulsions with K19 of FcγRIIIa to electrostatic attractions (Fig. 4A and B); A330K would make a new electrostatic interaction with E163 of FcγRIIIa and enhance van der Waals contacts with I85 of FcγRIIIa (Fig. 4A and B). The conformation of these side chain residues and the distances of ion-pairs are slightly different between the two complexes. This might reflect the weakness of these long-range electrostatic interactions. The contribution of K334E to the enhancement of FcγRIIIa binding seems mediated by a different mechanism from those of other substitutions. K334E makes a hydrogen bond with the carbohydrate chain attached to N297 of the C_H2-A of complex 1 and complex 2 (Fig. 4C and D), which could result in changing and stabilizing the carbohydrate chain conformation. The carbohydrate chain of the heavy chain Fc region is known to be critical for the binding to FcγRs (Ferrara et al., 2011; Krapp et al., 2003), so modifying and stabilizing the carbohydrate chain conformation could contribute to enhancing the binding activity to FcγRs.

The interfaces between the C_H2-B of Fc (asym-mAb23) and FcγRIIIa in complex 1 and 2 are depicted in Fig. 5. The substitutions introduced into the C_H2-B domain of Fc (asym-mAb23), L234Y/L235Y/G236W/S239M/H268D/S298A/A327D, affect not only the side chain structures around the substituted residues, but also the main chain structure of the lower hinge region, loop 265–273, and loop 325–331. Structural superposition of the C_H2-B of complex 1 with the C_H2-B of FcγRIIIa and Fc (IgG1) complex (PDB ID: 3SGJ) results in 1.13 Å rms difference of the main chain atoms. The lower hinge and some of the loops show larger deviations; with regard to residues 235–237 in the lower hinge, loop 265–273, and loop 325–331, the largest rms differences of the main chain are observed at Y235, P271, and D327, respectively, and their values are 4.85 Å, 2.18 Å, and 3.91 Å, respectively. Similar lower hinge and loop deviations are observed in the C_H2-B of complex 2. Structural superposition of the C_H2-B of complex 2 in this crystal structure with the C_H2-B of FcγRIIIa and Fc (IgG1) complex (PDB ID: 3SGJ) results in 0.77 Å rms difference of the main chain atoms. On the other hand, with regard to residues 235–237 in the lower hinge, loop 265–273, and loop 325–331, the largest rms differences of the main chain are observed at the same residues as in the C_H2-B of complex 1 (Y235, P271, and D327, respectively) and their values are 3.00 Å, 2.59 Å, and 2.27 Å, respectively. Compared with the FcγRIIIa and Fc (IgG1) complex, the electron density of the lower hinge is not well observed, especially in the C_H2-B. In both of the complexes, the conformation of L234Y and the preceding residues are not defined.

Some structural differences are observed around L235Y and G236W between the C_H2-B of complex 1 and complex 2; the main difference being that the two residues are interchanged between the two complexes and adopt conformations that are both different from that of the FcγRIIIa and Fc (IgG1) complex. In complex 1, W236 is involved in a hydrophobic core of the C_H2-B domain with P238, L328, V323, and I332 of the same domain, which can shift loop 325–331 considerably from the corresponding loop observed in the Fc (IgG1) and FcγRIIIa complex. L235Y of C_H2-B in complex 1 forms a van der Walls contact with K117 and edge-to-face interactions with H116 and H132 of FcγRIIIa (Fig. 5A). On the other hand, in the C_H2-B domain of complex 2, W236 is not involved in the hydrophobic core of the same domain, as is observed in the C_H2-B of complex 1. Instead, it forms a stacking interaction with H116 of FcγRIIIa, with L235Y of C_H2 making contact with L328 and P329 in the same domain (Fig. 5B). In complex 1, H268D would make a new electrostatic interaction with K128 of FcγRIIIa. Moreover,

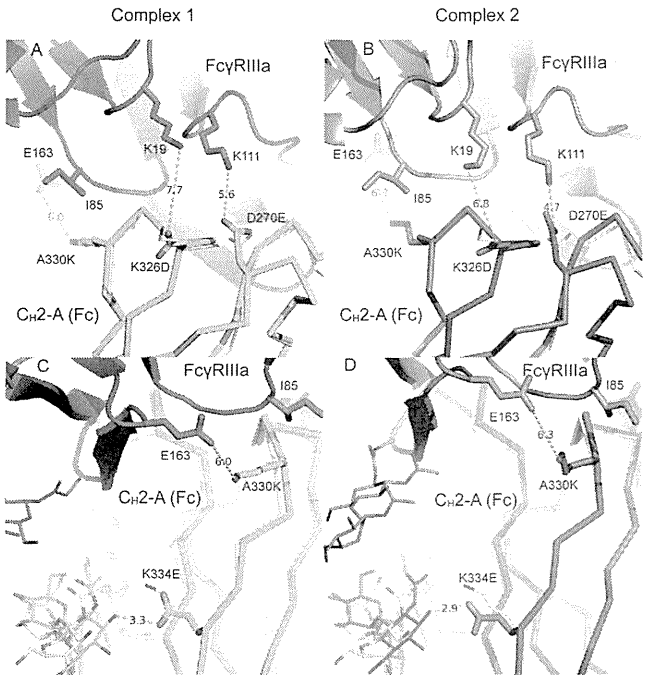

Fig. 4. The binding interfaces between the C_H2-A of Fc (asym-mAb23) and FcγRIIIa in complexes 1 and 2. The binding interfaces between the C_H2-A (shown in green) of Fc (asym-mAb23) and FcγRIIIa (shown in magenta) in complex 1 and the corresponding binding interfaces between the C_H2-A (shown in red) of Fc (asym-mAb23) and FcγRIIIa (shown in orange) in complex 2 are depicted in (A) and (B), respectively. The binding interfaces of another angle between the C_H2-B of Fc (asym-mAb23) and FcγRIIIa in complex 1 and 2 are depicted in (C) and (D), respectively. The corresponding C_H2 domain structure of the Fc (IgG1) (PDB ID: 3SGJ) (shown in yellow) is superimposed on the C_H2-A domain of Fc (asym-mAb23).

H268D may change the side chain conformation of neighboring residues E269 and E294 in C_H2-B of complex 1 and thus may contribute to optimizing the electrostatic interactions of those residues with K128 and K125 of FcγRIIIa, respectively (Fig. 5A). On the other hand, in complex 2, the conformations of K125 and K128 of FcγRIIIa are not completely defined because their electron density is poor (Fig. 5B), and this suggests that the long-range electrostatic interactions related to H268D might be weaker than others. As shown in Fig. 5A and B, in complex 1 and complex 2, S298A reduces the size of the side chain of the residue, which might result in optimizing a van der Waals interaction with FcγRIIIa to achieve closer binding in the whole binding surface of the C_H2-B in the Fc region. S239M makes new van der Waals contacts with K117 of FcγRIIIa and with the carbohydrate chain attached to N297 of the C_H2-B of complex 1 and complex 2 (Fig. 5C and D). This mutation might also contribute to stabilizing the carbohydrate chain conformation and enhancing the binding activity for FcγRs. The direct contribution of A327D to the improved binding affinity to FcγRIIIa is not obvious from the structural analysis, because even the nearest possible partner residues in FcγRIIIa, K117 and K128, are too far (approximately 14 Å) to form effective electrostatic interactions in either of the complexes. In the Fc (IgG1) and FcγRIIIa complex, A327 is located close enough to D270, so A327D might introduce an electrostatic repulsion with D270 to trigger the conformational change of loop 265–273 and loop 324–331. This would be the reason why the side chain of D270 of Fc (asym-mAb23) forms a hydrogen bond with the side chain of H131 of FcγRIIIa, which was not observed in Fc (IgG1) bound to FcγRIIIa. As a result, this substitution may contribute to the improvement of binding activity to FcγRIIIa.

As described above, the X-ray crystal structure suggests that the contribution of each substitution to the binding affinity is moderate. This is indicated by the distant electrostatic interactions (4–9 Å) observed in the structure and is also suggested by the fact that two types of binding mode were observed in some parts of the interface between Fc (asym-mAb23) and FcγRIIIa. Some of the substitutions seem to contribute to the binding enhancement indirectly by stabilizing the carbohydrate chains of the heavy chain Fc region or changing the loop conformation. Nevertheless, asym-mAb23 showed approximately 1000-fold enhanced binding affinity for FcγRIIIa. This would be achieved by the cumulative effect of these weak direct effects and the indirect effects caused by the stabilization of the carbohydrate chain conformation and the change of loop conformation.

A previous report suggested the difficulty of maintaining the high stability and improving the binding affinity for FcγRs at the same time by protein-engineering of Fc region (Oganesyan et al.,

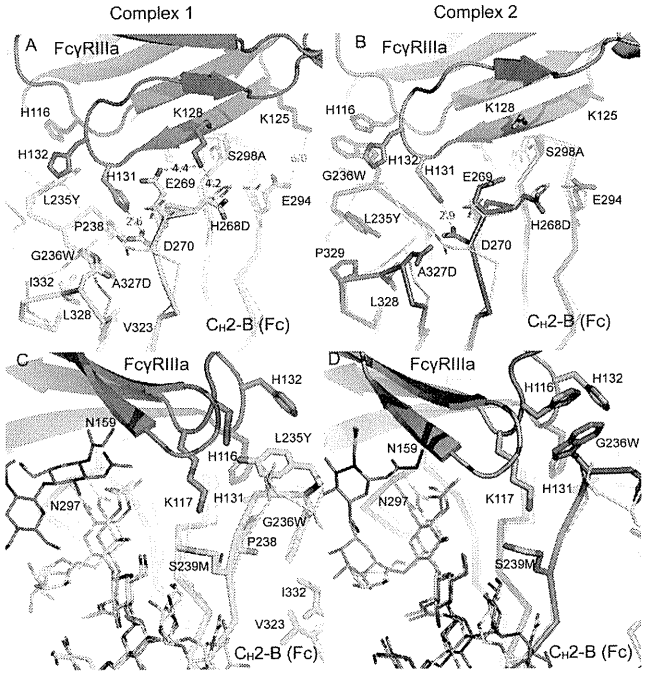

Fig. 5. The binding interfaces between the C_H2-B of Fc (asym-mAb23) and FcγRIIIa in complexes 1 and 2. The binding interfaces between the C_H2-B (shown in cyan) of Fc (asym-mAb23) and FcγRIIIa (shown in magenta) in complex 1 and the corresponding binding interfaces between the C_H2-B (shown in blue) of Fc (asym-mAb23) and FcγRIIIa (shown in orange) in complex 2 are depicted in (A) and (B), respectively. The binding interfaces of another angle between the C_H2-B of Fc (asym-mAb23) and FcγRIIIa in complex 1 and 2 are depicted in (C) and (D), respectively. The corresponding C_H2 domain structure of the Fc (IgG1) (PDB ID: 3SGJ) (shown in yellow) is superimposed on the C_H2-B domain of Fc (asym-mAb23).

2008). However, asymmetric Fc engineering can minimize the number of total substitutions in the Fc region, as we discussed in the previous report (Mimoto et al., 2013). In other words, asymmetric Fc engineering enables us to utilize a large number of substitutions and to exploit their contributions, even those conferring weak enhancement.

4. Conclusion

This is the first report describing the crystal structure of an asymmetrically engineered Fc variant in complex with FcγRIIIa. The structural analysis suggested that the asymmetrically introduced substitutions fine-tuned the interaction in each interface between the C_H2 domain and FcγRIIIa. Thus, the application of asymmetric Fc engineering would enable us to optimize the interaction in each interface independently and thus design Fc variants with a variety of FcγRs binding profiles more precisely. This crystal structure could be utilized when we design a more potent asymmetric Fc variant.

Acknowledgments

We thank our colleagues at Chugai Research Institute for Medical Science, Inc. and Chugai Pharmaceutical Co., Ltd., M. Fujii, Y. Nakata, A. Maeno, and S. Masujima for antibody generation; M. Saito for carrying out SPR analysis; and A. Sakamoto, M. Okamoto, and M. Endo for carrying out preparation of FcγRs. This work was fully supported by Chugai Pharmaceutical Co., Ltd.

Appendix A. Supplementary data

Supplementary data associated with this article can be found, in the online version, at http://dx.doi.org/10.1016/j.molimm.2013.11.017.

References

DeLano, W.L., 2002. The PyMOL Molecular Graphics System. Schrodinger, LLC. Palo Alto, CA.
Emsley, P., et al., 2010. Features and development of Coot. Acta Crystallogr. 66D, 486–501.
Evans, P., 2006. Scaling and assessment of data quality. Acta Crystallogr. 62D, 72–82.
Ferrara, C., et al., 2011. Unique carbohydrate–carbohydrate interactions are required for high affinity binding between FcgammaRIII and antibodies lacking core fucose. Proc. Natl. Acad. Sci. U. S. A. 108, 12669–12674.
Green, S.K., et al., 2002. Disruption of cell–cell adhesion enhances antibody-dependent cellular cytotoxicity: Implications for antibody-based therapeutics of cancer. Cancer Res. 62, 6691–6696.

Jung, S.T., et al., 2010. Aglycosylated IgG variants expressed in bacteria that selectively bind FcgammaRI potentiate tumor cell killing by monocyte-dendritic cells. Proc. Natl. Acad. Sci. U. S. A. 107, 604–609.
Kabsch, W., 1976. A solution for the best rotation to relate two sets of vectors. Acta Crystallogr. A 32, 922–923.
Kabsch, W., 2010. XDS. Acta Crystallogr. 66D, 125–132.
Klein, C., et al., 2012. Progress in overcoming the chain association issue in bispecific heterodimeric IgG antibodies. MAbs 4, 653–663.
Krapp, S., et al., 2003. Structural analysis of human IgG Fc glycoforms reveals a correlation between glycosylation and structural integrity. J. Mol. Biol. 325, 979–989.
Lazar, G.A., et al., 2006. Engineered antibody Fc variants with enhanced effector function. Proc. Natl. Acad. Sci. U. S. A. 103, 4005–4010.
McCoy, A.J., et al., 2007. Phaser crystallographic software. J. Appl. Crystallogr. 40, 658–674.
Mimoto, F., et al., 2013. Novel asymmetrically engineered antibody Fc variant with superior FcγR binding affinity and specificity compared with afucosylated Fc variant. MAbs 5, 229–236.
Murshudov, G.N., et al., 2011. REFMAC5 for the refinement of macromolecular crystal structures. Acta Crystallogr. 67D, 355–367.
Oganesyan, V., et al., 2008. Structural characterization of a mutated, ADCC-enhanced human Fc fragment. Mol. Immunol. 45, 1872–1882.
Radaev, S., et al., 2001. The structure of a human type III Fcgamma receptor in complex with Fc. J. Biol. Chem. 276, 16469–16477.
Ramsland, P.A., et al., 2011. Structural basis for Fc gammaRIIa recognition of human IgG and formation of inflammatory signaling complexes. J. Immunol. 187, 3208–3217.
Richards, J.O., et al., 2008. Optimization of antibody binding to FcgammaRIIa enhances macrophage phagocytosis of tumor cells. Mol. Cancer Ther. 7, 2517–2527.
Sazinsky, S.L., et al., 2008. Aglycosylated immunoglobulin G1 variants productively engage activating Fc receptors. Proc. Natl. Acad. Sci. U. S. A. 105, 20167–20172.
Scott, A.M., et al., 2012. Monoclonal antibodies in cancer therapy. Cancer Immun. 12, 14.
Shields, R.L., et al., 2002. Lack of fucose on human IgG1 N-linked oligosaccharide improves binding to human Fcgamma RIII and antibody-dependent cellular toxicity. J. Biol. Chem. 277, 26733–26740.
Shinkawa, T., et al., 2003. The absence of fucose but not the presence of galactose or bisecting N-acetylglucosamine of human IgG1 complex-type oligosaccharides shows the critical role of enhancing antibody-dependent cellular cytotoxicity. J. Biol. Chem. 278, 3466–3473.
Sondermann, P., et al., 2000. The 3.2-A crystal structure of the human IgG1 Fc fragment-FcgammaRIII complex. Nature 406, 267–273.
Stavenhagen, J.B., et al., 2007. Fc optimization of therapeutic antibodies enhances their ability to kill tumor cells in vitro and controls tumor expansion in vivo via low-affinity activating Fcgamma receptors. Cancer Res. 67, 8882–8890.
Winter, G., 2010. xia2: an expert system for macromolecular crystallography data reduction. J. Appl. Crystallogr. 43, 186–190.

Protein Engineering, Design & Selection vol. 26 no. 10 pp. 589–598, 2013
Published online June 5, 2013 doi:10.1093/protein/gzt022

Engineered antibody Fc variant with selectively enhanced FcγRIIb binding over both FcγRIIa^{R131} and FcγRIIa^{H131}

F.Mimoto, H.Katada, S.Kadono, T.Igawa[1], T.Kuramochi, M.Muraoka, Y.Wada, K.Haraya, T.Miyazaki and K.Hattori

Research Division, Chugai Pharmaceutical Co., Ltd., Gotemba, Shizuoka, Japan

[1]To whom correspondence should be addressed.
E-mail: igawatmy@chugai-pharm.co.jp

Received November 22, 2012; revised April 24, 2013; accepted May 8, 2013

Edited by Dario Neri

Engaging inhibitory FcγRIIb by Fc region has been recently reported to be an attractive approach for improving the efficacy of antibody therapeutics. However, the previously reported S267E/L328F variant with enhanced binding affinity to FcγRIIb, also enhances binding affinity to FcγRIIa^{R131} allotype to a similar degree because FcγRIIb and FcγRIIa^{R131} are structurally similar. In this study, we applied comprehensive mutagenesis and structure-guided design based on the crystal structure of the Fc/FcγRIIb complex to identify a novel Fc variant with selectively enhanced FcγRIIb binding over both FcγRIIa^{R131} and FcγRIIa^{H131}. This novel variant has more than 200-fold stronger binding affinity to FcγRIIb than wild-type IgG1, while binding affinity to FcγRIIa^{R131} and FcγRIIa^{H131} is comparable with or lower than wild-type IgG1. This selectivity was achieved by conformational change of the C_H2 domain by mutating Pro to Asp at position 238. Fc variant with increased binding to both FcγRIIb and FcγRIIa induced platelet aggregation and activation in an immune complex form *in vitro* while our novel variant did not. When applied to agonistic anti-CD137 IgG1 antibody, our variant greatly enhanced the agonistic activity. Thus, the selective enhancement of FcγRIIb binding achieved by our Fc variant provides a novel tool for improving the efficacy of antibody therapeutics.

Keywords: antibody engineering/FcγRIIb/Fc engineering/inhibitory FcγR/platelet activation

Introduction

IgG-based monoclonal antibodies (mAbs) have become important therapeutic options for numerous diseases (Brekke and Sandlie, 2003; Maggon, 2007). Fcγ receptors (FcγR)-dependent cytotoxicity plays an important role in the antitumor activity of mAbs for cancer immunotherapy (Nimmerjahn and Ravetch, 2012).

Several works describe engineering the Fc region to enhance the effector function of mAbs by increasing the binding affinity for active FcγRs (FcγRIa, FcγRIIa and FcγRIIIa) with amino acid substitutions. For example, antibodies engineered to have increased binding affinity for FcγRIIIa exhibited superior *in vitro* ADCC activity and *in vivo* antitumor activity compared with wild-type mAbs (Stavenhagen *et al.*, 2007; Zalevsky *et al.*, 2009). In addition to protein engineering, glyco-engineered tumor-specific mAbs with afucosylated N-linked oligosaccharides at Asn297 in the Fc region showed increased binding affinity for human FcγRIIIa and mouse FcγRIV, which resulted in enhancing the therapeutic activity in mouse models (Nimmerjahn and Ravetch, 2005; Mossner *et al.*, 2010).

In contrast to these activating FcγRs that function as immunostimulatory receptors, inhibitory FcγRIIb is reported to function as an immunomodulatory receptor (Li and Ravetch, 2011; White *et al.*, 2011). The inhibitory receptor FcγRIIb is the only IgG Fc receptor expressed on B-cells and plays a critical role in regulating B-cell homeostasis (Heyman, 2003; Nimmerjahn and Ravetch, 2008). Immune complexes (ICs) coengage FcγRIIb and B-cell receptor (BCR) and then selectively suppress B-cells that recognize cognate antigen (Heyman, 2003). FcγRIIb also regulates other B-cell stimulators that amplify B-cell proliferation and differentiation and suppresses the expression of costimulatory molecules (Leibson, 2004; Crowley *et al.*, 2009).

FcγRIIb also plays an inhibitory role in a homeostatic checkpoint of dendritic cells (DCs) for inducing tolerance or immunity by ICs, in contrast to FcγRIIa. While ligation of FcγRIIa led to DC maturation, targeting FcγRIIb alone did not activate DCs (Boruchov *et al.*, 2005). FcγRIIb on DCs induced peripheral tolerance by inhibiting antigenic processing and DC activation to suppress T-cell activation (Desai *et al.*, 2007).

Besides these inhibitory effects of FcγRIIb, several groups have recently reported that FcγRIIb enhances the agonistic activity of anti-tumor necrosis factor receptor (TNFR) superfamily antibody by working as a scaffold (White *et al.*, 2013). Proliferation of antigen-specific T-cells induced by anti-CD40 antibodies was abrogated in FcγRIIb-deficient mice (White *et al.*, 2011; Li and Ravetch, 2012). Anti-death receptor 5 (DR5) agonist antibody also required FcγRIIb to exert its agonistic activity and initiate apoptosis in lymphoma cells (Wilson *et al.*, 2011). The FcγRIIb-expressing cells are considered to work as a scaffold to efficiently crosslink anti-CD40 or DR5 antibodies bound to target cells via FcγRIIb.

In order to exploit these properties, engineering Fc region to increase the binding affinity to FcγRIIb is considered to be a promising approach. Introducing S267E/L328F substitutions

into the Fc region of human IgG1 increased the binding affinity to FcγRIIb 430-fold without increasing that to FcγRI, FcγRIIa^{H131} or FcγRIIIa (Chu *et al.*, 2008). Anti-CD19 antibody with the Fc promoted suppression of B-cell activation and proliferation in SLE mouse model by coengaging FcγRIIb with BCR (Horton *et al.*, 2011). Recent reports noted that anti-IgE antibody with S267E/L328F Fc variant reduced the production of IgE *in vivo* (Chu *et al.*, 2012) and that the Fcε domain fused with S267E/L328F Fc variant suppressed degranulation and calcium mobilization of mast cells (Cemerski *et al.*, 2012). Moreover, agonistic antibodies against CD40 or DR5 showed more potent agonistic activity *in vivo* with enhanced FcγRIIb binding (Li and Ravetch, 2011, 2012). These reports clearly demonstrate that engineered Fc with enhanced binding to FcγRIIb has various therapeutic applications. However, it was reported that S267E/L328F substitutions also enhanced the binding to one of the FcγRIIa allotypes, FcγRIIa^{R131}, to a level similar to the binding to FcγRIIb (Smith *et al.*, 2012). Therefore, when applying the substitutions to mAb therapeutics, the consequence of increasing the binding to FcγRIIa should be considered.

It is reported that a high incidence of thromboembolic complication was observed in patients treated with anti-CD154 or anti-VEGF antibody in clinical settings (Boumpas *et al.*, 2003; Scappaticci *et al.*, 2007). The ICs composing of these antibodies and the antigens activated platelets and induced thrombosis in human FcγRIIa transgenic mice by crosslinking FcγRIIa expressed on the platelets (Meyer *et al.*, 2009; Robles-Carrillo *et al.*, 2010). Moreover, intravenous immunoglobulins also induced FcγRIIa-mediated platelet aggregation *in vitro* (Pollreisz *et al.*, 2008). These results demonstrate that even wild-type IgG1 generally has a potential risk of inducing thromboembolism through an FcγRIIa-dependent mechanism, suggesting that this risk could be increased if the binding to FcγRIIa is enhanced. Therefore, considering the therapeutic applications, antibody with selectively enhanced binding to FcγRIIb relative to both FcγRIIa^{R131} and FcγRIIa^{H131} is preferred.

In this work, we investigated antibodies with selectively enhanced binding to FcγRIIb over both FcγRIIa^{R131} and FcγRIIa^{H131}. We screened a large set of single substituted variants of human IgG1 for binding to human FcγRs and found a distinct variant that distinguishes FcγRIIb from both FcγRIIa allotypes. We solved its crystal structure in complex with human FcγRIIb and elucidated the structural recognition mechanism by which it recognizes FcγRIIb over both FcγRIIa allotypes. In order to improve its FcγRIIb binding, we conducted further optimization and identified a novel antibody variant with over 200-fold more enhanced binding to FcγRIIb without increasing the binding to either FcγRIIa allotype. Structural analysis of this variant revealed the mechanism of the improved binding to FcγRIIb. We also report that antibody that also has enhanced binding to FcγRIIa is more likely to activate platelets and induce aggregation and would have a shorter *in vivo* half-life compared to wild-type IgG1. We also confirmed that this variant enhanced the agonistic activity of anti-CD137 antibody *in vitro*. Our results indicate that the novel Fc variant with purely selectively enhanced binding to FcγRIIb is applicable to a broad range of therapeutic antibodies, since it avoids increasing the potential to activate or aggregate platelets and to have rapid clearance *in vivo*.

Materials and methods

Preparation of IgG1 variants

IgG1 variants used in the experiments were expressed transiently in FreeStyle™ 293F cells transfected with plasmids encoding heavy and light chain and purified from culture supernatants using protein A. Site-directed mutagenesis of the Fc region was performed using QuikChange Site-Directed Mutagenesis Kit (Stratagene) or In-Fusion HD Cloning Kit (Clontech).

Construction, expression and purification of FcγRs

The genes encoding the extracellular region of human FcγRs were synthesized based on the sequence information obtained from the National Center for Biotechnology Information. FcγRs were fused with 6× His-tag at their C-terminus. Vectors containing FcγRs were transfected into FreeStyle™ 293F cells. The receptors were purified from the harvested culture supernatants by using ion exchange chromatography, nickel affinity chromatography and size exclusion chromatography.

Binding and affinity analysis for human FcγRs by surface plasmon resonance (SPR)

The interaction of antibody variants with FcγRs was monitored using Biacore instruments (GE Healthcare), as previously described (Richards *et al.*, 2008). Antibody variants were captured on the CM5 sensor chip (GE Healthcare) on which antigen peptide or protein A/G (Thermo Scientific) was immobilized, followed by injection of FcγRs. The binding of each variant to each FcγR was normalized by the captured amount of antibody on the sensor chip and was expressed as a percentage of that of IgG1. Kinetic analysis was performed by global fitting of binding data with a 1 : 1 Langmuir binding model using Biacore Evaluation Software (GE Healthcare).

Crystalization, data collection and structure determination of the complex of Fc fragment of human IgG1 with P238D substitution, Fc(P238D) and FcγRIIb

Crystals were obtained by 1 : 1 mixing of protein complex (10 mg/ml) with 0.1 M Bis-Tris pH6.5, 0.2 M ammonium acetate, 2.7% (w/v) D-galactose, 17% PEG3350 in sitting drop vapor diffusion setups at 20°C. For data collection, crystals were flash frozen at 95 K in precipitant solution containing 22.5% ethylene glycol. Diffraction data to 2.6 Å were collected using the Photon Factory beamline BL-1A. Data were processed with Xia2 (Winter, 2010), XDS Package (Kabsch, 2010) and Scala (Evans, 2006). The structure was determined by molecular replacement with PHASER (McCoy *et al.*, 2007) using Fc part of Fc(IgG1)/FcγRIIa structure (PDB ID: 3SGJ) and FcγRIIb structure (PDB ID: 2FCB) as search models. The asymmetric unit was formed by a single 1 : 1 complex. A model was built with the program Coot (Emsley *et al.*, 2010) and refined with the program REFMAC5 (Murshudov *et al.*, 2011).

Crystalization, data collection and structure determination of the complex of Fc fragment of V12 variant, Fc(V12) and FcγRIIb

Crystals were obtained by 1 : 1 mixing of protein complex (10 mg/ml) with 0.1 M Bis-Tris pH6.5, 0.2 M potassium phosphate dibasic, 19% PEG3350 in hanging drop vapor diffusion

setups at 20°C. For data collection, crystals were flash frozen at 95 K in precipitant solution containing 20% ethylene glycol. Diffraction data to 2.86 Å were collected at the SPring-8 beamline BL-32XU. After data processing and structure determination by molecular replacement using Fc(P238D)/FcγRIIb structure, a model was built with the program Coot and refined with the program REFMAC5. The asymmetric unit was formed by a single 1 : 1 complex.

Data collection and refinement statistics of both crystals are summarized in Supplementary Table S1. All graphical presentations were prepared with PyMOL (DeLano, 2002).

Preparation of Fc fragment and FcγRIIb complexes

We cloned recombinant Fc fragments corresponding to the heavy chain residues from 216 (EU numbering) to C-terminus for the crystallization. Cys 220 was replaced with Ser so that the free cysteine would not make disulfide bonds. FcγRIIb expressed by FreeStyle™ 293F cells in the presence of the mannosidase I inhibitor, kifunensine, was purified and treated with endoglycosidase F1 fused with glutathione *S*-transferase for deglycosylation as described previously to minimize the heterogeneity of the oligosaccharide (Grueninger-Leitch *et al.*, 1996). The complexes of Fc fragment and the deglycosylated FcγRIIb were prepared by mixing Fc fragment with a little excess of the deglycosylated FcγRIIb, and purified by size exclusion chromatography.

Thermal shift assay

Melting temperature (T_M) of the C_H2 region was measured as previously described (He *et al.*, 2010). The SYPRO orange dye (Invitrogen) was added to 0.1 mg/ml protein solutions at a final dilution of 1 : 500. Fluorescence measurements were employed using a real-time polymerase chain reaction instrument, Rotor-Gene Q (QIAGEN). The temperature was increased from 30 to 99°C at a heating rate of 4°C/min.

Stability study of high concentration antibodies

Antibodies were concentrated to 100 mg/ml in a histidine buffer (20 mM histidine, 150 mM NaCl, pH6.0) by ultrafiltration (Millipore). The solutions were stored at 25°C to assess the stability of the antibodies. High-molecular-weight (HMW) species were analyzed with TSK-GEL G3000SWXL column (TOSOH) by size exclusion high-performance liquid chromatography at initial time point and after 4 weeks. The mobile phase contained 300 mM NaCl in 50 mM phosphate at pH7.0. The percentage of HMW species peak in total protein peak area was calculated using Empower Waters software.

Binding affinity analysis of antibodies for human FcRn

Recombinant, soluble human FcRn (hFcRn) was expressed in HEK293 cells and prepared as described previously (Dall'Acqua *et al.*, 2006). The interaction of soluble hFcRn was monitored as described previously (Igawa *et al.*, 2010).

Pharmacokinetic studies of monoclonal antibodies in hFcRn transgenic mouse

Anti-human interleukin-6 receptor (hIL-6R) IgG1 or V12 variant was administered to human FcRn (hFcRn) transgenic mice (B6.mFcRn$^{-/-}$ hFCRN Tg32 B6.Cg-Fcgrt<tm1Dcr> Tg(FCGRT)32Dcr; Jackson Laboratories) by single intravenous injection together with 1 g/kg Sanglopor (CSL Behring K.K.) to mimic endogenous IgG in human. Blood samples were collected. The concentration of each antibody was determined by capture with anti-idiotype antibody (in-house), followed by addition of hIL-6R and biotinylated anti-hIL-6R antibody (R&D Systems) and detected by Streptavidin-Poly HRP80. The half-life was calculated from the plasma concentration–time data using non-compartmental analysis with WinNonlin Professional software (Pharsight).

Platelet aggregation and activation study using washed platelets

Fresh blood from healthy volunteers whose FcγRIIa genotype is R/R or H/H was anticoagulated with 0.5 ml of 3.8% sodium citric acid–citrate in blood collection tubes. Platelet-rich plasma (PRP) was obtained by centrifuging at 200 *g* for 15 min and then removing the supernatant. PRP was washed in modified Tyrode buffer (137 mM NaCl, 2.7 mM KCl, 12 mM $NaHCO_3$, 0.42 mM NaH_2PO_4, 2 mM $MgCl_2$, 5 mM HEPES, 5.55 mM dextrose, 0.35% bovine serum albumin) with 1.5 U/ml apyrase and resuspended at a concentration of 3×10^8/ml in modified Tyrode buffer. Washed platelets were then incubated with preformed IC for 5 min. The Preformed IC was prepared by mixing the anti-IgE mAb having different Fc variants (200 μg/ml) with its antigen (229 μg/ml), human IgE, at a molar ratio 1 : 1. Five minutes after the incubation, 30 μM ADP was added to induce the first wave of platelet aggregation. Platelet aggregation was measured by an aggregometer (MCM Hema Tracer 712; MC Medical) at 37°C with stirring at 1000 rpm.

Cells and reagents

CTLL-2 cells (mouse T lymphocyte cell line, No.RCB0637) were provided by the RIKEN BRC through the National Bio-Resource Project of the MEXT, Japan. Raji cells (human Burkitt's lymphoma cell line, ATCC No.CCL-86) were purchased from the American Type Culture Collection. Both cell lines were cultured in RPMI 1640 medium (Nacalai tesque), supplemented with 10% heat-inactivated foetal bovine serum (Bovogen). The culture medium for CTLL-2 was supplemented with 10 ng/ml recombinant mouse interleukin (IL)-2 (PeproTech). The culture medium for Raji cells was supplemented with 10 mM HEPES, 1 mM sodium pyruvate (Nacalai tesque), 4.5 g/l D-glucose, 1.5 g/l sodium bicarbonate (Sigma-Aldrich).

Flow cytometry analysis of CD137 expression

To analyze mouse CD137 expression on CTLL-2 cells, anti-mouse CD137 clone 1D8 variable region fused with the Fc domain of human IgG1 (Shuford *et al.*, 1997) or human IgG1 isotype control (Alexis, Lausen) was applied. Goat F(ab')2 anti-human IgG-FITC #732596 (Beckman Coulter) was used as the detection antibody. Cell Lab Quanta SC MPL system (Beckman Coulter) was used for cell acquisition and data analysis was conducted using FlowJo software (Tree Star Inc.).

Measurement of T-cell activation by anti-CD137 antibody by cytokine production

CTLL-2 cells (2×10^5/mL) and Raji cells (2×10^5/ml) were co-cultured in RPMI 1640 medium supplemented with 10% heat-inactivated foetal bovine serum (Bovogen), 10 ng/ml mouse IL-2 (PeproTech), 10 ng/ml phorbol 12-myristate 13-acetate, 0.5 μg/ml ionomycin (Sigma-Aldrich). The cells were treated with 3 μg/ml anti-CD137 antibodies with

different Fc (Fc of human IgG1, S267E/L328F or V12 variant) for 24 h at 37°C, 5% CO_2. Mouse interferon (IFN)-γ concentration in the cultured medium was determined by ELISA system (PeproTech), according to the manufacturer's protocol.

Results

Screening and characterization of variants to selectively enhance FcγRIIb binding by comprehensive mutagenesis

We screened a large set of over 500 variants prepared by replacing each of about 30 residues in the lower hinge and C_H2 region with every naturally occurring amino acid except for cysteine, for binding to human FcγRIIa^{H131}, FcγRIIa^{R131} and FcγRIIb in order to identify substitutions that selectively enhance FcγRIIb binding relative to both FcγRIIa allotypes. The effect of each substitution on the binding to FcγRIIa^{R131}, FcγRIIa^{H131} and FcγRIIb is compared in Fig. 1A and B. Only two substitutions, P238D and L328E, were found to enhance FcγRIIb binding while decreasing the binding to both FcγRIIa allotypes, although previously reported S267E and L328F increased both binding.

We compared the dissociation constant (K_D) of wild-type human IgG1, P238D variant and L328E variant (Supplementary Table S2) and the changes in affinity from

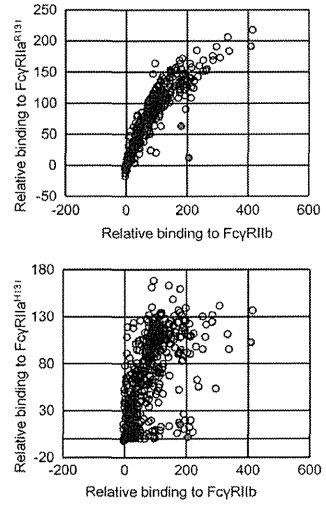

Fig. 1. Comprehensive mutagenesis of the lower hinge and C_H2 region. Binding affinity for FcγRIIa^{R131}, FcγRIIa^{H131} and FcγRIIb was evaluated. The binding to FcγRIIa^{R131}, FcγRIIa^{H131} or FcγRIIb of template antibody was normalized to 100. The binding to FcγRIIa^{R131} and FcγRIIb is shown in panel **A** and the binding to FcγRIIa^{H131} and FcγRIIb is shown in panel **B**. Novel substitutions to selectively improve FcγRIIb binding, L328E and P238D, are indicated in blue and red, respectively. Previously reported substitutions, S267E and L328F, to improve FcγRIIb but also FcγRIIa^{R131} binding are indicated in green and yellow, respectively.

IgG1 are shown in Fig. 2. Both P238D and L328E variants enhanced affinity to FcγRIIb, while reduced affinity to both FcγRIIa^{R131} and FcγRIIa^{H131}. P238D variant reduced the affinity for all the active FcγRs and enhanced that for FcγRIIb more significantly than L328E variant.

Crystal structure of the FcγRIIb complex with IgG1 Fc fragment with P238D

Fc(P238D) bound to FcγRIIb in an asymmetric fashion between the two C_H2 domains (C_H-A and C_H-B) like previously reported Fc(IgG1) and FcγR complexes. In Fig. 3A, the overall structure of Fc(P238D)/FcγRIIb was compared with known Fc(IgG1)/FcγRIIa^{R131} (PDB ID: 3RY6) (Ramsland *et al.*, 2011). Despite the high-sequence homology between FcγRIIb and FcγRIIa^{R131} (Supplementary Fig. S1), the domain arrangement of C_H2-B in Fc(P238D)-FcγRIIb interface was different from that in Fc(IgG1)/FcγRIIa^{R131}.

Structural comparisons of both C_H2 domains with those of Fc(IgG1) complexed with FcγRIIa^{R131} revealed conformational changes of loops around position 238 in both C_H2 domains (Fig. 3B and C). Pro238 in wild-type human IgG1 formed an inside hydrophobic core with Val263, Val266, V323, Asn325 and Leu328. On the other hand, Asp238 in P238D variant shifted out of the core and it was exposed to the solvent region. Instead, Leu235 occupied the vacated space which Pro238 occupied in Fc(IgG1), forming another hydrophobic core in C_H2-A, but not in C_H2-B. As a result, there was a large cavity surrounded by Val263, Val266, Val273, Val323, Asn325 and Leu328 in C_H2-B. Asp238 in C_H2-B formed an electrostatic interaction with Lys334 in the same chain.

In the C_H2-A domain, the main chain of Gly237 formed a novel hydrogen bond with Tyr160 of FcγRIIb (Fig. 3B). A weak hydrogen bond between the main chain of Asp238 and the side chain of Thr158 of FcγRIIb was also observed. In addition, the side chain of Asp238 formed van der Waals contacts with the side chain of Thr158 in FcγRIIb. In the C_H2-B domain, the conformation of the loop around Asp270 changed from that of Fc(IgG1) complexed with FcγRIIa^{R131}, and Asp270 formed a salt bridge with Arg131 of FcγRIIb (Fig. 3C).

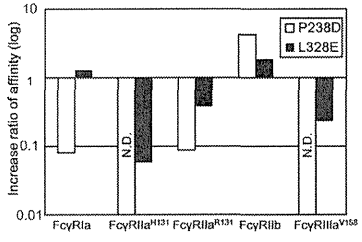

Fig. 2. Affinity ratio of Fc variants identified by comprehensive mutagenesis for all the human FcγRs. The binding of P238D variant to FcγRIIa^{H131} and FcγRIIIa^{V158} and that of L328E variant to FcγRIIa^{H131} were not detected. Affinity ratio was calculated by the equation, K_D (IgG1)/K_D (Fc variant).

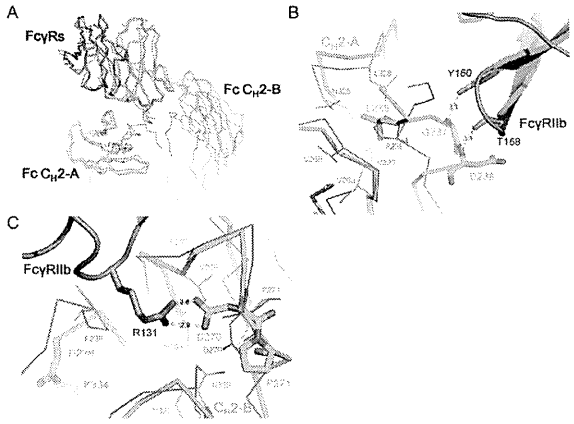

Fig. 3. Structural comparison of Fc(P238D)/FcγRIIb complex with Fc(IgG1)/FcγRIIa^{R131} complex. (**A**) The overall structural comparison of Fc(P238D)/FcγRIIb complex with Fc(IgG1)/FcγRIIa^{R131} complex. (**B**) The binding interface between the C_H2-A domain of Fc(P238D) and FcγRIIb. (**C**) The binding interface between the C_H2-B domain and FcγRIIb. The structural changes and novel interactions introduced by P238D in both interfaces are shown by comparing Fc(P238D)/FcγRIIb and Fc(IgG1)/ FcγRIIa^{R131}. Fc(P238D)/FcγRIIb and Fc(IgG1)/FcγRIIa^{R131} are shown in green and magenta, respectively. FcγRIIb and FcγRIIa^{R131} are shown in the darker color, respectively.

Table I. Effect of additional substitution(s) into P238D variant on binding affinity for FcγRIIb

Variant no.	Amino acid change					Fold (K_D for FcγRIIb)
Single substitution						
V1	E233D					1.7
V2		G237D				1.5
V3			H268D			1.7
V4				P271G		5.0
V5					A330R	1.2
Two substitutions						
V6	E233D				A330R	1.9
Three substitutions						
V7	E233D			P271G	A330R	8.2
V8		G237D	H268D	P271G		9.5
V9		G237D		P271G	A330R	33
Four substitutions						
V10	E233D		H268D	P271G	A330R	9.0
V11		G237D	H268D	P271G	A330R	40
Five substitutions						
V12	E233D	G237D	H268D	P271G	A330R	62

Fold = K_D (P238D variant)/K_D (Fc variants).

Screening, characterization and design of variants to further enhance FcγRIIb binding by comprehensive mutagenesis using the P238D variant as a template

In order to further enhance the affinity to FcγRIIb, we combined P238D with L328E or S267E/L328F, previously known variant to increase binding to FcγRIIb and FcγRIIa^{R131}. Unexpectedly, the additive effect by combining P238D with those substitutions was not observed. Affinities for FcγRIIb of these variants are listed in Supplementary Table S3.

Then, we screened substitutions to improve FcγRIIb binding when they were combined with P238D by comprehensive mutagenesis using the P238D variant as a template. Approximately 400 variants with an additional single substitution onto the P238D variant were generated, and the affinity for FcγRIIb was determined. Six effective substitutions (E233D, G237D, H268D, P271G, Y296D and A330R) were identified. We further combined these substitutions to create V12 variant having all the six substitutions described above. The fold increases of the variants against FcγRIIb over P238D variant are listed in Table I.

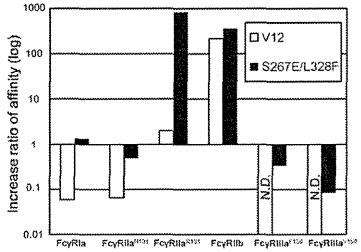

Fig. 4. Affinity ratio of S267E/L328F and V12 variant for all the human FcγRs. The binding of V12 variant to FcγRIIa^{F158} or FcγRIIa^{V158} was not detected. Affinity ratio was calculated by the equation, K_D (IgG1)/K_D (Fc variant).

K_Ds of wild-type IgG1, S267E/L328F variant and the most potent variant, V12 variant, to all the FcγRs are listed in Supplementary Table S2 and the changes in affinity from IgG1 are shown in Fig. 4. V12 variant showed 217-fold increase in affinity for FcγRIIb, yet bound to FcγRIIa^{R131} with similar affinity to that of wild-type IgG1 and to the other activating FcγRs with affinity significantly lower than that of IgG1. On the other hand, S267E/L328F variant increased the affinity for FcγRIIb 355-fold and that for FcγRIIa^{R131} even greater, 864-fold.

Crystal structure of the FcγRIIb complex with Fc(V12)

The same conformational changes around Asp238 induced by P238D substitution in Fc(P238D)/FcγRIIb were also observed in Fc(V12)/FcγRIIb.

In the C_H2-A domain, the introduced residues, Asp233, Asp237 and Arg330, were located in the interface with FcγRIIb (Fig. 5A). The weak electron density of Asp233, replaced from Glu, was observed. As Lys113 of FcγRIIb is located near Asp233, they might interact with each other. In the C_H2-A domain, Asp237, replaced from Gly, made van der Waals contacts with Trp87 and Tyr160 of FcγRIIb. In addition, the hydrogen bond distance between NH of the main chain at position 237 in Fc and OH of the Tyr160 side chain in FcγRIIb changed from 3.1 Å in Fc(P238D) (Fig. 3C) to 2.9 Å in Fc(V12) (Fig. 5A). A weak hydrogen bond between the side chain of Asp238 and the side chain of Thr158 of FcγRIIb was also observed. The electron density of the side chain of Arg330, which replaced Ala, was not clearly observed. As Glu86 of FcγRIIb is located near Arg330, a weak interaction between those residues could be present.

In the C_H2-B domain, H268D and P271G substitutions induced a further conformational change of a loop around Asp270 (Fig. 5B). The substitution from Pro to Gly at position 271 caused the main chain to flip and consequently rearranged the 266–273 loop and Arg131 of FcγRIIb, which also formed a salt bridge with Asp270 in C_H2-B of Fc(V12) as well as in Fc(P238D). In addition, the electron density of Gly271 in C_H2-B was clearly observed, though in Pro271 in Fc(P238D) it was not. This conformational change of the loop caused a rearrangement of Arg292 in C_H2-B of Fc(V12). The other substituted residue, Asp268, formed an electrostatic interaction with the shifted Arg292.

Pharmacokinetic and biophysical property assessment of V12 variant

In order to characterize the pharmacokinetic aspect of V12 variant, we measured the affinity for hFcRn and the pharmacokinetics in hFcRn transgenic mice. The binding affinity of V12 variant for hFcRn at pH6.0 was comparable with that of wild-type IgG1 and the *in vivo* half-life was also comparable (Table II).

T_M of the C_H2 domain was measured by thermal shift assay. The T_M of V12 variant decreased by 8°C relative to wild-type IgG1 (Table II). To assess the real-time stability for pharmaceutical application of V12 variant, a stability study at an antibody concentration of 100 mg/ml was performed. The formation of HMW species of V12 variant after storage for 4 weeks at 25°C was comparable with that of wild-type IgG1 (Table II).

In vitro activation and aggregation of platelets by ICs consisting of IgE and anti-IgE antibody with S267E/L328F variant or V12 variant

Platelets obtained from two donors homozygous for FcγRIIa^{R131} genotype and incubated with IC consisting of IgE and anti-IgE S267E/L328F variant increased the expression of CD62p and PAC-1 on the platelets, but those incubated with IC consisting of IgE and anti-IgE with the V12 variant did not (Supplementary Fig. S2A and B). On the other hand, when we used platelets obtained from two donors homozygous for FcγRIIa^{H131} genotype, IC consisting of IgE and anti-IgE S267E/L328F variant slightly upregulated the expression of CD62p and PAC-1 on the platelets but IC consisting of anti-IgE with the V12 variant did not after the incubation compared with the control (phosphate-buffered saline) (Supplementary Fig. S2C and D).

Next, the platelet aggregation induced by ICs was evaluated with an aggregometer. After the addition of ADP, only IC consisting of IgE and anti-IgE with S267E/L328F substitutions aggregated the platelets obtained from two donors homozygous for FcγRIIa^{R131} genotype, while IC consisting of IgE and anti-IgE with V12 variant did not (Fig. 6A and B). On the other hand, IC consisting of neither variant induced the aggregation of the platelets obtained from two donors homozygous for FcγRIIa^{H131} genotype (Fig. 6C and D).

Enhancement of agonistic activity of anti-CD137 antibody with enhanced FcγRIIb binding Fc

Several reports have described that agonistic anti-TNFR superfamily antibodies generally require FcγRIIb coengagment for their agonistic activity and that enhancing the binding affinity of the antibodies for FcγRIIb could increase the agonistic activity (White *et al.*, 2011; Wilson *et al.*, 2011; Li and Ravetch, 2012). Therefore, we tested whether V12 also has the same property using agonist antibody against CD137 (clone 1D8), which is one of the TNFR superfamily.

Mouse T lymphoma cell line CTLL-2 was used as mouse CD137-expressing cells (Fig. 7A), and human B lymphoma cell line Raji was used as human FcγRII-positive cells (Hernández *et al.*, 2010). T-cell activating agonistic activity of anti-CD137 antibody was measured with the production of mouse IFN-γ production of CTLL-2 co-cultured with Raji cells. Consistent with the previous reports, V12 variant as well as S267E/L328F variant increased IFN-γ production induced by agonist anti-CD137 antibody compared with intact human IgG1 by more than 5-fold (Fig. 7B).

Discussion

Several efforts to improve FcγR binding by Fc engineering have been reported to date. While most of the engineering enhances the binding affinity for activating FcγRs (Stavenhagen *et al.*, 2007; Zalevsky *et al.*, 2009; Mossner *et al.*, 2010), engineering to enhance binding affinity to inhibitory FcγR is limited (Chu *et al.*, 2008). S267E/L328F variant, the Fc variant reported to have the highest affinity for inhibitory FcγR binding, enhanced the binding affinity for FcγRIIb by 355-fold; however, it also enhanced the binding affinity for FcγRIIa^{R131} to the same level as FcγRIIb (Smith *et al.*, 2012). The high similarity between FcγRIIb and FcγRIIa^{R131} suggests that discriminating FcγRIIb and FcγRIIa^{R131} by Fc engineering is challenging (Supplementary Fig. S1).

In this work, we investigated the substitutions to distinguish FcγRIIb from FcγRIIa^{R131} by comprehensive mutagenesis and discovered a highly selective substitution, P238D, which provides the highest selectivity for FcγRIIb relative to all the other active FcγRs including FcγRIIa^{R131}. Fc variants which discriminate FcγRIIb from FcγRIIa^{R131} were extremely rare, probably because FcγRIIb is highly homologous to

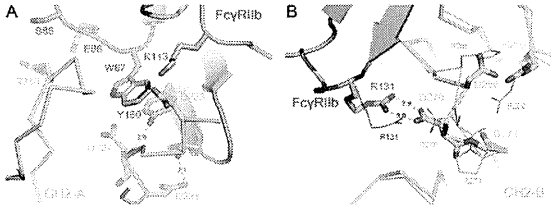

Fig. 5. Structure of Fc(V12)/FcγRIIb complex. (**A**) The binding interface between the C_H2-A domain of Fc(V12) and FcγRIIb. The substitutions in Fc(V12) and the residues in FcγRIIb with a minimum distance of 3.8 Å from these substitutions are shown as sticks. (**B**) The binding interface between the C_H2-B domain of Fc(V12) and FcγRIIb. The structural changes around Asp270 in the C_H2-B domains shown by comparing Fc(P238D)/FcγRIIb (green) and Fc(P238D)/FcγRIIb (cyan) complexes. FcγRIIb in each complex is shown in the darker color.

Table II. Characterization of V12 variant

	T_M (CH2) (°C)	HMW formation after storage (%)	K_D for FcRn (μM)[a]	Half-life (day)[b]
IgG1	70	0.30	1.5 ± 0.0	12.8 ± 3.8
V12	62	0.33	1.4 ± 0.0	12.6 ± 3.2

The group mean ± SD are given for the parameter ($n = 3$ each).
[a]K_D for FcRn was measured at pH6.0 by SPR.
[b]Half-life of intravenously injected IgG1 and V12 variant at 1 mg/kg in hFcRn transgenic mouse.

FcγRIIa^{R131} (Supplementary Fig. S1) and the Fc-FcγRIIb interface would be also highly homologous to the Fc-FcγRIIa^{R131}. To the best of our knowledge, this is the first report illustrating an Fc variant that enhances FcγRIIb binding while distinguishing FcγRIIb and FcγRIIa^{R131} precisely.

To elucidate the structural mechanism by which P238D variant discriminates FcγRIIb from FcγRIIa^{R131}, we solved the crystal structure of the complex of Fc(P238D) and FcγRIIb. Our structural analysis indicated that the high selectivity of P238D variant was achieved by a dynamic conformational change of the Fc-FcγRIIb interface that was induced by P238D substitution into wild-type IgG1. In reported Fc(IgG1) structures, Pro238 forms a hydrophobic core with its surrounding residues. Therefore, substituting this hydrophobic Pro238 to hydrophilic Asp should cause large free energy loss for desolvation of Asp to maintain the same structure. To avoid this free energy loss, Asp238 showed a large shift out of its original position to achieve access to the solvent region. Additionally, the position of Pro238 in Fc(IgG1) was occupied by Leu235 instead in C_H2-A of Fc(P238D) complexed with FcγRIIb. As the result, the large conformational change of loop233–240 attached to the hinge region was observed. This change would affect the domain arrangement between the C_H2-A and B domains because both C_H2 domains connect by S–S bonds in the hinge region and cannot move independently. In fact, the relative arrangement of C_H2-A and B domains in the Fc(P238D)/FcγRIIb complex was different from that of Fc(IgG1)/FcγRIIa^{R131}, despite FcγRIIb having the highest homology to FcγRIIa^{R131}. As the result of these dynamic conformational changes, Fc(P238D) acquired two novel interactions with FcγRIIb. One is the hydrogen bond between the main chain of Gly237 in C_H2-A and the side chain of Tyr160 in FcγRIIb. Both FcγRIIa allotype cannot make this hydrogen bond because corresponding residue of this Tyr is Phe in FcγRIIa (Supplementary Fig. S1). So, this interaction would play a critical role for distinguishing FcγRIIb from FcγRIIa. The other one is the salt bridge between Asp270 in C_H2-A and Arg131 of FcγRIIb. This salt bridge would contribute to improve not only the binding affinity to FcγRIIb but also the selectivity over FcγRIIa^{H131} because this allotype has His as the corresponding residue of Arg131 in FcγRIIb. On the other hand, the S267E/L328F variant increased binding affinity to both FcγRIIb and FcγRIIa^{R131} to the same extent, while it did not increase binding affinity to FcγRIIa^{H131} or other FcγRs. From the reported complex structure of Fc(IgG1)/FcγRIIa^{R131}, we elucidated that Glu267 of the Fc with S267E/L328F substitution would form a salt bridge with Arg131 of the FcγRIIb and also of the FcγRIIa^{R131}. This might explain the reason for the lack of selectivity of the S267E/L328F variant to FcγRIIb over FcγRIIa^{R131}, both of which have Arg at position 131. Large conformational change induced by P238D would also explain the reason for lack of additive effect of combining P238D with L328E or S267E/L328F.

Then, in order to further increase the binding affinity to FcγRIIb, we conducted a second comprehensive mutagenesis using the P238D variant as a template rather than combining substitution(s) effective for wild-type IgG1 template, since the interface of Fc(P238D)/FcγRIIb was considered to be significantly changed from that of Fc(IgG1)/FcγRIIb. P238D-based comprehensive and combinatorial study identified V12 variant whose affinity for FcγRIIb was significantly increased from P238D variant. Especially, P271G markedly increased affinity for FcγRIIb. The substitution of fixed proline to flexible glycine would contribute to release conformational stress when a salt bridge between Asp270 in Fc (V12) and Arg131 in FcγRIIb is formed, which is considered to contribute to the affinity improvement for FcγRIIb.

Structural analysis of P238D suggests that P238D substitution seemed to destabilize the hydrophobic core of C_H2 domain, although this could be partially compensated by Leu235 as found in C_H2-A domain. The conformational changes seem to be the cause of decreased T_M for V12 variant. Although this reduced T_M raised concern regarding the storage stability of Fc(V12) for pharmaceutical application, its stability (aggregation tendency at 100 mg/ml) was comparable with that of wild-type IgG1.

It is known that, for IgG1 antibody to have a long half-life *in vivo*, binding to FcRn at acidic pH is important. The affinity of V12 variant for hFcRn was comparable with that of wild-type IgG1 and, consistently, the *in vivo* half-life of V12

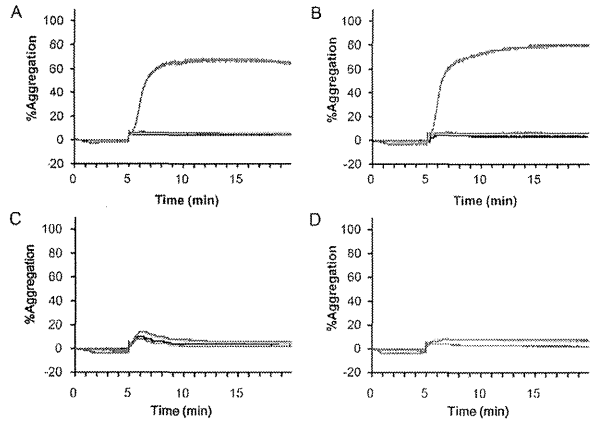

Fig. 6. Platelet aggregation studies incubated with ICs. Platelet aggregation was evaluated after platelets were incubated with ICs consisting of IgE with anti-IgE V12 variant (blue), that of anti-IgE S267E/L328F variant (red), IgE and anti-IgE IgG1 (green) or phosphate-buffered saline (black) for 5 min after being primed with ADP. Aggregation of the platelets from two donors with FcγRIIa R/R131 homozygous genotype are shown in panels **A** and **B**, respectively. Aggregation of the platelets from two donors with FcγRIIa H/H131 homozygous genotype are shown in panels **C** and **D**, respectively.

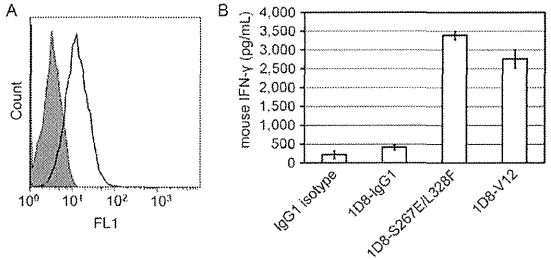

Fig. 7. V12 variant enhanced the T-cell activating agonistic activity of anti-CD137 antibody 1D8. (**A**) CD137 surface expression on CTLL-2 cells. Open histogram indicates 1D8-IgG1 and filled histogram indicates IgG1 isotype control. (**B**) T-cell activation induced by anti-CD137 antibody with different Fc (IgG1, V12 variant and S267E/L328F variant) was measured as mouse IFN-γ production of CTLL-2 co-cultured with Raji. Each bar shows mean ± SEM of three independent experiments.

variant was also comparable with that of wild-type IgG1. However, it should be noted that because the binding affinity of V12 variant to murine FcγRIIb (the mouse counterpart of human FcγRIIb) was not increased, its effect on the pharmacokinetics was not addressed in this study.

ICs induce platelet aggregation and activation when antibody binds to FcγRIIa expressed on the platelet surface (Boumpas *et al.*, 2003; Scappaticci *et al.*, 2007). The previous studies suggest that ICs consisting of IgG with enhanced binding to FcγRIIa have the potential to induce platelet aggregation and activation more intensively than IC consisting of wild-type IgG. However, the effect of engineered Fc with enhanced binding affinity to FcγRIIa on platelet activation and aggregation induced by IC has not so far been investigated. In this report, IC consisting of IgE and anti-IgE antibody with enhanced binding affinity to both FcγRIIb and FcγRIIa^{R131} (S267E/L328F variant) induced the activation and aggregation of platelets obtained from FcγRIIa genotype of R/R131 homozygous donors, but not from FcγRIIa genotype of H/H131 homozygous donors. On the other hand, anti-IgE antibody with selectively enhanced binding affinity to FcγRIIb did not induce the activation or aggregation of platelets from donors with either genotype. Platelets whose FcγRIIa genotype is R/H131 are considered to express both FcγRIIa allotypes on their surface, while platelets whose FcγRIIa genotype is R/R131 express only FcγRIIa^{R131}. Therefore, a similar tendency will be observed in the platelets from heterozygous donors, although the induction of the aggregation and activation might be milder.

It is known that FcγRIIa internalizes ICs by endocytosis and transfers them to lysosomal degradation (Zhang and Booth, 2010), while FcγRIIb recycles the internalized ICs